

Neutral Hydrogen in Local Group Dwarf Galaxies

Jana Grcevich

Submitted in partial fulfillment of the
requirements for the degree
of Doctor of Philosophy
in the Graduate School of Arts and Sciences

COLUMBIA UNIVERSITY

2013

©2013
Jana Grcevich
All rights reserved

ABSTRACT

Neutral Hydrogen in Local Group Dwarfs

Jana Grcevich

The gas content of the faintest and lowest mass dwarf galaxies provide means to study the evolution of these unique objects. The evolutionary histories of low mass dwarf galaxies are interesting in their own right, but may also provide insight into fundamental cosmological problems. These include the nature of dark matter, the disagreement between the number of observed Local Group dwarf galaxies and that predicted by Λ CDM, and the discrepancy between the observed census of baryonic matter in the Milky Way's environment and theoretical predictions.

This thesis explores these questions by studying the neutral hydrogen (HI) component of dwarf galaxies. First, limits on the HI mass of the ultra-faint dwarfs are presented, and the HI content of all Local Group dwarf galaxies is examined from an environmental standpoint. We find that those Local Group dwarfs within 270 kpc of a massive host galaxy are deficient in HI as compared to those at larger galactocentric distances. Ram-pressure arguments are invoked, which suggest halo densities greater than $2-3 \times 10^{-4} \text{ cm}^{-3}$ out to distances of at least 70 kpc, values which are consistent with theoretical models and suggest the halo may harbor a large fraction of the host galaxy's baryons. We also find that

accounting for the incompleteness of the dwarf galaxy count, known dwarf galaxies whose gas has been removed could have provided at most $2.1 \times 10^8 M_{\odot}$ of HI gas to the Milky Way. Second, we examine the possibility of discovering unknown gas-rich ultra-faint galaxies in the Local Group using HI. The GALFA-HI Survey catalog is searched for compact, isolated HI clouds which are most similar to the expected HI characteristics of low mass dwarf galaxies. Fifty-one Local Group dwarf galaxy candidates are identified through column density, brightness temperature, and kinematic selection criteria, and their properties are explored. Third, we present hydrodynamic simulations of dwarf galaxies experiencing a constant velocity and density wind which emulates relative motion of the dwarf and the host's hot halo. These simulations resolve instabilities which can contribute to gas loss, such as the effects of the Kelvin Helmholtz instability. The results of these simulations support the hypothesis that rapid gas loss occurs when the ram pressure stripping criterion is met, with complete stripping occurs with a timescale of about half a Gyr. This stripping would occur in less than an orbital period for ultra-faint like dwarfs. Models which do not meet the ram-pressure stripping criterion show slower but constant mass loss which does not depend on the residual dwarf's gas mass. Extrapolating the stripping timescales, we show low-mass dwarf galaxies can be stripped on timescales between 1.1 and 3.3 Gyrs. These simulations are a first step towards accurate ram-pressure and dynamical mass loss rates for low mass Local Group galaxies orbiting within a hot halo. They suggest that the lack of low mass galaxies within 250 kpc of the Milky Way can be explained via ram-pressure and dynamical interactions between the satellite galaxy's gas and the hot halo.

(This page left intentionally blank.)

Contents

1	Introduction	1
1.1	Dwarf Galaxies in a Cosmological Context	1
1.2	Ultra-Faint Dwarfs	2
1.3	Gas in Dwarf Galaxies	4
1.4	Galactic Hot Halo	6
1.5	Dark Matter in Dwarf Galaxies	7
1.6	Thesis Summary	8
1.6.1	Chapter 2: Neutral Hydrogen in Known Local Group Dwarfs	8
1.6.2	Chapter 3: Local Group Dwarf Galaxy Candidates in the GALFA-HI Survey	9
1.6.3	Chapter 4: Simulations of Mass Loss in Dwarf Satellite Galaxies . . .	9
2	Neutral Hydrogen in Known Local Group Dwarfs	13
2.1	Introduction	13
2.2	Observations	15
2.3	Results	16
2.3.1	Nondetections	16
2.3.2	Ambiguous Detections	20
2.3.3	Confident Detections	21
2.3.4	HI Mass and Galactocentric Radius	22
2.4	Discussion	23

2.4.1	Dwarf Gas Loss	25
2.4.2	Halo Density	29
2.4.3	Comparison to Halo Models	32
2.5	Summary	33
3	Local Group Dwarf Galaxy Candidates in the GALFA-HI Survey	47
3.1	Introduction	47
3.2	The GALFA-HI Survey and Compact Cloud Catalog	49
3.3	Dwarf Candidate Selection	51
3.4	Results	54
3.4.1	Spatial and Kinematic Characteristics	54
3.4.2	Comparison to Leo T	56
3.4.3	Search for Associated Stellar Populations with SDSS	57
3.5	Discussion	59
3.5.1	Two Candidates with Optical Counterparts	60
3.5.2	The CC Clouds	62
3.5.3	M31 Satellite Candidates	63
3.5.4	Remaining Group 1 Candidates	64
3.5.5	Remaining Group 2 Candidates	65
3.6	Summary	67
4	Simulations of Mass Loss in Dwarf Satellite Galaxies	86
4.1	Introduction	86
4.2	Simulation Setup	90
4.2.1	The Code	90
4.2.2	Basic Characteristics	90
4.2.3	Gravitational Potential	91
4.2.4	Gas Profile	92
4.3	Results	95

4.3.1	Stripping Timescales	95
4.3.2	Gas Loss Trends	96
4.3.3	Resolution Study	97
4.3.4	Discussion	98
4.3.5	Ram Pressure Stripping	98
4.3.6	Kelvin-Helmholtz Instability	100
4.3.7	Models as Compared to Observations	102
4.3.8	Implications for Dwarf Galaxy Evolution	103
4.4	Summary	104
5	Conclusion	113
5.1	Future Work	113
5.1.1	Searching for Unknown Local Group Dwarf Galaxies	113
5.1.2	Dwarf Galaxy Simulations	114
5.2	Conclusion	115

List of Figures

1.1	Number of known Local Group member galaxies over time	11
1.2	The structural properties of galaxies	12
2.1	Neutral Hydrogen maps for the Tucana, Sculptor, and Fornax dwarfs	41
2.2	Neutral Hydrogen mass versus distance	42
2.3	Mass fraction of neutral Hydrogen versus distance	43
2.4	HI mass divided by V-band luminosity versus distance	44
2.5	Halo density as a function of distance	45
2.6	Satellite velocities required for ram-pressure stripping	46
3.1	Integrated brightness temperature maps for group 1 dwarf candidates . . .	75
3.2	Integrated brightness temperature maps for group 1 dwarf candidates, continued	76
3.3	Integrated brightness temperature maps for group 2 candidates	77
3.4	Integrated brightness temperature maps for group 2 candidates, continued	78
3.5	Spatial and kinematic distribution of compact clouds	79
3.6	Velocity versus angle to apex of solar motion	80
3.7	Spatial profiles of candidate clouds	81
3.8	Mass estimation method	82
3.9	Sloan Digital Sky Survey image of candidate 22	83
3.10	Sloan Digital Sky Survey image of candidate 23	84
3.11	Sloan Digital Sky Survey identified stars in the vicinity of candidate 22 . . .	85

4.1	Fractional gas mass in the dwarf's original extent	107
4.2	Density maps for models A1 and A2	108
4.3	Density maps for models B1 and B2	109
4.4	Density maps for models C1 and C2	110
4.5	Mass loss in resolution study	111
4.6	Ram pressure strength versus initial central density	112

(This page left intentionally blank.)

List of Tables

2.1	HI Mass of Newly Discovered Satellites	36
2.2	HI Mass of Andromeda Satellites	37
2.3	HI Mass of Additional Local Group Satellite Galaxies	38
2.3	HI Mass of Additional Local Group Satellite Galaxies	39
2.4	Orbital Characteristics and Hot Halo Densities	40
3.1	Coordinates and Kinematics for Group 1 Dwarf Galaxy Candidates	68
3.2	Observational Characteristics for Group 1 Dwarf Galaxy Candidates	69
3.3	Coordinates and Kinematics for Group 2 Galaxy Candidates	70
3.3	Coordinates and Kinematics for Group 2 Galaxy Candidates	71
3.4	Observational Characteristics for Group 2 Galaxy Candidates	72
3.4	Observational Characteristics for Group 2 Galaxy Candidates	73
3.5	Range and Mean Values for Candidate Clouds as Compared to Leo T	74
4.1	Parameters for Models	106

(This page left intentionally blank.)

DEDICATION

I dedicate this work to my father and the memory of my mother. Of all that I have learned, their lessons of kindness, love, and generosity are the ones I most hope to remember.

ACKNOWLEDGEMENTS

I am truly fortunate to have so many supportive people in my life. Without their encouragement this work would not exist. My deepest thanks go to my advisor Mary Putman. Not only was her guidance and knowledge invaluable, but she also lent me her confidence when I found my own lacking. I cannot thank you enough for your support, draft revisions, and patience. Thanks to Fabian Heitsch, whose guidance on simulations was essential, and who acted as my advisor in residence my last year at the University of Michigan. Thanks as well to the additional members of my thesis committee and those who sat in on committee meetings: Marla Geha, Kathryn Johnston, and Greg Bryan, Jacqueline van Gorkom, and David Helfand.

I thank the faculty of the Department of Astronomy at Columbia for welcoming and supporting me, and special thanks go to my fellow graduate students at Columbia for accepting me as a friend and colleague. I am particularly grateful to Lia Corrales, Taka Tanaka, Duane Lee, Cameron Hummels, Destry Saul, Josh Schroeder, and Jeff Andrews. To officemates Lauren Corlies, Yuan Li, Emily Bowsher, Maria Periera, Kyle Parfrey, Andrew Brown, Brandon Horn, and Nitza Santiago, thank you for sharing your space with me.

I also would like to extend appreciation to the faculty of the University of Michigan, where I began graduate school. Thanks to my first graduate advisor, Mario Mateo, my professors, and particularly to Nuria Calvet, who provided the perfect balance of academic rigor and unwavering advocacy. I wish to thank my colleagues from Michigan, especially

my fellow graduate students, especially Janet Collucci, Zhaohuan Zhu, Jess Werk, and Laura Ingleby. I would also like to thank Nicholas Dahl for years of love, care, and support during my time in Michigan and before. Thanks to Eric Wilcots at the University of Wisconsin for getting me started in astronomy. I will never forget my awe that first day at a research telescope, and how I didn't know the difference between UNIX and IRAF. To my REU advisor Yancy Shirley, not only for an amazing and productive summer at NRAO Socorro, but for continued advice and encouragement.

I would like to thank the staff of the Arecibo Observatory and the ALFALFA observing team for their indispensable help in conducting the GALFA-HI Survey observations. I would also like to thank the members of the GALFA-HI collaboration, including Ayesha Begum, Kevin Douglas, Steven Gibson, Carl Heiles, Bon-Chul Koo, Eric Korpela, Min-Young Lee, and Snezana Stanimirovic, and especially to my local colleagues Josh Peek, Destry Saul, and Mary Putman.

Thanks to Milile and Ayone for running the department and for being such excellent advocates for the graduate students. Trudy, Donna, Krystal, and Julie, thank you for making sure that the students are able to receive reimbursements on time. Francisco, thanks for making sure all our academic expenses are paid for. Thank you Nelson, for your upkeep of the building and the Pupin lobby plants.

To my students and outreach attendees for reminding me how rewarding it is to share wonder and excitement with others. To my early teachers, particularly Elaine Barthelemy, Nels Dokken, and Ted Seifkis – thank you for fostering a love of knowledge. To my non-astronomy friends Jessica Raddatz, Andrea Swensson, Kristin Lindholm, Matt Lat-

turner, David Purdy, Jason Hagaman, James Stuart, and Stephanie Wykstra, thanks for de-stressing me. To Katie Hartman, thanks for your help with figures. To Kristen and Logan Lewis, thanks for the many IM encouragements and for providing a second home in Michigan. Thanks to my brother Geoff Grcevich and my sister-in-law Sarah Grcevich for their support, visits, and Skype chats. To my niece Mira, thanks for the excitement you provided before and after you were born – I look forward to watching you grow up and sharing the stars with you. Thanks to Josh, Katie, and Maxwell Peek. Josh, your support both as a friend, colleague, cheerleader, and IDL guru has been absolutely indispensable. Thanks especially to Spencer Greenberg for encouragement and co-working, letting me literally run your printer dry of ink, and for reminding me of the wonder that originally drove me to study astronomy. I am deeply grateful for your companionship and love.

January 2013, New York City

Chapter 1

Introduction

1.1 Dwarf Galaxies in a Cosmological Context

While the archetypical image of a galaxy is that of a luminous spiral, the vast majority of galaxies in the universe are dwarf galaxies. Disproportionate to their relatively small mass, dwarf galaxies are unusually useful for unraveling the mysteries of galactic evolution and cosmology. One of the most important unexplained phenomena in astrophysics is that of dark matter. First inferred through the motion of cluster galaxies, this “missing mass” was later observed via the rotation curves of spiral galaxies (Zwicky 1933; Rubin & Ford 1970). Later it became known that dwarf galaxies, particularly the faintest dwarf galaxies, are highly dark matter dominated systems (Simon & Geha 2007).

Simulations of structure formation conducted using the most studied dark matter model, called Λ cold dark matter (Λ CDM), suggest there may be hundreds of dark matter

concentrations clustered about more massive spiral galaxies (Diemand et al. 2007). Despite great success of Λ CDM on larger scales (> 1 Mpc), on smaller scales there is a divergence between the number of subhalos in the simulations and the number of observed dwarf galaxies. This apparent discrepancy is called the missing satellites problem (Klypin et al. 1999; Moore et al. 2006; Strigari et al. 2007).

1.2 Ultra-Faint Dwarfs

It may be that the Milky Way harbors numerous dark matter subhalos, but that many of these subhalos do not host a galaxy or host faint galaxies which have not yet been discovered. These possible resolutions to the missing satellites problem are supported by the fact that many extremely faint dwarf galaxies in the Local Group have eluded discovery until recent times. The discovery of these faint dwarfs has increased the Local Group galaxy count dramatically, from 35 in 2000 to 73 in 2012 (McConnachie 2012). Figure 1.1 shows the approximate number of Local Group galaxies known to humanity as a function of time. The recently discovered dwarf galaxies are termed ultra-faints due to their extremely low luminosities. The most luminous of them is Canis Venetici I, which has a V-band luminosity of only $2.3^{+0.4}_{-0.3} \times 10^5 L_{\odot}$ (Zucker et al. 2006a). They are so faint and their stars so sparse they cannot be identified by eye in images, but rather must be discovered through careful analysis of the colors of resolved stars. The Sloan Digital Sky Survey (SDSS) has allowed such searches to take place over a large fraction of the sky and have proven effective in discovering ultra-faint galaxies (York et al. 2000; Abazajian et al. 2009; Wilman et al. 2002; Willman et al. 2005b,a; Martin et al. 2007; Zucker et al. 2006c,b;

Belokurov et al. 2006b, 2007a; Irwin et al. 2007; Walsh et al. 2007).

Including the known population of ultra-faints dwarfs in the dwarf galaxy census reduces the severity of the missing satellites problem. Correcting for the detection efficiency of dwarf galaxy searches, the total number of galaxies is similar to that predicted by semi-analytic models. However, there are still some issues, as the luminosity distribution of observed galaxies doesn't agree with the predicted distribution for an NFW-like or isothermal distribution of satellite galaxies (Koposov et al. 2007b). Combining the completeness limits with a subhalo distribution taken from the Via Lactea simulation (Diemand et al. 2007), observations of the ultra-faint dwarfs are consistent with an underlying population of about 500 subhalos within the virial radius, which is in rough agreement with simulations. Thus the missing satellite problem may not necessarily represent a strong disagreement between models and observations, but may primarily be due to an incomplete galaxy count (Tollerud et al. 2008).

Even if the theoretical missing satellites problem is less dire than previously thought, we are still missing satellites in an observational sense. It is extremely unlikely that the ultra-faint satellites discovered to date are the only ones that exist. Faint dwarf galaxies that lie outside the SDSS coverage region likely lie undiscovered, and SDSS has currently mapped only 20% of the sky. Satellites within the SDSS sky coverage may have stars too faint to be detected, too distant to be resolved, or which have too sparse a stellar distribution to be detected. In particular, dwarf galaxies of comparable magnitudes to known ultra-faints ($M_V > -4$) would be undetectable beyond the virial radius of the Milky Way using current detection methods. Observation of the neutral hydrogen component of

these galaxies may be a useful complementary discovery method, particularly for dwarfs which are on the outskirts of the Local Group (see Chapter 3).

The new population of ultra-faint dwarf galaxies are about as faint as globular clusters in terms of M_V , but have lower surface brightness and larger half light radii. The top panel of Figure 1.2, taken from Tolstoy's 2009 review article, shows the surface brightness of all Local Group dwarf galaxies is plotted vs. M_V . There is a gap in this apparent linear relationship which separates the classical dwarfs and ultra-faints. Leo T is an ultra-faint dwarf galaxy with properties intermediate between those expected for dwarf spheroidal and dwarf irregular galaxies, and is the only ultra-faint known to contain neutral hydrogen (HI) gas. It spans the gap seen in Figure 1.2 which separates ultra-faint and classical dwarf galaxies (Tolstoy et al. 2009). It is possible Leo T is a unique object, but there are reasons to believe there are additional Leo-T like galaxies which have not yet been discovered. If those galaxies exist, there are observational and theoretical motivations to think they would be at a larger average distance from us, and thus remain unobserved due to selection effects (See Chapter 2).

1.3 Gas in Dwarf Galaxies

While studies of the resolved stellar populations of dwarf galaxies have produced exciting results, it is important not to overlook what the gas - or even the absence of gas - can reveal about the evolutionary history of Local Group dwarfs. According to hierarchical formation scenarios and cosmological simulations, the lower mass halos ($< 10^8 M_\odot$) and the galaxies they host formed before more massive galaxies. It has been suggested that some or most

dwarf spheroidal (dSph) galaxies formed stars prior to reionization, and are devoid of gas due to photoionization during the epoch of reionization (Efstathiou 1992; Gnedin 2000; Bullock et al. 2001; Ricotti & Gnedin 2005; Gnedin & Kravtsov 2006; Bovill & Ricotti 2009; Madau et al. 2008; Muñoz et al. 2009). This would also have the effect of reducing the severity of the missing satellites problem by lowering the number of observable satellites associated with the (relatively unchanged) underlying subhalo population. It should also leave a signature in the star formation histories of the dwarfs which has not been observed (Grebel & Gallagher 2004). While the SDSS discovered galaxies lack gas to low limits and have old, metal-poor populations, Leo T has gas and evidence of recent star formation, which is difficult to explain if reionization was the means of gas loss for all dSph galaxies. Also, it is possible that a greater average distance has discouraged the discovery of a population of gas rich, low mass dwarf galaxies.

Dwarf spheroidal (dSph) galaxies may be evolutionarily connected to dwarf irregular (dIrr) galaxies - dSph galaxies may be dIrr galaxies which have undergone transformative processes which removes their gas and restructures their stars. Suggested mechanisms for such transformation are tidal effects due to interaction with a massive host galaxy, galactic harassment (tidal effects from interactions with other dwarf galaxies), stellar feedback, ram-pressure stripping, and dynamical gas stripping processes. There is a distance dependence of the gas content of Local Group dwarfs, despite the similarity in total masses and other characteristics (see Chapter 2). This suggests that gas removal occurs at least partially via means which are sensitive to the dwarf's environment, specifically, the dwarf's galactocentric distance. Of the gas loss mechanisms discussed earlier, those

that are distance dependent include tidal gas stripping, galactic harassment, interaction with the disk, ram pressure, and dynamical stripping. The relative influence of several of these mechanisms depends strongly on the physical characteristics of the hot halo gas of the Milky Way.

1.4 Galactic Hot Halo

The hot, shocked component of gas which accretes onto the dark matter scaffold of spiral galaxies may have partially remained ionized and diffuse, and have become what we today call the warm-hot intergalactic medium (WHIM). Observations of the cosmic microwave background as well as deuterium abundances combined with big bang nucleosynthesis (BBN) theory suggest a cosmological baryon density of 4.5% (Komatsu et al. 2011; Burles et al. 2001; O’Meara et al. 2006; Pettini et al. 2008). There is strong motivation from theory and simulations for the existence of an extended hot gas halo surrounding not only in galaxy clusters, but also in individual spiral galaxies and galaxy groups (White & Frenk 1991; Sommer-Larsen 2006).

Our current census of present-day baryonic matter is deficient (Shull et al. 2011; Fukugita 2004; Fukugita et al. 1998). It is possible that a significant portion of these “missing baryons” reside in the WHIM, which, because it absorbs and emits primarily in the ultraviolet and X-ray bands and is diffuse, is extremely difficult to detect directly. Several marginal detections of highly ionized gas which might be associated with a galactic corona or local hot intergalactic medium have been observed, suggesting the existence of 10^{-4} to 10^{-5} cm^{-3} , 10^6 K gas (Sembach et al. 2003; McKernan et al. 2004; Wang et al. 2005).

Neutral hydrogen observations can help constrain the hot halo properties. The morphology of high velocity clouds (HVCs) has been used to measure the halo density. In this model, the ambient hot halo exerts a drag on HVCs, which affects their morphological and kinematic structure. Detailed analysis along these lines suggest a halo density of approximately $2 \times 10^{-4} \text{ cm}^{-3}$ at $R \sim 20 \text{ kpc}$ (Peek et al. 2007). Observations of HI in dwarf galaxies can also be used in this manner. By making reasonable assumptions about the dwarf's orbital characteristics and the conditions under which ram-pressure stripping will occur, limits can be placed on the properties of the hot halo gas (see Chapter 3). The conditions under which significant gas loss can be refined, which may lead to improved halo density estimates (see Chapter 4).

1.5 Dark Matter in Dwarf Galaxies

We now know from baryon acoustic oscillations in the cosmic microwave background as measured by the Wilkinson Microwave Anisotropy Probe (WMAP) that 22% of the mass/energy density of the universe is non-baryonic “dark matter” (Jarosik et al. 2011). Analysis of the stellar velocity dispersions of ultra-faint dwarf galaxies suggest they are extremely dark matter dominated, with all of the ultra-faint dwarf galaxies known today having mass to light ratios greater than 100 and several possibly exceeding 1000 (Simon & Geha 2007). The fact that ultra-faint dwarfs are highly dark matter dominated, their close proximity, and possible large numbers means they may be the best candidates as targets for detecting dark matter indirectly, through the high energy photons thought to be produced via self-annihilation in some popular dark matter particle theories (Strigari

et al. 2008; Kuhlen 2010; Wakker et al. 2012).

It should also be noted that even if the underlying assumptions of Λ CDM are incorrect and the solution to these contradictions lies in a theory of modified dynamics, dwarf galaxies are the environments which show the most apparent effect, regardless of the detailed phenomenology.

1.6 Thesis Summary

1.6.1 Chapter 2: Neutral Hydrogen in Known Local Group Dwarfs

We examine the HI content and environment of all of the Local Group dwarf galaxies ($M_{tot} < 10^{10} M_{\odot}$), including the numerous newly discovered satellites of the Milky Way and M31. All of the new dwarfs, with the exception of Leo T, have no detected HI. The majority of dwarf galaxies within ~ 270 kpc of the Milky Way or Andromeda are undetected in HI ($< 10^4 M_{\odot}$ for Milky Way dwarfs), while those further than ~ 270 kpc are predominantly detected with masses $\sim 10^5$ to $10^8 M_{\odot}$. Analytical ram-pressure arguments combined with velocities obtained via proper motion studies allow estimates of the halo density of the Milky Way at several distances. This halo density is constrained to be greater than $2-3 \times 10^{-4} \text{ cm}^{-3}$ out to distances of at least 70 kpc. This is broadly consistent with theoretical models of the diffuse gas in a Milky Way-like halo and is consistent with this component hosting a large fraction of a galaxy's baryons. Accounting for completeness in the dwarf galaxy count, gas-less dwarf galaxies could have provided at most $2.1 \times 10^8 M_{\odot}$ of HI gas to the Milky Way, which suggests that most of our Galaxy's star formation

fuel does not come from accreted small satellites in the current era.

1.6.2 Chapter 3: Local Group Dwarf Galaxy Candidates in the GALFA-HI Survey

Gas rich dwarf galaxies are preferentially observed at larger distances from the Milky Way than gas poor dwarfs. If dwarfs with luminosities less than a few times $10^5 L_{\odot}$ exist at distances of ~ 270 kpc to 1 Mpc, they are likely to have escaped detection. Using HI to search for Local Group dwarf galaxies is a method that provides complementary observational biases to stellar searches. This chapter presents a list of dwarf galaxy candidates selected from a catalog of compact, isolated neutral hydrogen clouds identified in the GALFA-HI survey. Clouds were selected based on how well their observational characteristics matched those of known Local Group dwarf galaxies, and in particular the characteristics of the only known ultra-faint galaxy to contain HI, Leo T. These candidate clouds may represent the HI component of Local Group dwarf galaxies which have not been previously discovered. Three of the HI-selected candidates have optical counterparts, which most likely represent extra-Local Group dwarf galaxies.

1.6.3 Chapter 4: Simulations of Mass Loss in Dwarf Satellite Galaxies

I present a set of six wind-tunnel simulations of a gas-containing, low-mass (Leo-T-like) dwarf galaxies experiencing a constant velocity wind. The wind is modeled after the expected characteristics of the Milky Way's hot halo. The satellite galaxy's gas and the hot halo interact via ram-pressure and dynamical instabilities, leading to gas loss from the

dwarf. These simulations are novel in that they resolve small scale instabilities which can contribute to gas loss, such as the effects of the Kelvin Helmholtz instability. The results of these simulations support the hypothesis that rapid gas loss occurs when the ram pressure stripping criterion (Gunn & Gott 1972) is met, with complete stripping occurring on a timescale of about half a Gyr for galaxies with Leo-T like characteristics. This stripping would occur in less than an orbital period as these dwarfs have typical orbital periods of a few Gyrs. For those models where the ram-pressure stripping criterion is not met, mass is lost at a slower but constant rate which does not seem to depend on the residual dwarf's gas mass. Extrapolating the stripping timescales, we expect these dwarfs to be stripped between 1.1 and 3.3 Gyrs. These simulations are a first step towards accurate ram-pressure and dynamical mass loss rates for low mass Local Group galaxies orbiting within a hot halo. They suggest that the lack of low mass galaxies within 250 kpc of the Milky Way can be explained via ram-pressure and dynamical interactions between the satellite galaxy's gas and the hot halo.

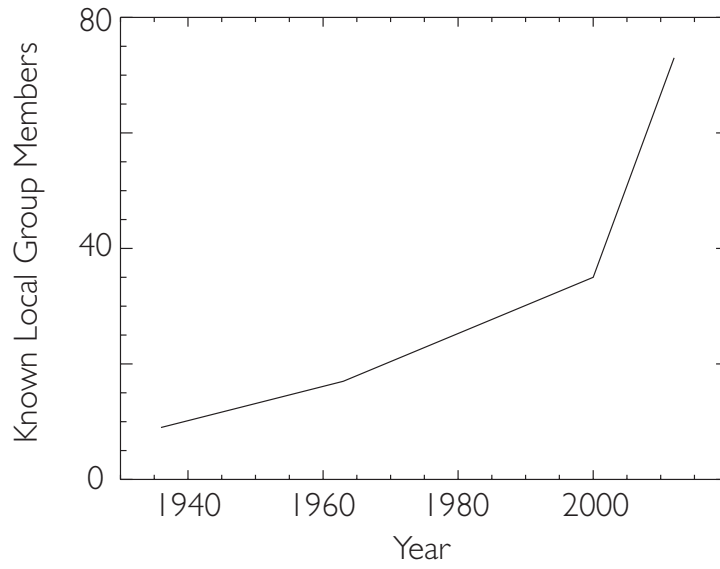


Figure 1.1 Approximate number of Local Group dwarf galaxies known to humanity over time.

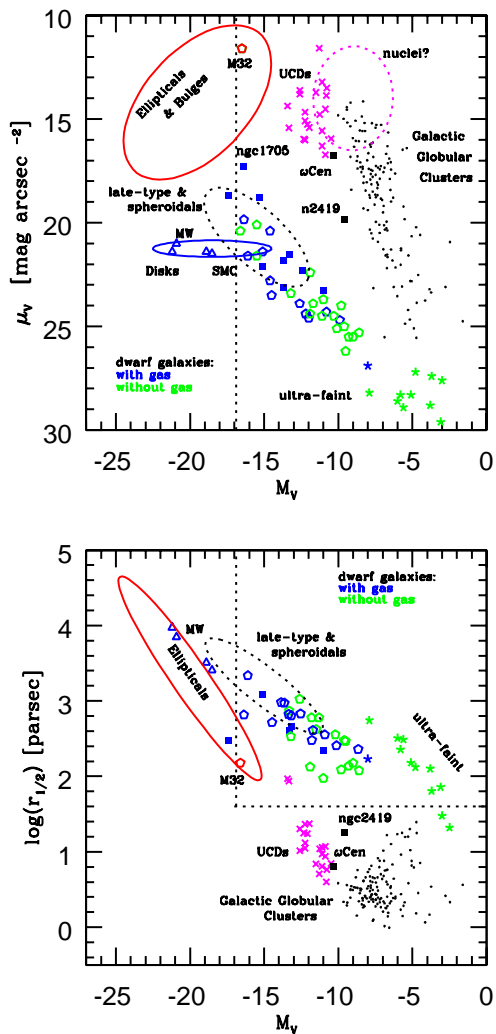


Figure 1.2 The structural properties for different types of galaxies, from Tolstoy 2009 and similar to Kormendy 1985 and Binggeli 1994. Top panel shows absolute magnitude (M_V) vs. central surface brightness, μ_V , bottom panel shows M_V versus half light radius, $r_{0.5}$. Courtesy of Eline Tolstoy.

Chapter 2

Neutral Hydrogen in Known Local Group Dwarfs

2.1 Introduction

The Sloan Digital Sky Survey data (York et al. 2000) have led to the discovery of 13 new satellites of the Milky Way (Belokurov et al. 2006a; Zucker et al. 2006c; Willman et al. 2005a,b; Belokurov et al. 2006b; Irwin et al. 2007; Walsh et al. 2007; Zucker et al. 2006b; Belokurov et al. 2008). Similar objects have been found in the vicinity of M31 (Zucker et al. 2004a; Martin et al. 2006; Zucker et al. 2007; Majewski et al. 2007). These satellites have absolute magnitudes between those of globular clusters and dwarf spheroidal galaxies, with most resembling faint dwarf spheroidals. The discovery of these satellites has implications for the nature of the smallest galaxies in the universe and the building up of larger galaxies. In particular, the newly discovered satellites partially alleviate

the “missing satellites problem”, or the order of magnitude discrepancy between the dark matter haloes predicated by Λ CDM simulations and the number of dwarf galaxies observed in the Local Group (Klypin et al. 1999; Moore et al. 1999; Koposov et al. 2007a). Knowledge of the composition of these satellites is important to determine the mechanisms responsible for the formation and evolution of the smallest galactic building blocks and the fuel they bring to larger galaxies like the Milky Way. In addition, the satellites can be used to probe the extended gaseous halo of the parent galaxy, a galactic component which is difficult to detect directly and may harbor a significant fraction of the galaxy’s baryons (Sommer-Larsen 2006; Maller & Bullock 2004).

This chapter presents a study of the gaseous environments of the dwarf galaxies of the Local Group. These dwarfs are found at a wide range of galactocentric distances with most of the newly discovered dwarfs well within the Milky Way’s dark matter halo (~ 200 kpc). The close proximity of the Milky Way satellites and their range in Galactocentric radii make them an excellent choice to study stripping and gas loss mechanisms. In this chapter we use existing HI observations to put constraints on the neutral gas content of Local Group dwarf galaxies and use this information to examine what dictates their gas content and probe the diffuse Galactic halo. This chapter includes all newly discovered dwarfs through November 2008 as well as the previously known dwarf galaxies listed in Mateo (1998) which have total masses less than $10^{10} M_{\odot}$.¹

¹The SMC and LMC are not included due to their large combined total mass and the complex 3-body interaction of this system.

2.2 Observations

The HI data are from the HI Parkes All-Sky Survey (HIPASS: Barnes et al. 2001) and the Leiden/Argentine/Bonn Survey (LAB: Kalberla et al. 2005). The HIPASS data cover the sky at $\delta < +25^\circ$, and has been reprocessed using the MINMED5 algorithm which increases the sensitivity to resolved structures by using the entire 8° HIPASS scan to calculate the bandpass correction (rather than only using a 2° section of the scan; see Putman et al. 2003 for details). The reprocessed data range from -700 to 1000 km s^{-1} with reference to the LSR. The channel spacing is 13.2 km s^{-1} , and the spectral resolution after Hanning smoothing is 26.4 km s^{-1} . The average single channel rms noise level in the northern data ($\delta = 2^\circ - 25^\circ$) is 14 mK , and the main beam FWHM is $15.5'$ after gridding the data into cubes. The 5σ HI mass detection limit for the reprocessed HIPASS data and using the 26.4 km s^{-1} velocity resolution is $M_{HI} = 2.38 \times 10^{-2} D_{kpc}^2 M_\odot$.

The LAB survey, the Leiden/Argentine/Bonn Galactic HI Survey (Kalberla et al. 2005), covers the entire sky by combining the Leiden/Dwingeloo survey (LDS: Hartmann & Burton 1997) and the Instituto Argentino de Radioastronomía Survey (IAR: Arnal et al. 2000; Bajaja et al. 2005). The data have also been recorrected for stray radiation. The LAB survey spans velocities from -450 to 400 km s^{-1} at a resolution of 1.3 km s^{-1} . The main beam FWHM is $35.7'$, and the rms brightness temperature noise ranges from 70 to 90 mK for a single 1.3 km s^{-1} channel. Assuming a dwarf has a minimum velocity range of 10 km s^{-1} , the 5σ LAB detection limit as a function of distance is $M_{HI} = 6.24 \times 10^{-1} D_{kpc}^2 M_\odot$.

The HIPASS data represent an important improvement in sensitivity and spatial resolution as compared to the LAB data. While we are not the first to use HIPASS data to

study the HI in dwarf galaxies (see Bouchard et al. 2006; hereafter BCS06), the environment of the newly discovered dwarfs have not been previously explored, and we are also able to set deeper limits on several other Local Group dwarf galaxies and collate the results of the entire sample. It is important to note that the HI mass limits obtained with the above are only valid if the size of the dwarf is smaller than the beam width, which is $\sim 36'$ for the LAB data and $15.5'$ for the HIPASS data. This corresponds to a physical size of 305 pc for the nearest dwarf with limits obtained from LAB data (Ursa Major II at 30 kpc) and 2.2 kpc for the furthest dwarf with a LAB limit (Canis Venatici I at 220 kpc). Minimum physical sizes for confident nondetection of the galaxies in the HIPASS region range from 103 pc for Segue I at a distance of 23 kpc to 721 pc for Leo IV at a distance of 160 kpc. In all cases the half light radius of the dwarf is smaller than the beam width.

2.3 Results

2.3.1 Nondetections

2.3.1.1 Newly Discovered Milky Way Satellites

We have examined the HIPASS and LAB data in the vicinity of the newly discovered satellites of the Local Group. In all the optical centers of the new satellites examined, except that of Leo T, there was no detection of an HI cloud along the line of sight. There was no evidence of HI near Leo IV, Leo V, Segue I, Coma Berenices, Boötes II, or Hercules in the HIPASS data, and we confirm non-detection and improve HI mass limits with HIPASS for Boötes I (Bailin & Ford 2007). LAB data show no evidence of HI in Canis Venatici I or

II, Ursa Major I or II, or Willman I. Upper limits for the HI mass in the undetected satellites are determined by the 5σ detection limit and the distance to the satellite, and range from $13 M_{\odot}$ to $3 \times 10^4 M_{\odot}$ (see Table 2.1).

The search for emission was completed within 100 km s^{-1} of the optical velocity of the dwarf. In four cases the optical velocity has not yet been determined and so the entire velocity range of the data was searched. In some channels Galactic emission is present which interferes with the ability to detect emission from the dwarf. This “Galactic Interference Range” is noted in Table 2.1. For three of the dwarf galaxies the optical velocity lies within the Galactic Interference Range. In these cases the diffuse Galactic emission causes a higher noise level, and in order to set accurate mass limits the noise is calculated at the optical velocity. For the four galaxies without optical velocities the limit was set by the noise level beyond the channels with Galactic emission. These limits may need to be adjusted when optical velocities are obtained for these dwarfs. The discrete nature of dwarf galaxy HI emission does generally make a detection rise out of the Galactic emission, as in the case of Leo T (Irwin et al. 2007). None of the new dwarfs show this type of discrete emission in their vicinity.

2.3.1.2 New and Previously Known M31 Satellites

The HI environment of both the previously known and newly discovered M31 satellites were examined. This section describes only those satellites with non-detections that have been clearly defined as M31 satellites. Upper limits for the HI mass were determined with LAB data for Andromeda IX, X, XI, XII, XIII, XIV, XV, XVI, and XVII. We also confirm

HI nondetections for Andromeda I, II, and VII with LAB data and And VI with HIPASS data (Blitz & Robishaw 2000; hereafter BR00). Nondetection of HI towards And III was confirmed by Robishaw et al. (2000), and the velocity measured by Harbeck et al. (2001) of Andromeda V indicates that the detection in BR00 is false.

The HI upper limits for undetected M31 satellites are listed in Table 2.2. We list the 5σ detection limits for the LAB data, except for the case of And VI, in which we use the 5σ HIPASS limit, and for NGC 147 and M32 whose limits come from other sources. Andromeda IV is not included because it is not associated with M31 (Ferguson et al. 2000), and Andromeda VIII is excluded because its existence is in dispute (Merrett et al. 2006). Andromeda XI, XII, and XIII have uncertain distances; for the purpose of calculating an HI mass upper limit they are assumed to be at the distance of M31 (784 kpc, Stanek & Garnavich 1998), but the limits listed in Table 2.2 for these dwarfs are approximate and they are excluded from Figure 2.2.

2.3.1.3 Other Previously Known Local Group Dwarfs

Prior studies have examined the HI environment of the previously known dwarf galaxies. In the case of Cetus, an HI cloud within 1.5° of the optical center was found at a velocity of -280 km s^{-1} (BCS06). Since that time the optical velocity of Cetus has been measured by Lewis et al. (2007) as being -87 km s^{-1} , so the cloud is not associated with the galaxy. A detection of low significance near the position and optical velocity of the Sextans dwarf galaxy was found using data with less sensitivity and resolution than the HIPASS data (BR00), but no cloud was found after inspection of the HIPASS cubes. A cloud reported

near the position of Leo I at a velocity 26 km s^{-1} from the optical velocity of the dwarf (BR00) was also not found upon inspection of the HIPASS data, in agreement with BCS06.

Three clouds were reported near the Carina galaxy by BCS06. Of the three clouds, two are near the optical edge of the galaxy at a distance of about $80'$ (2.3 kpc) from the optical center, and have velocities close to the optical velocity of Carina. There is no HI within the optical radius of the galaxy and the clouds lie outside the tidal radius, so it is unlikely that the gas and the dwarf are physically associated (BCS06).

HI in the general direction of Tucana was first detected by Oosterloo et al. (1996) who claimed it was associated with the Magellanic Stream. BCS06 also detect this cloud at a velocity of about 130 km s^{-1} , and offset from central position of the dwarf by $\sim 18'$. The optical velocity for Tucana has been found by Tolstoy et al. (2004) to be 182 km s^{-1} , so the difference in velocity between the HI cloud and the optical dwarf is 52 km s^{-1} . Figure 2.1 shows the average velocity along the line of sight with the integrated intensity contours overlaid for the vicinity of the Tucana Dwarf. The optical position of the dwarf is marked with a plus sign. Due to its proximity to the Magellanic Stream and the offset velocity of the cloud near the Tucana dwarf, we consider it a non-detection.

To summarize our findings for the non-detections of previously known Local Group dwarfs, we confirm the non-detections or improve HI mass limits with HIPASS for Leo I and Leo II (Knapp et al. 1978), Cetus, Carina, Sextans (BCS06), and the core of the Sagittarius stream (Koribalski et al. 1994) and find that the gas in the vicinity of Tucana is unlikely to be associated. We confirm non-detections in the LAB data for Ursa Minor and Draco (Knapp et al. 1978), and NGC 147 (Young & Lo 1997). The HI limits for previously

known Local Group dwarfs except the Andromeda dwarfs are given in Table 2.3.

2.3.2 Ambiguous Detections

In the case of two of the dwarfs, it is unclear if a cloud is associated with the dwarf galaxy or has a separate origin. We refer to these as ambiguous detections, but note the mass of the cloud at the distance of the galaxy in Table 2.3. One of these is the Sculptor Dwarf, near which two HI clouds were discovered by Carignan et al. (1998). The velocity of the HI ($\sim 105 \text{ km s}^{-1}$) and the optical velocity of the dwarf galaxy (102 km s^{-1}) agree. Despite this, the Sculptor dwarf is in the same direction as the Magellanic Stream and another complex of HI clouds in the general direction of the Sculptor Group (Putman et al. 2003), and numerous clouds near that velocity are found in this region that could be mistaken for gas associated with the Sculptor dwarf (see Figure 2.1). For these reasons, as well as the offset of the clouds from the optical center and the lack of recent star formation in this dwarf, we consider the Sculptor detection ambiguous.

Another ambiguous case is that of the Fornax dwarf. The Fornax dwarf has an optical velocity of 53 km s^{-1} . The cloud in question suffers from contamination from Galactic HI emission in the HIPASS data and is offset $28'$ from the optical center of Fornax. In the analysis by BCS06 the removal of the Milky Way's spectrum was incomplete, and it was unclear if the cloud was part of the Milky Way, a cloud of separate origin, or associated with the Fornax dwarf. We confirm that the origin of the cloud is unclear from the HIPASS data, which is shown in its environment in Figure 2.1.

2.3.3 Confident Detections

Clear detections of HI at the position and velocity of the dwarf have been made for Antlia, Phoenix, Pegasus, DDO 210, WLM, IC 5152, UGCA 438, LGS3, Sextans B, IC1613, Sextans A, GR8, Sagittarius, and SagDIG. We confirm all of these detections in the HIPASS data, although the Phoenix dwarf blends into Galactic emission. The HI masses of these and additional Local Group dwarfs as well as references are listed in Table 2.3.

The HI detection of LGS3 (Hulsbosch & Wakker 1998; BCS06) is unusual in that it has one cloud at the optical position of the dwarf and two clouds offset from the optical center which have diffuse HI connecting them. Only the cloud aligned with the position of LGS3 has a velocity which agrees closely with the optical velocity of LGS3, so only the mass of that cloud is considered.

Leo T is one of the newly discovered SDSS dwarf galaxies and is a particularly interesting object due to its low luminosity, recent history of star formation, and gas content. The HIPASS data show a compact HI cloud in the direction of the Leo T dwarf which was first reported by Irwin et al. (2007), and confirmed by Ryan-Weber et al. (2008) with synthesis data. Leo T has a velocity of about 35 km s^{-1} , and in the HIPASS data a maximum velocity of about 46 km s^{-1} . The lower velocity cutoff and the total width in velocity are uncertain due to Galactic interference. Our reanalysis of the HI cloud as it appears in the HIPASS data reduced to recover extended emission indicates Leo T has a total HI mass of about $4.3 \times 10^5 M_{\odot}$ assuming a distance of 420 kpc.² Ryan-Weber et al.

²The HI mass of Leo T was also checked with new data from the Galactic Arecibo L-band Feed Array (GALFA) HI Survey, which has a velocity resolution of 0.74 km s^{-1} (e.g., Stanimirovic et al. 2006), and found to be $4.8 \times 10^5 M_{\odot}$.

(2008) found a total HI mass of $2.8 \times 10^5 M_{\odot}$ and a peak HI column density of $7 \times 10^{20} \text{ cm}^{-2}$. Our higher total mass may be due to extended emission of Leo T not recovered in the synthesis maps and/or some level of diffuse Galactic emission included in the integrated intensity map.

2.3.4 HI Mass and Galactocentric Radius

Figure 2.2 shows the HI mass or upper limit of each Local Group dwarf vs. the distance to the center of the Milky Way or Andromeda from the dwarf, whichever is closer to the given satellite. Nondetections are associated with upper limits in HI mass, and are marked with downward arrows. Confident detections are marked with diamonds and the two ambiguous detections with plus signs. The apparent lines of upper limits in Figure 2.2 arise due to the distance dependence of the HI mass limits.

As illustrated in Figure 2.2, there is a cutoff in the distance to the Milky Way or Andromeda within the range of 260 to 280 kpc (which corresponds to log values of 2.41 and 2.45) within which galaxies are undetected in HI to low levels, and beyond which the majority of galaxies have significant amounts of HI. A similar type of relationship was noted by other authors (Einasto et al. 1974; Lin & Faber 1983; Blitz & Robishaw 2000; Grebel et al. 2003). There are only two satellite galaxies with significant amounts of HI at galactocentric radii less than 270 kpc, NGC 185 and NGC 205. These galaxies are dwarf ellipticals that have total masses between $10^{8-9} M_{\odot}$, much greater than that of the typical satellites in our sample. The two ambiguous detections, Sculptor and Fornax, are at intermediate Galactocentric distances of 88 and 138 kpc respectively. Of those galaxies

beyond 270 kpc, 19 galaxies are detected confidently at masses greater than $10^5 M_{\odot}$, and two are not detected (Tucana and Cetus). The HI mass of galaxies detected beyond 270 kpc ranges from $4.3 \times 10^5 M_{\odot}$ (Leo T), which is significantly greater than all of our upper limits for Milky Way satellites, to HI masses as high as $1.5 \times 10^8 M_{\odot}$ (IC 10). The mean HI mass of detected galaxies beyond 270 kpc is $2.8 \times 10^7 M_{\odot}$, and the median HI mass is $6.1 \times 10^6 M_{\odot}$.

Figure 2.3 shows HI mass normalized by total mass versus galactocentric distance for those dwarfs with measured dynamical masses. All of the dwarfs with measured total masses within 270 kpc, with the exception of Canis Venatici II and possibly Sculptor, have limits on their gas fractions that are less than any galaxy beyond 270 kpc. We have also plotted the HI mass normalized by V band luminosity (in L_{\odot}) in Figure 2.4. All dwarfs except possibly Fornax within 270 kpc have M_{HI}/L_V limits approximately at or below the values of those beyond 270 kpc. Figures 2.3 and 2.4 indicate that our limits on HI mass are significant even accounting for a simple scaling by total mass or luminosity. The fact that the main outliers in these plots are the two ambiguous detections suggests the HI clouds are less likely to be directly associated with the galaxies.

2.4 Discussion

Including the information for the newly discovered satellites and updating the HI detections of Local Group dwarfs further supports the idea that those dwarfs at small galactocentric radii have less HI than dwarf galaxies at large radii. We find there is a cutoff at approximately 270 kpc, within which most galaxies are undetected at low levels

and beyond which all the galaxies are confident detections with the exception of Cetus and Tucana. The two galaxies with ambiguous detections, Sculptor and Fornax, are at distances of 88 and 138 kpc. These galaxies could be devoid of gas and the detections are the result of chance superpositions, or the nearby clouds may have originated from the dwarf and been offset from the optical center during the process of gas removal. The lack of HI in most satellites within about 270 kpc of the Galactic and M31 center indicates the dominant gas removal mechanism is related to the proximity to the primary galaxy. It is important to note that many of the newly discovered SDSS dwarfs are near the detection limit, and if similar objects existed at greater distances they would not have been discovered (Koposov et al. 2007a). If these dwarfs were deficient in HI, the lower right region of Figure 2.2 as it stands now would be underpopulated. The existence of such galaxies would not affect the conclusion that those satellites within 270 kpc of the Galactic center tend to be HI deficient.

These galaxies are potential source of star formation fuel if their gas is accreted by the Milky Way. If we examine the case of the Milky Way alone, we can estimate the contributed amount of HI gas. First we assume that each of the satellite galaxies within 270 kpc had an average of 10% of their measured dynamical mass in neutral hydrogen, and that the gas of the galaxy was completely integrated into the Milky Way's disk. Galaxies or streams³ with unknown masses are assumed to have the same HI mass as Leo T ($4.3 \times 10^5 M_{\odot}$) on average. In this scenario, the total amount of gas recently accreted by the

³This calculation includes destroyed galaxies seen as streams, including the Monoceros Stream, the Orphan Stream, and the Virgo overdensity (Newberg et al. 2002; Belokurov et al. 2007b; Newberg et al. 2007). The number of streams which have fully integrated into the disk is unknown and their contribution is not included.

Milky Way from known satellite dwarf galaxies would be $\sim 2.1 \times 10^7 M_{\odot}$.

The previous calculation does not account for incompleteness in the total satellite galaxy count due to limited sky coverage and survey detection limits. Tollerud et al. (2008) predicted the total number of Milky Way satellite galaxies within various radii assuming that the Via Lactea N-body simulation (Diemand et al. 2007) is a good representation of the spatial distribution of Milky Way satellites and also by using the SDSS detection efficiencies given in Koposov et al. (2007). They estimate that there are 322 satellite galaxies within 300 kpc of the Milky Way, with a 98% confidence range between 246 and 466 satellites. These galaxies must be relatively faint, or they would have otherwise been discovered, so it is reasonable to say that on average their HI mass may be similar to that of Leo T. Adding in the contribution from the predicted but undiscovered satellite galaxies, the total amount of HI recently contributed to the Milky Way by dwarfs is in the range of $1.2 - 2.1 \times 10^8 M_{\odot}$. Since most chemical evolution models suggest we need an average of $\sim 1 M_{\odot} \text{ yr}^{-1}$ of infalling fuel over the past 5-7 Gyrs in order to explain the metallicity of the long lived G and K stars (Chiappini et al. 2001; Fenner & Gibson 2003), dwarf galaxies alone cannot provide sufficient fuel to the Milky Way in the current era.

2.4.1 Dwarf Gas Loss

Proposed methods by which dwarf satellites have their gas removed include ram pressure stripping, tidal stripping, feedback from supernovae or stellar winds, and the effects of reionization. In the process known as ram pressure stripping, as a satellite moves through the halo medium it experiences a pressure whose strength depends on the satellite's

velocity, total mass, and gas density and the properties of the ambient gas (Gunn & Gott 1972). If the orbit of a dwarf brings it into a region of sufficient density the pressure will be great enough to allow the gas to escape the potential well of the satellite. If ram pressure stripping is taking place, we can estimate the density of the diffuse hot halo gas that a satellite has experienced. The general equation describing the condition necessary for stripping to take place is,

$$n_{halo} \sim \frac{\sigma^2 n_{gas}}{3 v_{sat}^2} \text{ cm}^{-3} \quad (2.1)$$

where n_{halo} is the ambient gas number density, σ is the central stellar velocity dispersion of the dwarf, v_{sat} is the relative motion of the dwarf through the medium, and n_{gas} is the average gas density of the dwarf in the inner regions. It should be noted that this equation assumes that stripping is instantaneous, occurs in a homogeneous medium, and does not trigger star formation which can heat the gas and increase stripping efficiency; some of these factors may play an important role (e.g., Mayer et al. 2006).

Another way to strip a galaxy of its gas is via the effects of massive star evolution. Internal mechanisms such as stellar winds and supernovae may cause gas loss from the shallow potential wells of the dwarfs. Though star formation and the resulting feedback may play a role in heating the gas and making it easier to strip, it is unlikely to result in the distant dependent mass loss shown in Figure 2.2. This is emphasized by Figures 2.3 and 2.4, which show the limits on the gas content of the dwarfs is significant even when scaling by total mass and stellar content. If gas-loss due to stellar feedback was dominant, a relationship between gas content and the quantity of stars and/or the total mass of the galaxy (depth of the potential well) may be apparent. Strigari et. al. (2008) have shown

that both the newly discovered and previously known dwarf spheroidals have similar total mass of $\sim 10^7 M_{\odot}$ interior to 300 pc. Since the gas would not escape more easily from the nearby dwarfs, there is no evidence that stellar feedback is the dominant gas loss mechanism. Though the products of stellar evolution can potentially also contribute HI to galaxies (van Loon et al. 2006; Bouchard et al. 2005), it would not create the distance dependent effect seen in Figures 2.2 - 2.4.

An additional gas loss mechanism is photoionization during the epoch of reionization (Gnedin & Kravtsov 2006; Dijkstra et al. 2004; Madau et al. 2008; Ricotti & Gnedin 2005). The effects of reionization inhibit the ability of the lowest mass halos to accrete gas. It has been proposed that the smallest dwarf galaxies of the Local Group formed their stars before reionization when they were still capable of accreting gas (Gnedin & Kravtsov 2006). The mass scale for the halos that are able to accrete gas from the IGM after reionization is somewhat uncertain (Dijkstra et al. 2004), however the gas-rich, low mass Leo T is difficult to explain unless its dark matter halo extends out to much larger radii than the observed baryons. In the case of reionization it may be possible that galaxies further from the main source of ionization would be more likely to retain gas. If the Milky Way and Andromeda were major sources of ionization at early times and there is a correlation with the current and past galactocentric distances of the dwarfs, then reionization may play a role in the HI-distance trend. Given the amount of time for the Local Group galaxies to evolve since reionization (e.g., Moore et al. 2006), it seems unlikely that reionization could lead to the present day HI-distance effect.

The lack of significant HI in nearby dwarfs is due to a distant dependent mechanism.

The two most widely studied distance dependent gas-loss mechanisms are tidal and ram pressure stripping, with simulations showing that the combination of tides and ram pressure is more effective than either mechanism alone. Ram pressure stripping is the dominant gas loss mechanism in the simulations (Mayer et al. 2006), with tides enhancing the effectiveness of ram pressure stripping by lowering the depth of the satellite's potential well. The limited effect of tidal forces in stripping the gas from the satellites is evident from calculations of tidal radii of the dwarf galaxies and studies of the galaxies stellar components. The tidal radius for a $10^7 M_{\odot}$ dwarf galaxy at a distance of 20 kpc from the center of the Milky Way is on the order of 1 kpc, and increasing the total mass of the satellite galaxy only serves to increase the tidal radius (Battaner & Florido 2000). This is significantly larger than the extent of HI in Leo T and is three times the average stellar extent of the newly discovered dwarf galaxies (Strigari et al. 2008). The stellar component of 18 Local Group dwarf galaxies was examined by Strigari et al. (2008) to search for the current effects of tidal forces on individual dwarfs. They searched for gradients in the line of sight stellar velocities across the face of the galaxies (including Willman I, Coma Berenices, and Ursa Major II, which are all within 44 kpc of the Milky Way) and found no significant detection of streaming motions indicative of tidal disruption. The dominant gas loss mechanism is likely to be ram pressure stripping for the dwarf satellites in the Local Group, as also concluded by BR00, and we address this further below.

2.4.2 Halo Density

Leo T still has a significant amount of HI and does not appear to have been affected by ram pressure stripping or tidal disruption (Ryan-Weber et al. 2008; Strigari et al. 2008). Given the total mass of Leo T and its diffuse stellar component, it is likely similar to the progenitors of the newly discovered dwarfs which do not have HI. The diffuse halo component required to completely strip this type of galaxy can be calculated. We assume a Leo T-like value for σ of 7.5 km s^{-1} (Simon & Geha 2007). We also estimate a range of possible dwarf gas densities; for the low end of the range, we take the mean gas density in the central region of Leo T, $n_{gas} = 0.12 \text{ cm}^{-3}$, and for the high limit we take the central density calculated from fitting a Plummer model to the column density profiles in Ryan-Weber et al. (2008), which yields $n_{gas} = 0.44 \text{ cm}^{-3}$. We approximate the value of v_{sat} as the one dimensional velocity dispersion of 60 km s^{-1} for Local Group dwarfs (van den Bergh 1999). Using these values and assuming the dwarfs are on circular orbits or experiencing their initial infall, we find that the newly discovered, gas-free dwarfs likely experienced a halo density greater than $n_{halo} \sim 0.6\text{-}2.3 \times 10^{-3} \text{ cm}^{-3}$ at the distance limit where the dwarfs have HI, or $\sim 270 \text{ kpc}$. Observations indicate densities on the order of 10^{-3} cm^{-3} are extremely unlikely at this distance (Gaensler et al. 2008; Sembach et al. 2003; Putman et al. 2004; Peek et al. 2007), as do simulations and calculations of the hot halo density profile (Kaufmann et al. 2008, 2007; Sommer-Larsen 2006; Maller & Bullock 2004; Peek et al. 2008). Figure 2.5 shows several of the hot halo density profiles from the simulations drop towards 10^{-5} cm^{-3} at distances greater than 200 kpc.

The most likely solution to the above is that the dwarf orbits have brought them

closer to the center of the parent galaxy than we see them today, and they therefore experienced a much higher halo density than that present in their current environment. In addition, they would have attained a much greater velocity through the halo medium as they approached the galaxy, and because the required density for stripping scales as v^{-2} , they would require lower densities for stripping during this portion of their orbit. It is also possible they have traveled through their parent galaxy's disk before arriving at their current position. Eccentric orbits could cause an overestimate of the typical stripping radius based on Figure 2.2, since the satellites would spend more time at apogalacticon than perigalacticon.

Several dwarfs do have proper motion measurements which give an estimation of their space velocity and orbital characteristics. The velocity at perigalacticon can be calculated by using the current radius and velocity in the galaxy rest frame to find the specific angular momentum of the orbit, $J = vR$. Using angular momentum conservation, the velocity at perigalacticon is $v_{peri} = J/R_{peri}$. We calculated v_{peri} for the dwarfs with proper motions and orbital analyses, Carina (Piatek et al. 2003), Ursa Minor (Piatek et al. 2005), Sculptor (Piatek et al. 2006), and Fornax (Piatek et al. 2002; Walker et al. 2008). We assume typical values for the central stellar velocity dispersion, $\sigma = 10 \text{ km s}^{-1}$ (Mateo 1998), and a central density, $n_{gas} = 0.5 \text{ cm}^{-3}$. For all of the dwarfs with proper motions there is a range of possible orbits and perigalacticons, and thus a range in the densities required for stripping. The 90% confidence range for the distance at perigalacticon from the proper motion references as well as the maximum and minimum density required for stripping within that range is listed for each dwarf in Table 2.4. In the case of Carina, we calculate

a lower limit for the halo density of $8.5 \times 10^{-5} \text{ cm}^{-3}$ at the most likely perigalacticon of 20 kpc. For Ursa Minor, the calculated lower limit for the density of the halo at the most likely perigalacticon of 40 kpc is $2.1 \times 10^{-4} \text{ cm}^{-3}$. Using the Sculptor orbital characteristics we calculate a halo density of $2.7 \times 10^{-4} \text{ cm}^{-3}$ at the most likely perigalacticon of 68 kpc. The case of Fornax is interesting because at 137 kpc, it may be near perigalacticon (Piatek et al. 2002). The most likely perigalacticon for Fornax is 118 kpc and at that distance the required density for stripping is $\sim 3.1 \times 10^{-4} \text{ cm}^{-3}$. We note that these calculations of the halo density do not include tidal effects which may play a small role in contributing to the effectiveness of ram pressure stripping for the closest perigalactica (as previously discussed).

Sculptor and Fornax are the most distant dwarf galaxies in Table 2.3 and are also labeled as ambiguous detections indicating there are clouds in the vicinity of these galaxies which may or may not be associated (see Figures 2.1 and 2.2). Since in both cases the HI clouds are offset from the optical center of the dwarf, even if the gas is associated with the dwarf galaxies it appears to have been partially removed. We also note the discrepant position of Sculptor and Fornax in Figures 2.3 and 2.4, possibly indicating the HI clouds may not be associated. The halo density estimate holds for these two galaxies if the gas has been recently stripped or is not associated with the dwarf.

We can now come back to the newly discovered dwarf galaxies (with a Leo T like progenitor) and give them a velocity at perigalacticon that is closer to that obtained by the above dwarf galaxies to estimate a more likely density required to strip them. We do not know the actual perigalactica of these galaxies, but if they were moving at velocities

between 200 - 400 km s⁻¹ halo densities of $\sim 1.0 - 4.2 \times 10^{-4}$ cm⁻³ would be required to strip them. This is much closer to the expected halo densities at the current distance of many of the newly discovered dwarf galaxies.

2.4.3 Comparison to Halo Models

The densities of the halo derived from the dwarf galaxies with proper motion estimates can be compared to theoretical models of hot gas confined within a Milky Way-sized dark matter halo. Figure 2.5 shows halo density vs. Galactocentric distance with the range in distances and halo densities for the dwarf galaxies taken from Table 2.4. The solid line is the theoretical density profile for gas whose initial distribution traces the central cusp in the NFW halo, while the dotted line represents the density profile which results from an initial gas distribution with a central core of high entropy (Kaufmann et al. 2007, 2008). The cored model is expected for haloes which have experienced pre-heating feedback early in their histories, and implies a more extended distribution for the hot halo gas, as well as an extended cloud population (Rasmussen et al. 2006; Li et al. 2007). The remaining density model plotted on Figure 2.5 is from Sommer-Larsen (2006) and is from high resolution cosmological SPH simulations of a Milky-Way like galaxy in a Λ CDM cosmology. The densities derived from the stripping of the dwarf galaxies are broadly consistent with the theoretical profiles. The exception is the value calculated with Fornax which predicts a halo density that is higher than the models in most cases. If the gas clouds in the vicinity of Fornax are in the process of being stripped, an overestimate could be due to the calculation of the halo density being for the complete stripping of the gas from the dwarf.

It is possible, given a halo model and a typical range of dwarf galaxy characteristics, to calculate the velocity required to strip a satellite galaxy at a given radius. This is plotted in Figure 2.6 for the three halo density models previously discussed and using a range in dwarf galaxy velocity dispersions ($\sigma = 5 - 12 \text{ km s}^{-1}$) and central densities ($n_{\text{gas}} = 0.1 - 0.8 \text{ cm}^{-3}$). As additional proper motions are determined this plot can be used to check consistency between the ram pressure stripping scenario and the halo density models. Also, if there is independent evidence that a dwarf is being stripped at its current radius (e.g., head-tail structure; Quilis & Moore 2001), Figure 2.6 could be used to estimate a lower limit on the velocity of the satellite.

2.5 Summary

We conducted an analysis of the HI content of Local Group dwarfs including those extremely low mass dwarfs discovered through November 2008 via SDSS and deep surveys of the M31 environment. We used HIPASS and LAB data to determine the HI mass or upper limits on the SDSS dwarfs and have made several conclusions.

- All of the Milky Way SDSS dwarfs except Leo T are devoid of gas to the level of our detection limits. The upper limits are well under $10^5 M_{\odot}$, which is lower than the HI mass of any known dwarf galaxy with an HI detection. The newly discovered Andromeda dwarfs also appear to be devoid of gas, but the limits set are higher ($M_{\text{HI}} < 10^{5.5} M_{\odot}$). This result is consistent with the lack of recent star formation in these galaxies.

- Local Group dwarf galaxies at small galactocentric distances (< 270 kpc) tend to not have HI while those at larger galactocentric distances usually do with HI masses above $10^5 M_{\odot}$. The exceptions at < 270 kpc are the two higher total mass dE's and two ambiguous detections (Fornax and Sculptor) at 88 and 138 kpc from the Milky Way for which the clouds detected may or may not be associated with the dwarf galaxies. Thirty five dwarf galaxies are devoid of gas within 270 kpc and 17 galaxies are clearly detected in HI beyond this radius. There is a clear relationship between galactocentric distance and HI content for dwarf galaxies in the Local Group. This relationship is still significant when scaling the HI mass by the total mass or luminosity of the dwarf galaxy.
- By assuming ram pressure stripping is the dominant gas loss mechanism and taking typical characteristics of the dwarf galaxies with gas, we approximate the density of the Galactic halo necessary to strip the Local Group dwarf galaxies. For those dwarfs with proper motions, we calculate the most likely velocity at perigalacticon and determine limits or approximate values of the Galactic halo density at specific distances from the center of the Galaxy. This method estimates the Milky Way's halo density as greater than $\sim 8.5 \times 10^{-5}$, 2.1×10^{-4} , 2.7×10^{-4} , and $3.1 \times 10^{-4} \text{ cm}^{-3}$ at 20, 40, 68, and 118 kpc respectively in order to strip the galaxies. These values are generally consistent with theoretical models of the hot gas within the Milky Way's extended halo. We also calculate the velocities required to strip dwarf galaxies without known proper motions given these theoretical halo gas profiles.
- Assuming that the HI gas was stripped and integrated into the Milky Way's disk, and

that the satellite galaxy progenitors had typical galaxy characteristics, we estimate that accretion of gas from known stripped galaxies and streams would have provided $\sim 1.1 \times 10^7 M_{\odot}$ of HI gas to the Milky Way. If the incompleteness in the satellite galaxy count is corrected, we expect about $\sim 1.2 - 2.1 \times 10^8 M_{\odot}$ of HI mass to be accreted by the Milky Way. This is not enough to sustain the star formation of the Milky Way in the current era.

Table 2.1. HI Mass of Newly Discovered Satellites

Object	Data	α (J2000)	δ (J2000)	Optical Velocity (km s ⁻¹)	Galactic Interference Range (km s ⁻¹)	Distance (kpc)	HI Mass (M _⊙)	Refs
Ursa Major II	LAB	08 ^h 51 ^m 30 ^s	63°07′48″	-117	-70 to 30	30	< 562	a,e
Leo T	HIPASS	09 ^h 34 ^m 53 ^s	17°02′52″	38	-73 to 46	420	~ 4.3 × 10 ⁵	b,e
Segue I	HIPASS	10 ^h 07 ^m 04 ^s	16°04′56″	...	-73 to 46	23	< 13	c
Ursa Major I	LAB	10 ^h 34 ^m 53 ^s	51°55′12″	-55	-70 to 25	100	< 6.24 × 10 ³	d,c,e
Willman I	LAB	10 ^h 49 ^m 22 ^s	51°03′04″	...	-75 to 5	38	< 901	i
Leo V	HIPASS	11 ^h 31 ^m 09 ^s	02°13′12″	173	-72 to 72	180	< 771	j
Leo IV	HIPASS	11 ^h 32 ^m 57 ^s	00°32′00″	132	-60 to 60	160	< 609	c,e
Coma Berenices	HIPASS	12 ^h 26 ^m 59 ^s	23°54′15″	98	-60 to 33	44	< 46	c,e
Canis Venatici II	LAB	12 ^h 57 ^m 10 ^s	34°19′15″	-129	-50 to 25	150	< 1.4 × 10 ⁴	c,e
Canis Venatici I	LAB	13 ^h 28 ^m 04 ^s	33°33′21″	30.9	-20 to 25	220	< 3.0 × 10 ⁴	c,e,f
Boötes II	HIPASS	13 ^h 58 ^m 00 ^s	12°51′00″	...	-33 to 33	60	< 86	h
Boötes I	HIPASS	14 ^h 00 ^m 06 ^s	14°30′00″	...	-33 to 33	60	< 86	g
Hercules	HIPASS	16 ^h 31 ^m 02 ^s	12°47′30″	45	-60 to 60	140	< 466	c,e

Note. — Upper limits for undetected objects are the HIPASS or LAB 5 σ detection limits at the distance of the dwarf. References for the optical data: a: Zucker et al. (2006b), b: Irwin et al. (2007), c: Belokurov et al. (2007c), d: Willman et al. (2005a), e: Simon & Geha (2007), f: Zucker et al. (2006c), g: Belokurov et al. (2006b), h: Walsh et al. (2007), i: Willman et al. (2005a), j: Belokurov et al. (2008)

Table 2.2. HI Mass of Andromeda Satellites

Object	α (J2000)	δ (J2000)	D_{\odot} (kpc)	D_{M31} (kpc)	HI Mass ($10^6 M_{\odot}$)	References
And I	00 ^h 45 ^m 39.8 ^s	+38°02'28''	745	59	< 0.35	a,b,c
And II	01 ^h 16 ^m 29.8 ^s	+33°25'09''	652	185	< 0.27	a,b,c
And III	00 ^h 35 ^m 33.8 ^s	+36°29'52''	749	76	< 0.35	a,b,c
And V	01 ^h 10 ^m 17.1 ^s	+47°37'41''	774	110	< 0.37	b,d
And VI	23 ^h 51 ^m 46.3 ^s	+24°34'57''	783	269	< 0.015	a,b,c,e
And VII	23 ^h 26 ^m 31 ^s	+50°41'31''	763	219	< 0.36	b,d,f
And IX	00 ^h 52 ^m 53 ^s	+43°11'45''	765	42	< 0.37	b,g
And X	01 ^h 06 ^m 33.7 ^s	+44°48'16''	783	112	< 0.38	b,i
And XI	00 ^h 46 ^m 20.0 ^s	+33°48'05''	...	103	< 0.38	j
And XII	00 ^h 47 ^m 27.0 ^s	+34°22'29''	...	95	< 0.38	j
And XIII	00 ^h 51 ^m 51.0 ^s	+33°00'16''	...	116	< 0.38	j
And XIV	00 ^h 51 ^m 35.0 ^s	+29°41'49''	740	167	< 0.34	l
And XV	01 ^h 14 ^m 18.7 ^s	+38°07'03''	630	170	< 0.25	k
And XVI	00 ^h 59 ^m 29.8 ^s	+32°22'36''	525	270	< 0.17	k
And XVII	00 ^h 37 ^m 07.0 ^s	+44°19'20''	794	45	< 0.39	m
M32	00 ^h 42 ^m 42 ^s	+40°51'54''	805	22	< 2.7	a,n
NGC 147	00 ^h 33 ^m 12 ^s	+48°20'12''	725	115	< 0.005	a
NGC 185	00 ^h 38 ^m 58 ^s	+48°20'12''	620	185	0.13	a
NGC 205	00 ^h 40 ^m 22 ^s	+41°41'24''	815	32	0.38	a

Note. — a: Mateo (1998), b: van den Bergh (2006), c: van den Bergh (1972), d: Armandroff et al. (1998), e: Armandroff et al. (1999), f: Karachentsev & Karachentseva (1999), g: Zucker et al. (2004b), h: Morrison et al. (2003), i: Zucker et al. (2007), j: Martin et al. (2006), k: Ibata et al. (2007), l: Majewski et al. (2007), m: Irwin et al. (2008), n: Grebel et al. (2003)

Table 2.3. HI Mass of Additional Local Group Satellite Galaxies

Object	α (J2000)	δ (J2000)	Optical Velocity (km s ⁻¹)	D _⊙ (kpc)	HI Mass (10 ⁶ M _⊙)	References
WLM	00 ^h 01 ^m 58 ^s	-15°27'48"	-78	925	61	a,j
IC 10	00 ^h 20 ^m 25 ^s	+59°17'30"	-344	825	153	a
Cetus	00 ^h 26 ^m 11 ^s	-11°02'40"	-87	755	< 0.014	a,f,h
SMC ^a	00 ^h 52 ^m 44 ^s	-72°49'42"	175	60	402	a,i
Sculptor ^b	01 ^h 00 ^m 09 ^s	-33°42'33"	102	88	(0.234)	a,b,h,v,z
LGS3	01 ^h 03 ^m 55 ^s	+21°53'06"	-287	810	0.16	a,d,h,o,p
IC 1613	01 ^h 04 ^m 54 ^s	+02°08'00"	-237	700	54	a,q,r
Phoenix	01 ^h 51 ^m 06 ^s	-44°26'41"	-13	445	0.17	a,b,l
Fornax ^b	02 ^h 39 ^m 59 ^s	-34°26'57"	53	138	(0.15)	a,h,aa
UGCA 092	04 ^h 32 ^m 01 ^s	+63°36'24"	-99	1300	16	a
LMC ^a	05 ^h 23 ^m 34 ^s	-69°45'24"	324	50	500	a,b,i
Carina	06 ^h 41 ^m 37 ^s	-50°57'58"	224	101	< 0.00021	a,h,bb
Leo A	09 ^h 59 ^m 24 ^s	+30°44'42"	22.3	690	8	a,k
Sextans B	10 ^h 00 ^m 00 ^s	+05°19'42"	300	1345	45	a,m,r
Antlia	10 ^h 04 ^m 04 ^s	-27°19'52"	351	1235	0.72	a,b,e
Leo I	10 ^h 08 ^m 28 ^s	+12°18'23"	286	250	< 0.0015	a,h,bb
Sextans A	10 ^h 11 ^m 06 ^s	-04°42'30"	328	1440	78	a,s,w
Sextans	10 ^h 13 ^m 03 ^s	-01°36'53"	140	86	< 0.00018	a,h
Leo II	11 ^h 13 ^m 29 ^s	+22°09'17"	76	205	< 0.01	a,v
GR8	12 ^h 58 ^m 40 ^s	+14°13'00"	214	1590	4.5	a,p,t,r
Ursa Minor	15 ^h 09 ^m 08 ^s	+67°13'21"	-247	66	< 0.04	a,v
Draco	17 ^h 20 ^m 12.4 ^s	+57°54'55"	-293	82	< 0.00016	a
Sagittarius	18 ^h 55 ^m 03 ^s	-30°28'42"	140	24	< 0.00014	a,u,bb
SagDIG	19 ^h 29 ^m 59 ^s	-17°40'41"	-75	1060	8.8	a,d,p,n
DDO 210	20 ^h 46 ^m 51.8 ^s	-12°50'53"	-141	800	1.9	a,b,p

Table 2.3—Continued

Object	α (J2000)	δ (J2000)	Optical Velocity (km s ⁻¹)	D _⊙ (kpc)	HI Mass (10 ⁶ M _⊙)	References
IC 5152	22 ^h 02 ^m 42 ^s	-51°17'42''	122	1590	67	a,m,x
Tucana	22 ^h 41 ^m 50 ^s	-64°25'10''	182	880	< 0.015	a,b,c,h
UGCA 438	23 ^h 26 ^m 27 ^s	-32°23'18''	62	1320	6.2	a,m,n
PegDIG	23 ^h 28 ^m 36 ^s	+14°44'35''	-183	760	3.4	b,g

Note. — References: a: Mateo (1998) and references therein, b: Grebel et al. (2003) and references therein, c: Tolstoy et al. (2004), d: Young & Lo (1997), e: Tolstoy & Irwin (2000), f: Lewis et al. (2007), g: Huchra et al. (1999), h: Bouchard et al. (2006), i: Brüns et al. (2005), j: Humason et al. (1956), k: Brown et al. (2007), l: Irwin & Tolstoy (2002), m: Huchtmeier & Richter (1986), n: Longmore et al. (1982), o: Thuan & Martin (1979), p: Lo et al. (1993), q: Lake & Skillman (1989), r: Hoffman et al. (1996), s: Huchtmeier & Richter (1988), t: Carignan et al. (1990), u: Koribalski et al. (1994), v: Knapp et al. (1978), w: Skillman et al. (1988), x: Blitz & Robishaw (2000), y: Oosterloo et al. (1996), z: Carignan et al. (1998), aa: Bouchard et al. (2006), bb: This chapter.

^aThe LMC and SMC are included here for reference, but are not included in the figures.

^bThe HI mass given is that of the nearby HI cloud which may or may not be associated with the galaxy.

Table 2.4. Orbital Characteristics and Hot Halo Densities

Satellite	Most Likely Perigalacticon (kpc)	Range in Perigalacticons (kpc)	n_{peri} ($\times 10^{-4} \text{ cm}^{-3}$)	Range in n_{peri} ($\times 10^{-4} \text{ cm}^{-3}$)	V_{peri} (km s^{-1})
Carina	20	3-63	0.85	0.55 - 3.9	443
Ursa Minor	40	10-76	2.1	0.13 - 7.2	283
Sculptor	68	31-83	2.7	0.51 - 3.9	251
Fornax	118	66-144	3.1	0.98 - 4.6	231

Note. — The range in perigalacticons are the 90% confidence level for the orbits listed in the references in the text and the range in densities correspond to that range of perigalacticons. n_{peri} and V_{peri} are the density and velocity at the most likely perigalacticon.

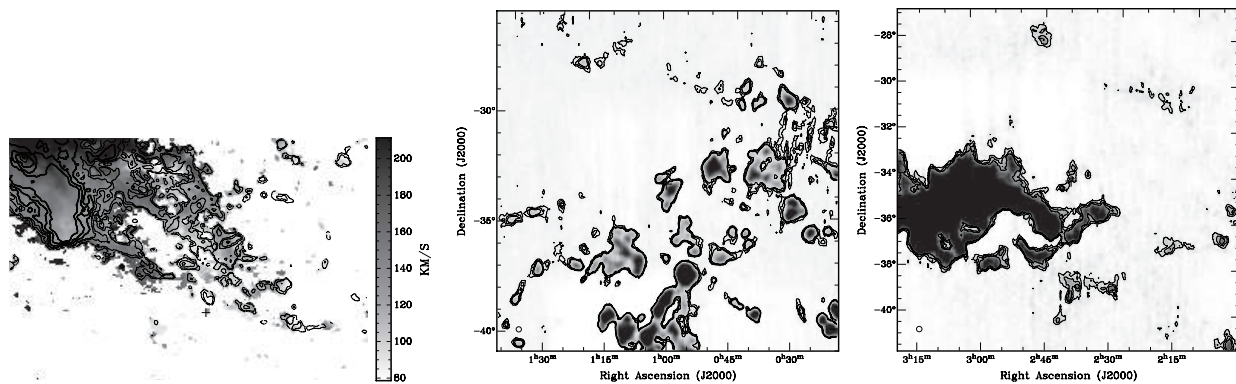


Figure 2.1 The average velocity along the line of sight with the integrated intensity contours overlaid for the region of Tucana (left), and integrated intensity maps for the regions of the Sculptor (middle) and Fornax (right) dwarfs. The optical positions of the dwarfs are marked with a plus sign. The contours for the Tucana region are at $0.911, 1.82, 5.47, 9.11, 18.2, 36.5,$ and $72.9 \times 10^{19} \text{ cm}^{-2}$. The contours are $0.50, 0.84,$ and $1.2 \times 10^{19} \text{ cm}^{-2}$ for Fornax and $0.81, 1.3,$ and $1.9 \times 10^{19} \text{ cm}^{-2}$ for Sculptor. The velocities included in the integrated intensity maps are 20 to 46 km s^{-1} for Fornax and 46 to 152 km s^{-1} for Sculptor, while the optical velocities are 53 and 102 km s^{-1} , respectively.

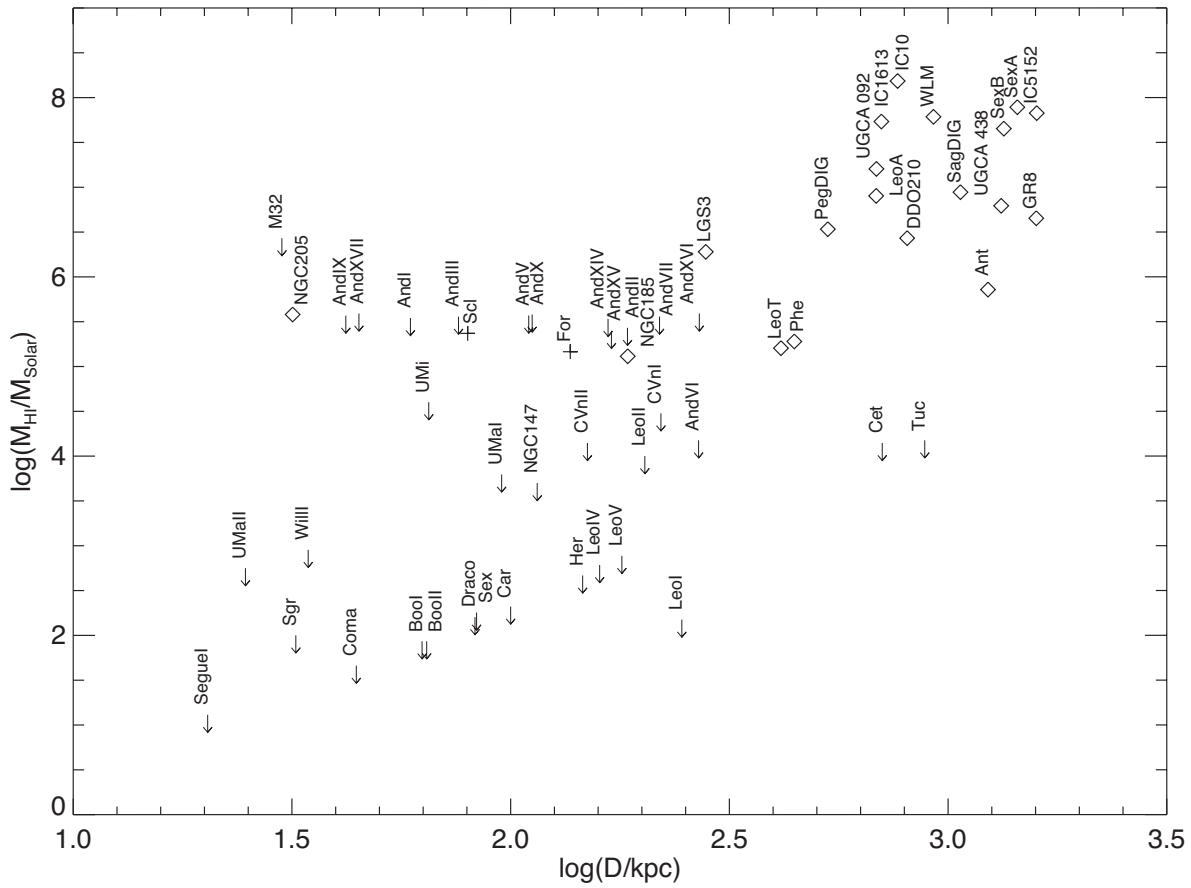


Figure 2.2 HI mass vs. distance to the center of the Milky Way or Andromeda, whichever is closer, for the dwarf galaxies of the Local Group. Downward arrows indicate upper limits, plus signs are ambiguous detections, diamonds indicate confident detections.

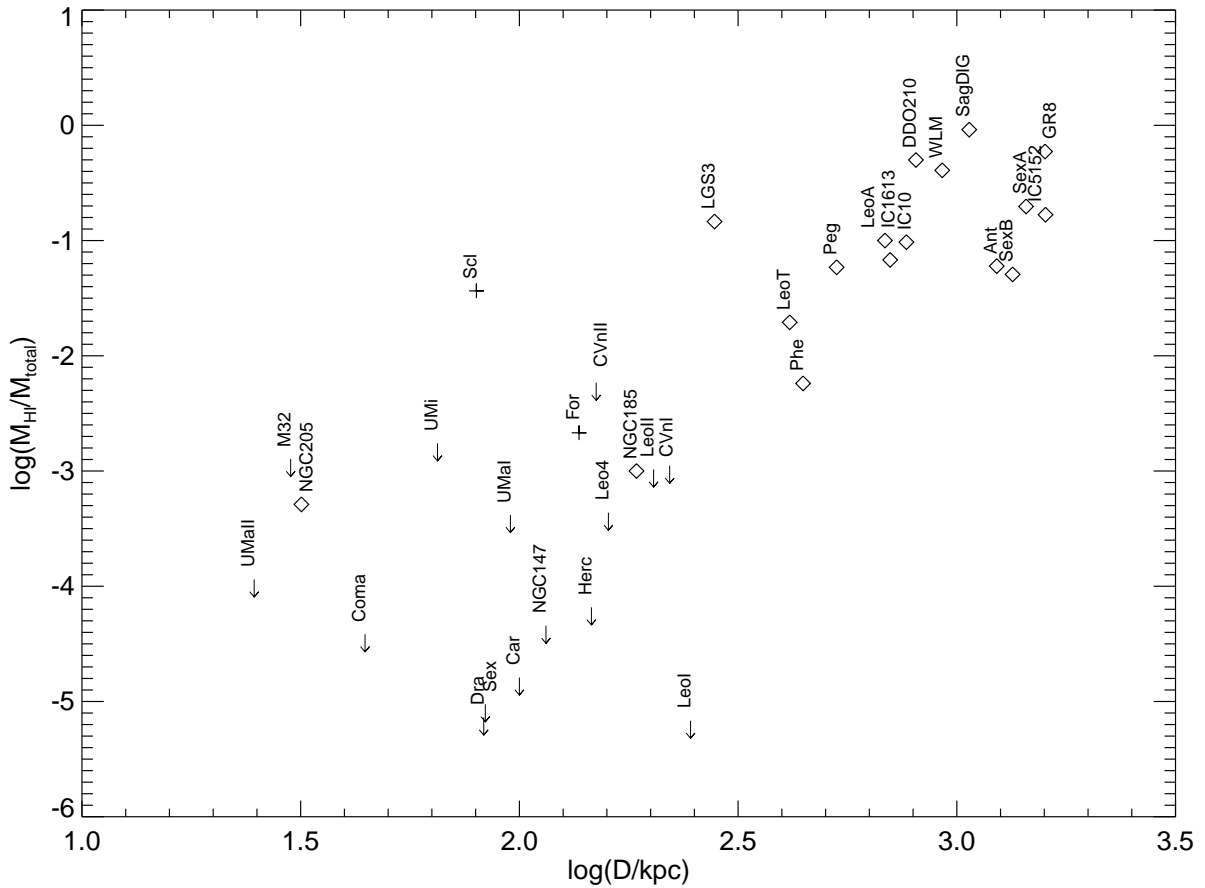


Figure 2.3 HI mass divided by total mass of dwarf galaxies in the Local Group vs. distance to the center of the Milky Way or Andromeda, whichever is closer, for those dwarf galaxies in Figure 1.2 with previously calculated total masses. Symbols are the same as Figure 1.2 with downward arrows indicating upper limits, plus signs as ambiguous detections, and diamonds as confident detections. Total masses are from Mateo (1998) except Canes Venatici I, Canes Venatici II, Coma Berenices, Hercules, Leo IV, Leo T, Ursa Major I, and Ursa Major II (Simon & Geha 2007), and Leo A (Brown et al. 2007).

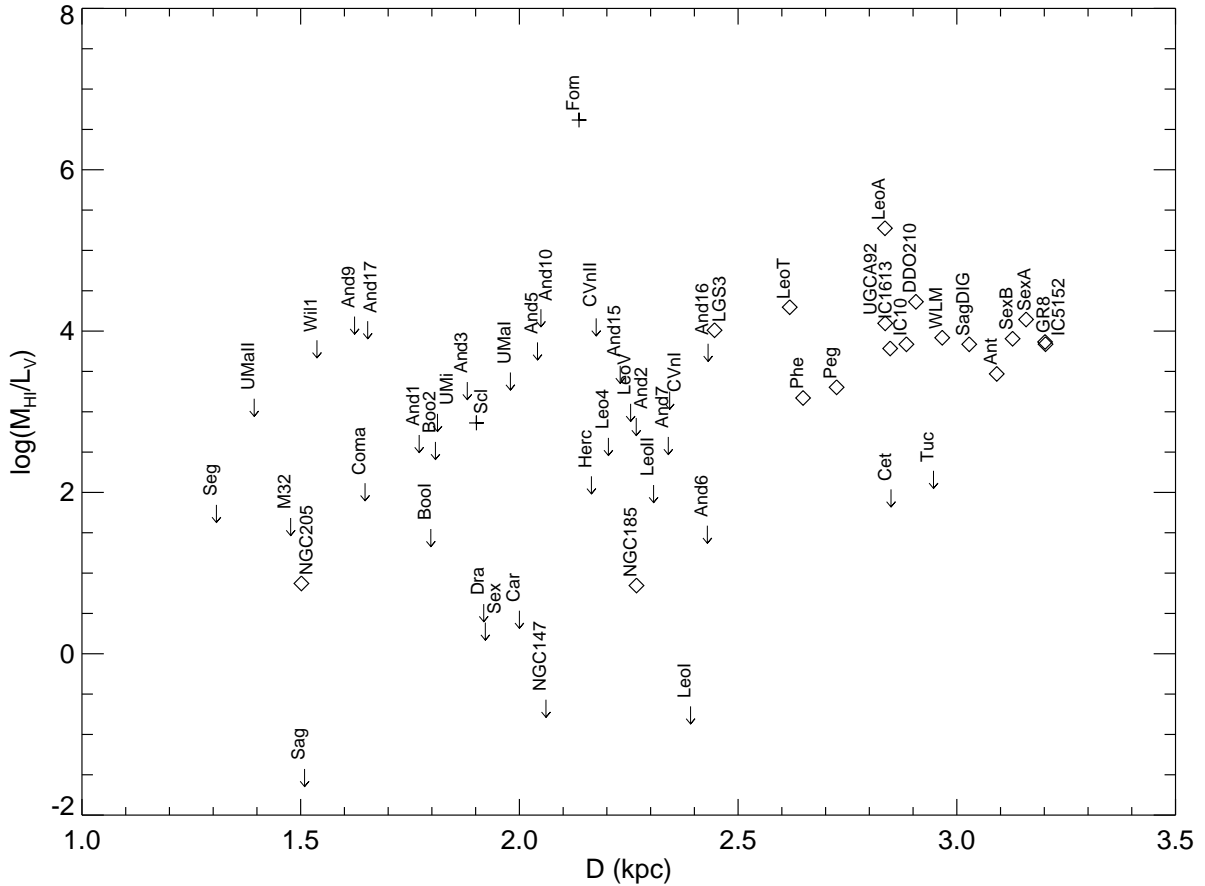


Figure 2.4 HI mass divided by V-band luminosity in solar units of Local Group dwarfs versus distance to center of the Milky Way or Andromeda, whichever is closer. Symbols are the same as Figure 2.2 with downward arrows indicating upper limits, plus signs as ambiguous detections, and diamonds indicating confident detections. V-band luminosities are from Mateo (1998) except Boötes I (Belokurov et al. 2006b), Boötes II (Walsh et al. 2007), Willman I (Willman et al. 2005a), Canes Venatici I, Canes Venatici II, Coma Berenices, Hercules, Leo IV, Leo T, Ursa Major I, and Ursa Major II (Simon & Geha 2007), Cetus (Whiting et al. 1999), Leo V (Belokurov et al. 2008), Andromeda V through X (van den Bergh 2006), Andromeda XI through XIII (Martin et al. 2006), and Andromeda XIV-XV (Ibata et al. 2007).

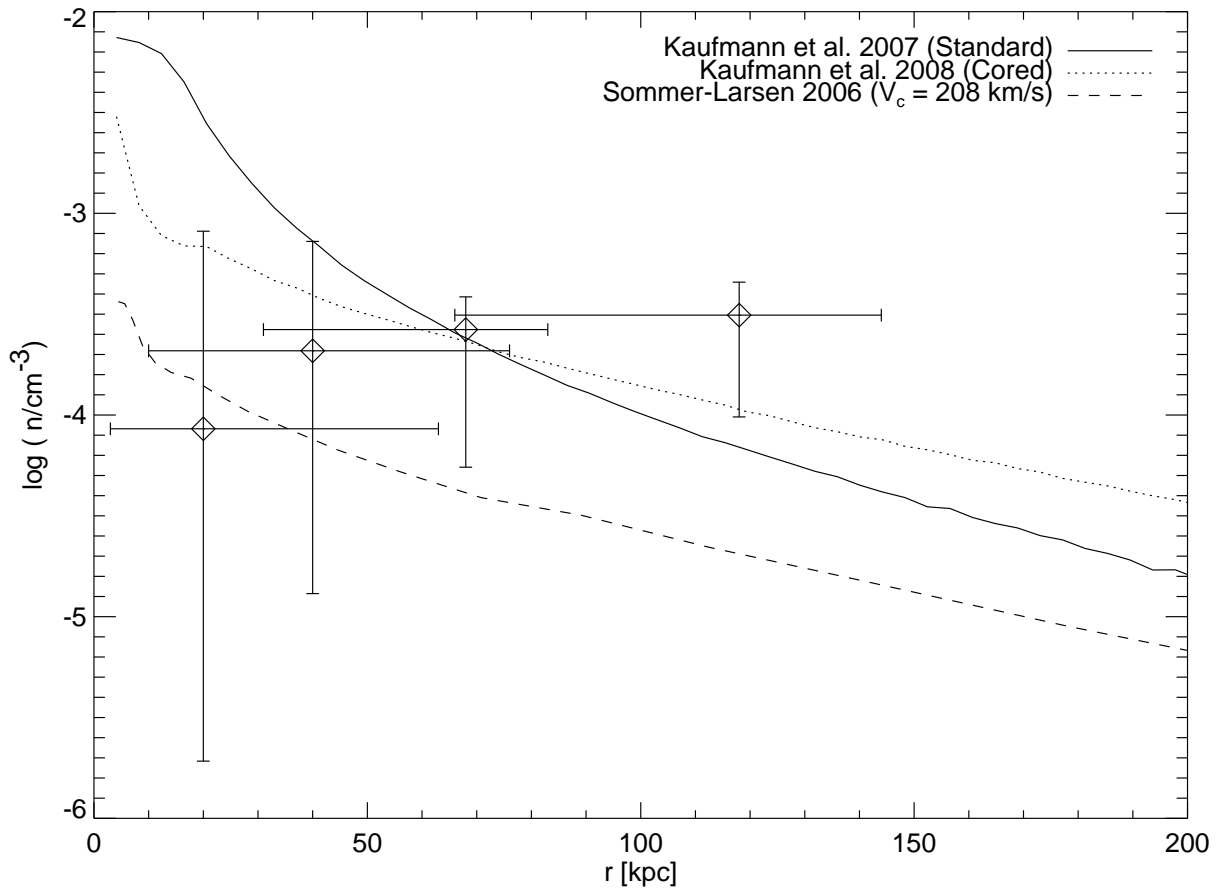


Figure 2.5 The diamonds represent estimates for the halo density as a function of Galactocentric distance calculated from the orbital characteristics of Carina, Ursa Minor, Sculptor, and Fornax (from left to right). The lines represent the model halo density profiles with the references given in the legend of the plot.

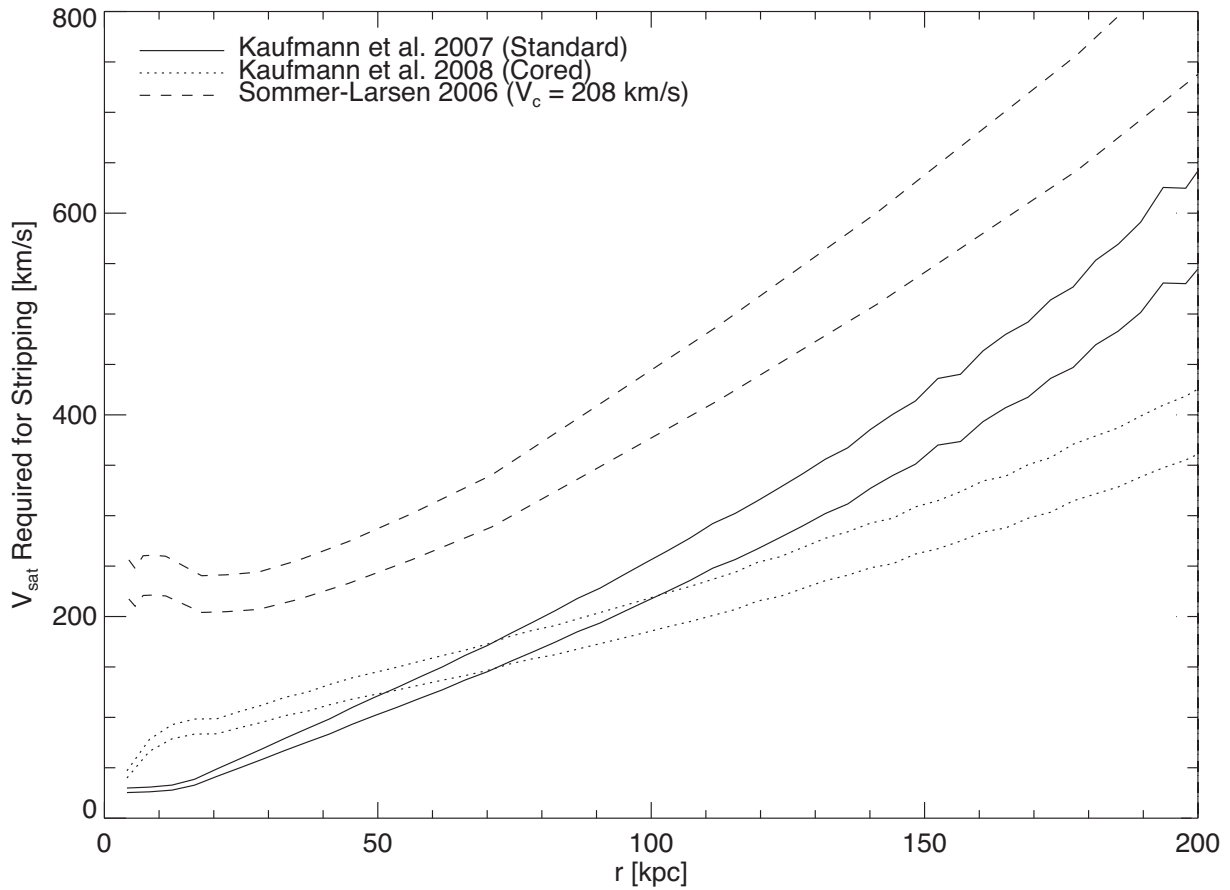


Figure 2.6 A plot of the satellite velocities required for ram-pressure stripping of a satellite galaxy using the density profiles of the Milky Way's hot halo gas shown in Figure 1.5. The two lines represent the range of typical satellite galaxy characteristics: $n_{\text{gas}} \sim 0.1 - 0.8 \text{ cm}^{-3}$, $\sigma \sim 5 - 10 \text{ km s}^{-1}$.

Chapter 3

Local Group Dwarf Galaxy Candidates in the GALFA-HI Survey

3.1 Introduction

A complete census of ultra-faint Local Group galaxies would allow better comparisons with Λ CDM simulations and theories of galactic evolution. It would be particularly helpful for determining what factors influence the baryon content and star formation history of low mass dark matter halos. Thirty dwarf galaxies, approximately half of the galaxies now known to make up the Local Group, have been discovered since 2004. Identified primarily through over-densities of red giant branch stars, these galaxies were previously hidden to observers and were discovered via analysis of deeper photometric surveys such as the Sloan Digital Sky Survey and the Pan-Andromeda Archeological

Survey (SDSS and PAndAS respectively; Abazajian et al. 2009; Martin et al. 2009). Recent dwarf discovery programs have been extremely successful, but they have limited sky coverage and the methods employed are largely insensitive to galaxies with characteristics similar to Leo T (the only ultra-faint known to have HI) which are located in the outskirts of the Local Group (Walsh et al. 2009). Since we generally expect HI rich dwarfs to be located more than 270 kpc from the Milky Way, searching for dwarfs first via their HI and then undertaking targeted optical observations is complementary to optical searches (Grcevich & Putman 2009).

An alternative to stellar dwarf searches is to first look for compact HI clouds which resemble the HI component of known dwarfs and then obtain deep optical observations which can easily reveal an associated stellar population. An important advantage of this method is that it is not subject to the same set of selection biases; targeted optical observations allow the discovery of less optically luminous, less concentrated, and more distant HI-containing dwarf galaxies. Dwarf galaxies outside the Local Group have been discovered first via their HI (e.g. Irwin et al. 2009; Santiago-Figueroa et al. 2011), but so far no Local Group dwarf galaxy candidates identified first via their HI have been confirmed (Giovanelli et al. 2010; Cannon et al. 2011).

Leo T is the only ultra-faint dwarf galaxy known to contain HI (Ryan-Weber et al. 2008; Grcevich & Putman 2009) and is also the furthest ultra-faint from its nearest massive neighbor galaxy. The fact that Leo T is the only ultra-faint dwarf to contain HI might be explained by its greater Galactocentric distance (Grcevich & Putman 2009). The greater distance also means that it is on the edge of current detectability, and if there are galaxies

with characteristics similar to Leo T at greater distances we are unlikely to detect them in existing large area photometric surveys. Though at the edge of detection in optical surveys, Leo T is easily detectable in some existing HI surveys. Leo T has $2.8 \times 10^5 M_{\odot}$ of HI, an HI radius of 300 pc, and a velocity dispersion of 6.9 km s^{-1} , making it clearly identifiable as a unique object in high sensitivity, high resolution HI surveys like the GALFA-HI Survey (Galactic Arecibo L-band Feed Array; Peek et al. 2001).

Recently data from the GALFA-HI survey were searched algorithmically for compact HI clouds, yielding a catalog of 1964 discrete clouds $< 20'$ in size (Saul et al. 2011). With the goal of discovering unknown Local Group dwarf galaxies, the collection of dwarf galaxy candidates have been selected out of this catalog. This chapter first discusses the GALFA-HI survey and compact cloud catalog, and then the selection criteria for candidates. The characteristics of candidates are then presented in the context of known Local Group dwarf galaxies. The possibility of stellar counterparts is explored with SDSS data where available. Finally, the probability the candidates represent Local Group dwarfs is discussed, and future work in this area is suggested.

3.2 The GALFA-HI Survey and Compact Cloud Catalog

The GALFA-HI survey is particularly suited to identifying dwarf-like clouds because of the high spatial ($4'$) and velocity (0.184 km s^{-1}) resolution. Four arcminutes ($4'$) corresponds to 291 pc at 250 kpc and 1.2 kpc at 1 Mpc, and low mass dwarf galaxies may have velocity widths $< 10 \text{ km s}^{-1}$. The sensitivity varies somewhat over the GALFA-HI coverage region and is typically between 50-120 mK in 0.74 km s^{-1} channels (see Saul et al. 2012 and Peek et

al. 2011 for more details). The GALFA-HI survey is sensitive to gas at velocities between -650 and 650 km s^{-1} (local standard of rest or lsr velocity) the GALFA-HI Data Release 1 (DR1) used here covers 7540 deg^2 of sky between declinations of -1° to 38° . GALFA-HI DR1 has over a 85% overlap with the SDSS DR-9 region, or about 1100 deg^2 of overlap. It is still worthwhile to look for undiscovered dwarfs in the overlap region as we expect to be sensitive to dwarfs which are more distant than those able to be detected in SDSS.

Candidate clouds are selected out of the GALFA-HI compact cloud catalog (Saul et al. 2012). Cataloging is largely automated and involves five main steps: 1. Galactic subtraction, 2. Convolution, 3. Region Detection, 4. Merging and Selection, 5. Visual Inspection, and 6. Removal of known Galaxies.

Galactic emission is removed by applying a 1 deg^2 median filter to each position for each channel, and subtracting the smoothed image from the data. The Galactic subtracted data cube is then convolved with four 3D kernels, yielding four convolved cubes. The kernels used for the convolution are the sum of a positive and a negative Gaussian component, with the negative component 1.2 times the full width at half maximum (FWHM) of the positive component (e.g. in the shape of the traditional Mexican Sombrero). The positive component of each of the four kernels have a different combination of spatial FWHM (5 or 15') and velocity FWHM (7 or 18 km s^{-1}). After convolution is applied a simple watertable technique is used to determine regions of interest. Starting with the highest unclassified peak in each convolved cube, any position where the convolved cube value exceeds 4σ is selected and grown to include all surrounding voxels (volumetric pixels) which exceeded the 4σ threshold. Regions larger than 34' or 36' (in the 5' and 15' kernels

respectively) are considered extended and rejected. For those regions of interest which are identified in more than one kernel, the one which has a higher response is selected because this indicates that it better matches the 3D cloud profile. Following the merging process, three individuals visually inspect each cloud by eye and the majority to agree that it is a compact cloud and not either an extended structure nor a data artifact. Clouds with a NASA extragalactic database (NED) identified galaxy within $10'$ which also have a velocity within 50 km/s are excluded from the catalog as they are likely to represent known galaxies. The clouds in the final catalog have a range of measured properties; e.g., $T_B = 0.2\text{-}1.8$ K, $N_{HI} = 1 - 70 \times 10^{19}$ cm $^{-2}$, and $\delta v = 2.5 - 70$ km s $^{-1}$. For more detail on the cataloging algorithm and to access the catalog, see Saul et. al. (2012).

3.3 Dwarf Candidate Selection

Dwarf galaxy candidates are selected because their observational characteristics are similar to those of Local Group dwarfs or because they are kinematic outliers compared to the general GALFA-HI catalog. As discussed in detail below, the candidates are referred to as group 1 candidates if they have peak column densities or brightness temperatures that are representative of Local Group dwarf galaxies, and group 2 candidates if they are clear velocity outliers in the catalog. No additional cutoff based on velocity width was applied to either group in order to remain sensitive to the range of dark matter halo masses possible for dwarf galaxies.

- **Group 1 Candidates** We found one of the best observed parameters that differentiates known Local Group dwarf galaxies from the general cloud population is the peak column density. Classical Local Group dwarfs typically have peak column densities greater than 10^{20} cm^{-2} in the central ALFA beam, and Leo T has a peak column density on the order of 10^{20} cm^{-2} in the GALFA-HI data. Since we are looking for dwarfs which likely are extremely low mass and low luminosity we wish to be sensitive to dwarfs which have slightly lower peak column densities than that of classical dwarfs, as well as those which may have a slightly reduced observed column density due to beam dilution. We select clouds from the GALFA-HI catalog that have peak column densities greater than $5 \times 10^{19} \text{ cm}^{-2}$, which represents the top 7% of the column density distribution of the general cloud population.

We also wish to include those clouds that have a small δv and are on the high end of the range of brightness temperatures. These clouds are promising candidates in that they may represent lower mass halos that despite being strongly concentrated, may be too distant or have too small a velocity spread to have a column greater than $5 \times 10^{19} \text{ cm}^{-2}$. Group 1 therefore also includes those clouds with peak brightness temperatures greater than 1.5 K, or the top 3% of cataloged clouds in terms of peak brightness.

Finally, we remove from this list clouds that lie close in position-velocity space to known HVCs using the criteria explained in Peek et al. (2007). These candidates are more likely to be small clouds associated with larger cloud complexes rather than isolated dwarf galaxies. Each candidate was inspected by eye and any candidates

that showed a hint of extension in the direction of Galactic emission or Galactic contamination were removed. The end result is a sample of 21 group 1 candidates that are listed in Table 3.1 and Table 3.2. Integrated brightness temperature maps along with the velocity profiles of each of the group 1 candidates are presented in Figures 3.1, 3.2.

- **Group 2 Candidates** HI containing Local Group dwarfs may exist whose size and distance lead them to be overlooked when only searching by peak column density or brightness temperature. A possible way to distinguish these from the general cloud population is to look for clouds whose velocities differ significantly from those of their neighbors. Each catalog member's v_{lsr} was compared to those of nearby catalog members, and those clouds that have a v_{lsr} outside the 3σ variation of the clouds lying within a 0.5 deg radius are considered velocity outliers. We also adopted the clouds that have velocities significantly beyond any of the catalogued clouds in the group 2 velocity outlier candidates (generally $> 150 \text{ km s}^{-1}$; see Saul et al. 2012). Finally, we examined each of these candidates individually as we did with the group 1 candidates and ended with a sample of 30 group 2 candidates. The properties of the group 2 candidates are noted in Table 3.3 and Table 3.4. Integrated brightness temperature maps of the group 2 candidates, along with velocity profiles are shown in 3.3, 3.4

3.4 Results

3.4.1 Spatial and Kinematic Characteristics

In order to determine the possible origin of the clouds, we analyzed the spatial, kinematic, environmental characteristics of the dwarf candidates listed in Table 3.1 and Table 3.3. Figure 3.5 shows the Galactic latitude and longitude, and v_{lsr} for all GALFA-HI cataloged compact clouds, known Local Group dwarfs, and group 1 and 2 candidate clouds. The solid line shows the limits of the Arecibo sky and thus the outer bounds of the GALFA-HI Survey; see Saul et al. (2012) for the precise areas observed in GALFA-HI DR1. Eight classical Local Group dwarfs (discovered before 2004 and generally $> 2.3 \times 10^5 L_{\odot}$) and 9 ultra-faint Local Group dwarfs lie in the GALFA-HI survey coverage. The dwarf candidates are relatively evenly distributed in position and in velocity, with the clear exception of one position-velocity cluster. Ten of the candidates are tightly clustered near $(l,b) = (78^{\circ}, -25^{\circ})$, and the majority of these have similar velocities to an intermediate velocity cloud (IVC) complex in that area (Wakker & van Woerden 1997). This suggests that these clustered candidates are associated with Galactic processes rather than representing unknown dwarfs, although the origin of IVCs is unknown. We will hereafter refer to this subgroup of candidates as the candidate cluster (CC). This type of association does not happen between candidates and HVCs because we have already excluded candidates close to HVCs in position-velocity space with HVC catalogs (see § 3.3). IVC catalogs do not exist as they are more complex structures that merge into Galactic emission. Visual inspection of the IVC sky did not reveal any other obvious correlations with our candidates.

The group 1 candidates were selected primarily by their column density or brightness temperature and if they represent dwarf galaxies we would expect them to be kinematically distinct from the general cloud population and potentially more likely to be orbiting the Local Group barycenter. The group 2 candidates were selected to be velocity outliers. The velocities of the great majority of candidates are consistent with the velocities of known Local Group dwarfs, whose radio velocities range from -342 (IC 10) to 404 km s^{-1} (NGC 3109) (Mateo 1998).

In order to determine if the velocities of the group 1 candidates are distinct, we performed a two sample Kuiper's test (also known as an invariant Kolmogorov-Smirnov test, or KS test) on the velocities of the candidates and general cloud population in three different reference frames, v_{lsr} (local standard of rest), v_{gsr} (Galactic standard of rest), and v_{lgsr} (Local Group standard of rest). We can strongly reject that the group 1 candidate population is drawn from the same velocity distribution as the general cloud population in v_{lsr} (98.6% confidence); however, we cannot reject that they may have the same underlying v_{gsr} or v_{lgsr} distribution. Due to the variance introduced in conversion to v_{lgsr} and v_{gsr} , the KS tests for those quantities are less informative. The test was repeated excluding the ten CC clouds as they are unlikely to be unassociated with one another. The candidate velocity distribution is more disparate from that of the general cloud population when we exclude the ten CC clouds, and we can reject that the candidate population is drawn from the same v_{lsr} (99.99% confidence) and v_{gsr} (93.8% confidence) distribution.

A common method used to constrain the probability of Local Group membership is to examine the cosine of the angle between a given dwarf's position and the apex of

solar motion versus the radial velocity. This is shown in Figure 3.6. Dwarf galaxies of the Local Group preferentially lie near the line representing the opposite of the component of the solar motion. The dispersion around the best fit line for known Local Group dwarfs, calculated from the radial velocities of the population of classical dwarf galaxies, is 61 km s^{-1} . The dotted line in Figure 3.6 represents 1σ , while the dot dashed line represents 3σ . Dwarf galaxies strongly affected by tidal interactions, for example the Sagittarius dwarf galaxy, vary from this relation. A dwarf candidate lying outside the 1σ line does not definitively indicate that it is not a Local Group dwarf, but it does make it less likely. Ten of the dwarf candidates lie within or very close to 1σ lines and as can be seen in the last columns of Table 3.2 and Table 3.4.

The members of the CC cluster are clearly outside the 3σ line to the extreme right in Figure 3.6. There are many group 2 candidates at high positive velocity that lie well outside 3σ of the Local Group best fit line. These are much more likely to represent previously undiscovered galaxies which lie outside the Local Group.

3.4.2 Comparison to Leo T

In Figure 3.7 the spatial intensity profiles of the candidates are compared to that of Leo T. The spatial profiles are averaged over two orthogonal axes of the candidates. In the top panel of Figure 3.7 the profiles are not scaled, however for the lower panel they are normalized by $T_{B,max}$ to allow a comparison of the profile shapes. The FWHM values of the group 1 candidates are comparable to Leo T, with over 80% of the sample with $4 - 15 \text{ km s}^{-1}$. The group 2 candidates have a wider FWHM range ($4 - 150 \text{ km s}^{-1}$). Both the

candidates and Leo T show primarily gaussian velocity profiles.

Table 3.5 shows the values for key observational parameters for Leo T and the mean and range of values for the group 1 and group 2 candidates. The observational traits of the candidates span the range of traits of Leo T, and a few candidates match along many dimensions. With these interesting exceptions, most of the candidates have central column densities an order of magnitude lower than Leo T. However, the physical column density may be higher if the candidate is distant or small enough to suffer from beam dilution. Leo T is found at low v_{lsr} , while the candidates have a wide range of velocities. This is especially true of the group 2 candidates, since many are velocity outliers. We expect there to be a wide range of expected velocities for Local Group dwarfs, as seen in 3.4.1.

Two candidates, 11 and 33, have column densities which exceed that of Leo T. Candidate 11 exceeds Leo T in column density, peak brightness temperature, and FWHM. It is one of the CC members. Candidate 33 was selected due to its high v_{lsr} of 423.9 km s^{-1} . It is unresolved in HI, has a FWHM of 103.9 km s^{-1} , and lies well outside the 3σ line of Figure 3.6. As discussed in § 3.5.5, this candidate and others are likely to represent new galaxies that lie beyond the Local Group.

3.4.3 Search for Associated Stellar Populations with SDSS

Thirty-one of the dwarf candidates have sufficient SDSS-DR9 coverage to allow a search for a diffuse optical counterpart or an underlying resolved stellar population at their position. In two cases, there is an obvious diffuse, blue optical counterpart near the

candidate position (see § 3.5.1). In searching for a resolved stellar population, we selected objects identified as stars in SDSS within a square degree around the position of each candidate. For each candidate with SDSS coverage a local σ for total stellar density was determined from the square degree area surrounding the position of each candidate.

Individual stellar density fields and color magnitude diagram were examined for all candidates with SDSS-DR9 coverage. Color magnitude diagrams for $g-r$ vs. r and $g-i$ vs. i were made both on and off the candidate position. The “on” CMDs were constructed by selecting stars within a $4'$, $6'$, and $8'$ radius, chosen to match both the typical size of stellar overdensities seen in previously discovered SDSS dwarfs, and the typical HI extent of the candidates. The “off” CMDs were made by selecting stars out of the corresponding equal area annulus surrounding the “on” region. The stellar density of each equal area annulus was measured, and plots of the normalized stellar density as a function of radius were created for those candidates with complete coverage within the square degree.

For the stellar density plots of each candidate, we also applied two color cuts to see if this resulted in any stellar overdensities. The cuts applied were based on the stellar population of Leo T: $-0.5 < g-r < 1$ and $21.5 < r < 23$, $0.25 < g-r < 0.75$ and $22 < r < 24.5$. These same cuts were applied with $g-i$ and i .

No 3σ overdensity at the candidate positions were seen in the combined or individual stellar positions in either the total stellar position plots or those with the color cut applied. The lack of overdensities of resolved stars at the candidate positions not exclude that they have a population too dim to be detected in SDSS, or that more detailed isochrone analysis could reveal a population in the existing data. However, candidates 1,10, 21, and

23 showed significant overdensities with a characteristic size of $\sim 3'$ at distances further than $15'$ from the candidate position, which is outside the HI extent in all cases. For each overdense position, there was no known galaxies with measured velocities within $15'$. It is possible some of these overdensities may represent clustered galaxies misidentified as stars by the SDSS pipeline.

3.5 Discussion

Distances are one of the primary uncertainties for interpreting the properties of the candidates.

To determine a distance the equation for the HI mass and the dynamical mass can be combined (e.g. Putman et al. 2002). The HI mass of the candidate is,

$$M_{HI} = 2.36 \times 10^{-1} D_{kpc}^2 \int F dv, \quad (3.1)$$

where D_{kpc} is the distance to the candidate in kpc, $\int F dv$ is its total HI line flux in Jy km/s, and the HI mass, M_{HI} is given in M_{\odot} .

The dynamical mass for a dispersion-supported dwarf galaxy can also be defined in terms of its distance,

$$M_{dyn,\sigma} = \frac{\sigma r}{G} = \frac{\left(\frac{FWHM}{2\sqrt{2\ln(2)}}\right)^2 \frac{\delta}{2} D_{kpc}}{G} \quad (3.2)$$

Where σ is the velocity dispersion in km s^{-1} , r is the radius of the dwarf candidate in kpc, G is the gravitational constant, FWHM is the full width at half maximum of the HI line,

D_{kpc} is the distance to the dwarf in kpc, and δ is the angular size of the dwarf candidate in radians (using the 4σ GALFA-HI contour). These two equations can be combined by assuming the HI mass is a fraction f of the total dynamical mass typical for dwarf galaxies, giving the distance in kpc

$$D_{kpc} = \frac{fFWHM\delta}{GF} \quad (3.3)$$

Where f is the gas fraction of the galaxy, FWHM is the full width at half maximum of the HI line, δ is the angular size in radians, F is the total flux in the HI line, and $G = 4.302 \times 10^{-3} \text{ pc } M_{\odot}^{-1} \text{ km s}^{-1}$. The distance D calculated with a fiducial gas fraction of 10% is listed for each of the candidates in Table 3.2 and Table 3.4. The value for the dynamical mass and therefore the calculated distances depend on the fraction of total mass which is HI, and there is a high scatter for known Local Group dwarf galaxies, leading to large uncertainty on distances calculated via this method. HI comprises 8.4% of the total mass of Leo T, and if this value is used in Equation 3.3 the derived distance is 390 kpc (true distance = 409_{-27}^{+29} kpc, Clementi 2012). The dynamical masses as a function of distance as well as the total masses expected at various gas fractions are shown for candidate 11 in Figure 3.8. This is discussed further below in the context of the individual candidates.

3.5.1 Two Candidates with Optical Counterparts

Two candidates show clear evidence of an optical counterpart in the SDSS images within $1'$ of the candidate position. Candidate 22 is located the position (R.A., Decl. (J2000)) = $(0^h 14^m 45.9^s, +10^{\circ} 49' 30.1'')$; Candidate 23 is at (R.A., Decl. (J2000)) = $(1^h 19^m 13.9^s, +11^{\circ} 7' 30.1'')$. Both are kinematically selected candidates which both have a high v_{lsr}

of 239.6 and 617.1 km/s respectively. The velocity of candidate 23 makes it very unlikely to be a Local Group dwarf, but the v_{lsr} of candidate 22 is in the range of observed velocities of Local Group dwarf galaxies. Note that both galaxies appear as resolved, extended, blue sources in the SDSS composite images (Figures 3.9 and 3.10) with semi-major axes of $\sim 12''$ and $15''$ respectively. The physical diameter corresponding to their optical extent at 300 kpc, 1 Mpc, and 5 Mpc are 17 pc, 58 pc, and 291 pc for candidate 22, and 22 pc, 73 pc and 367 pc at the same set of distances for candidate 23.

Figure 3.11 shows the positions of SDSS identified stars for these two objects. There appears to be a slight, but non-significant overdensity of stars at the positions of the optical counterparts. More detailed CMD analysis involving isochrone filtering may determine if these overdensities represent a population. If stars associated with these objects are resolved, that would be evidence that the galaxies are close enough to be within the outskirts of the Local Group.

The match distances for these two candidates, derived as described earlier assuming a 10% gas fraction, are 5.5 and 20.9 Mpc respectively. The corresponding HI masses are $9.2 \times 10^7 M_{\odot}$ and $1.9 \times 10^9 M_{\odot}$. Their v_{lsr} values also place them outside the 3σ range for Local Group galaxies on Figure 3.6. Overall, their characteristics suggest they represent star forming galaxies which lie just beyond the Local Group, and their high gas content suggests they have not had significant interaction with the inner regions of Local Group if they reside near it. These interesting objects warrant detailed follow up study, and are similar in characteristics to the Leo P dwarf galaxy which has been suggested to be a Local Group member (Salzer & Rhode 2012).

3.5.2 The CC Clouds

When IVC maps were inspected by eye it was found that the CC grouping lies near an IVC at $(l,b) = (67^\circ, -27^\circ)$ that has been called the g1 cloud (Wakker et al. 2008). Clouds associated with this IVC extend at least down to 55 km s^{-1} in velocity. The g1 cloud and CC candidates may also be related to the Galactic center positive (GCP, also called the Smith Cloud) HVC complex in this region of the sky (Wakker & Van Woerden 2011), though this complex is at higher velocities ($v_{lsr} = 91\text{-}126 \text{ km s}^{-1}$). The GALFA-HI data has partial coverage in this region, making it difficult to determine the relationship between the CC candidates, the GCP HVC complex, and the g1 IVC. While individually the CC clouds are promising candidates, their clustering in position-velocity, proximity to an IVC, and divergence from the typical kinematic trend of Local Group dwarfs as indicated by Figure 3.6 suggest they are more likely Milky Way associated clouds. However, even if the CC clouds do not represent individual galaxies, it is possible that the CC candidates, and possibly the nearby HVC/IVC complexes themselves, originated from a disrupted progenitor satellite (Bland-Hawthorn et al. 1998).

Cloud g1 is one of a few IVCs to have distance measurements derived from absorption lines associated with Galactic halo stars (Wakker et al. 2008). The distance measurements indicate g1 is between 1.8 to 3.8 kpc. If the candidate clouds are associated with cloud g1 and are at a similar distances, the mass of the individual candidate clouds would be between $7.3 M_\odot$ and $62.0 M_\odot$. The mass of entire g1 IVC was found to be $1000\text{-}4000 M_\odot$ (Wakker et al. 2008), so the candidates would represent very small components of this complex. In any case, the distinction of the CC candidates in column density from other

clouds in Saul et al. (2012) warrants further investigation of the cluster.

3.5.3 M31 Satellite Candidates

Several of the candidate clouds have small projected distances to M31. Estimates for the virial radius of M31 and the distance to M31 are $D = 770$ kpc and $r_{vir} = 260$ kpc (Seigar et al. 2007), and as viewed from the Milky Way the virial radius extends 18.6° from M31. While M31 itself is outside the GALFA-HI survey coverage region, lying at $\delta_{M31} = 41.2^\circ$, a significant fraction of the virial volume of M31 is observed. The projected distance to M31 is less than the virial radius of M31 for four of the dwarf candidates: 1, 2, 3, and 24. The near-M31 candidates all have positive velocities, ranging from 28 to 65 km s^{-1} . While M31 satellite galaxies are not strictly limited to any particular v_{lsr} range, the systemic v_{lsr} of M31 is -300 km s^{-1} , and known satellites of M31 have velocities ranging from -481 to -188 km s^{-1} . Because the candidates are located near to the edge of the projected virial radius they are more likely to be near apogalacticon and have a lower orbital velocity. Since these 4 candidates have a v_{lsr} similar to each other and also similar to the general cloud population in that region, and their velocities are outside the expected range of velocities of M31 satellites, it is less likely these candidates are closely bound M31 satellites.

Using a 10% gas fraction, these candidates have match distances of 250-400 kpc, beyond the Milky Way's virial radius and not yet within that of M31. This would be consistent with Local Group dwarf galaxies only having significant amounts of gas if they are beyond the virial radius of the Milky Way or M31 (e.g. Grcevich & Putman 2009). These candidates could also have larger gas fractions and lie beyond M31, or at distances

> 1 Mpc.

The velocities of these candidates are consistent with Leo T which is sitting at the outskirts of the Local Group. These candidates could be additional gas-rich faint galaxies that have not yet fallen into the Local Group. They are all within the 3σ line in Figure 3.6.

3.5.4 Remaining Group 1 Candidates

Group 1 candidates are those that have peak column densities that exceed $5 \times 10^{19} \text{ cm}^{-2}$ or peak brightness temperatures that exceed 1.5 K. Candidates 7, 8 and 9 are promising. All three are at $|b| < 15^\circ$, and therefore easily missed in optical surveys. They are within or very close to the 3σ line in Figure 3.6, and assuming a 10% gas fraction have match distances between 350-700 kpc. Their total mass estimates at these distance range from 3×10^6 to $1.2 \times 10^7 M_\odot$. Candidate 11 is notable due to its high peak column density of $1.49 \times 10^{19} \text{ cm}^{-2}$. It has a match distance of 261 kpc, at which its HI mass would be $1.3 \times 10^6 M_\odot$.

The HI masses of the group 1 candidates range from 9.9×10^4 to $1.7 \times 10^6 M_\odot$ at an assumed distance of 300 kpc, with an average value of 3.7×10^5 ($\sigma = 1.6 \times 10^5$). At 1 Mpc, the HI masses range between 1.1×10^6 and $1.9 \times 10^9 M_\odot$, with an average value of $4.1 \times 10^6 M_\odot$ ($\sigma = 1.8 \times 10^6 M_\odot$). If the dwarfs are located at a distance of 300 kpc, the range of dynamical masses calculated ranges from 2.2×10^5 to $8.8 \times 10^7 M_\odot$, with an average of $8.3 \times 10^6 M_\odot$ ($\sigma = 1.7 \times 10^6 M_\odot$). If the candidates are all considered to be at a distance of 1 Mpc, they range in estimated dynamical masses from from 1.5×10^6 to $5.9 \times 10^8 M_\odot$, with an average of $5.6 \times 10^{10} M_\odot$ ($\sigma = 1.4 \times 10^{10} M_\odot$).

3.5.5 Remaining Group 2 Candidates

Group 2 candidates are selected because they are local or absolute kinematic outliers. Ten of the 33 Group 2 candidates lie at velocities which exceed the escape velocity of the Local Group at 1 Mpc: 22, 25, 27, 29, 31, 33, 40, 41, 43, and 44. It is possible these candidates are transient Local Group dwarfs, but it is more likely they are newly discovered dwarf galaxies beyond the Local Group. Candidates 32 and 49 (49 is a CC member) both show area(s) with clear underdensities of SDSS stars at a position near the candidate. In both cases, this decrement is due to the presence of a bright star at that location which interferes with our stellar overdensity search. Candidate 34 shows a reduction of the number of stars observed by SDSS at a distance of 8' on two sides of the candidate position, but no reduction in the number of stars is observed at the cloud position. The obscuration is due to the nearby emission nebula NGC 2264, which lies 15' away from the cloud position and unlikely to be associated with the candidate cloud, which lies at an lsr velocity of 318 km/s.

Several candidates are located along the line of sight to known galaxies, but are well separated in velocity from them. These could be satellite galaxies, galaxy alignments due to larger scale structure, or chance alignments.

Candidate 40 ($v_{lsr} = 519.9 \text{ km s}^{-1}$) lies 45'' from SDSS J094805.89+070744.8 ($v_{lsr} = 819 \text{ km s}^{-1}$). Two group 2 candidates are likely associated with the Virgo cluster, candidates 43 and 44. Candidate 43 lies at close projected position to the Virgo cluster, and its velocity, 473 km s⁻¹, is within the range of Virgo Cluster galaxies (Binggeli et al. 1987). It is near the line of sight to NGC 4472, and a faint blue object may be present in SDSS images at

its position. It has a velocity FWHM of 33 km s^{-1} . This candidate may be an unknown member of the Virgo S sub-cluster and/or satellite of NGC 4472. Candidate 44 is very near the line of sight to M91, a barred spiral member of the Virgo cluster, being separated only by $44''$. It is possible this represents a low velocity extension of M91 associated gas, or a satellite galaxy. The FWHM of this candidate is 146 km s^{-1} and the central velocity is 92 km s^{-1} less than that of M91 (394 km s^{-1} vs. 486 km s^{-1}), so it may also represent a distinct Virgo cluster galaxy and/or satellite galaxy of M91.

The smaller average size, the larger FWHM, and their status as velocity outliers all strongly suggest Group 2 candidates may contain galaxies either on the outskirts of the Local Group or outside of it. The SHIELD galaxies may be appropriate analogs to these candidates (Cannon et al. 2011). The SHIELD galaxies were discovered in the Arecibo Legacy Fast Alfa (ALFALFA) survey, with which part of the GALFA-HI survey data is taken commensally. During the cataloging process several of the SHIELD galaxies were identified, but were removed from the final GALFA-HI catalog and candidate list when they were confirmed to have optical counterparts. The SHIELD sample galaxies' HI characteristics are consistent with the candidates in our sample, particularly many Group 2 candidates at high absolute V_{lsr} . They were found to have HI masses between 10^6 and $10^7 M_{\odot}$, HI column densities under 10^{21} cm^{-2} , and one for which additional data has been obtained shows ordered rotation indicating a dynamical mass of $10^8 M_{\odot}$ (Cannon et al. 2011). At an assumed distance of 1 Mpc, our group 2 candidates range from 2.8×10^5 to $1.4 \times 10^7 M_{\odot}$ in HI mass, with an average value of $2.1 \times 10^6 M_{\odot}$ ($\sigma = 1.2 \times 10^6 M_{\odot}$). The dynamical masses range from 9.2×10^5 to 3.4×10^9 at this distance with a large spread in

gas fractions.

Although there were no detections of a significant overdensity of SDSS-identified stars in any of the Group 2 candidates, as with the Group 1 candidates, this does not rule them out as possible dwarf galaxies. Since we are expecting gas rich dwarfs to be preferentially located in the outskirts of the Local Group, their stars may not be individually resolved at those distances, or their stars may be detected only in deeper optical observations. We also note that 9 out of 29 candidates in the Group 2 category are at $|b| < 15^\circ$, where discovery of galaxies by optical methods is strongly prohibited.

3.6 Summary

We have identified 51 Local Group dwarf galaxy candidates from the GALFA-HI Survey Catalog. Twenty-one of these candidates were selected due to their high-column density or peak brightness temperature, and 30 were selected due to having a V_{lsr} significantly different from their neighbors, or with a V_{lsr} exceeding 150 km s^{-1} . The column density selected candidates are on average of lower column than Leo T, but otherwise have a range of sizes, velocity and spatial profiles, and FWHM within the expected range for ultra-faint dwarfs. One candidate shows some evidence for a stellar overdensity at the cloud position in the SDSS data. The Group 2 candidates most likely largely represent galaxies beyond the Local Group. While it is difficult to discern if the majority of these clouds represent dwarf galaxies or clouds of other origin without additional observation, they provide an extremely promising pilot sample for HI motivated dwarf galaxy searches.

Table 3.1. Coordinates and Kinematics for Group 1 Dwarf Galaxy Candidates

ID number	α (J2000)	δ (J2000)	ℓ	b	V_{FWHM} (km s ⁻¹)	V_{lsr} (km s ⁻¹)	V_{gsr} (km s ⁻¹)	V_{lgsr} (km s ⁻¹)
1	1 ^h 23 ^m 21.9 ^s	+ 27° 50' 30.2"	131.5°	-34.5°	11.2	27.9	122.8	198.0
2	1 ^h 34 ^m 29.9 ^s	+ 32° 51' 30.2"	133.3°	-29.1°	8.1	37.4	-100.2	-142.7
3	1 ^h 46 ^m 9.9 ^s	+ 31° 43' 30.2"	136.3°	-29.7°	6.0	31.9	58.1	25.5
4	2 ^h 58 ^m 45.9 ^s	+ 31° 58' 30.2"	152.2°	-23.6°	4.5	-52.8	-50.1	-84.8
5	3 ^h 29 ^m 37.9 ^s	+ 5° 14' 30.0"	178.7°	-39.9°	56.1	-231.7	-280.1	-296.0
6	4 ^h 21 ^m 37.9 ^s	+ 4° 50' 30.0"	189.0°	-30.1°	6.7	-32.7	-11.8	-53.4
7	4 ^h 48 ^m 53.9 ^s	+ 21° 26' 30.2"	178.9°	-14.8°	12.3	-53.5	-81.4	-14.8
8	6 ^h 29 ^m 22.0 ^s	+ 13° 37' 30.1"	198.3°	1.4°	9.8	-64.3	-79.6	-106.5
9	6 ^h 56 ^m 22.0 ^s	+ 10° 31' 30.1"	204.1°	5.9°	14.1	69.4	92.4	167.1
10	11 ^h 42 ^m 34.0 ^s	+ 32° 9' 30.2"	190.2°	74.2°	6.4	-73.2	13.2	64.3
11	21 ^h 22 ^m 30.0 ^s	+ 23° 42' 30.2"	73.2°	-18.4°	14.3	31.1	-131.8	-144.4
12	21 ^h 34 ^m 10.1 ^s	+ 20° 17' 30.1"	72.5°	-22.7°	14.6	51.9	89.6	27.9
13	21 ^h 38 ^m 6.1 ^s	+ 22° 19' 30.2"	74.8°	-22.0°	18.7	57.5	188.5	262.9
14	21 ^h 47 ^m 42.1 ^s	+ 23° 34' 30.2"	77.4°	-22.6°	12.3	44.6	-114.1	-185.1
15	21 ^h 49 ^m 34.1 ^s	+ 20° 32' 30.1"	75.4°	-25.1°	8.5	54.8	62.9	1.9
16	22 ^h 3 ^m 30.1 ^s	+ 17° 36' 30.1"	75.8°	-29.5°	11.8	51.3	21.7	1.7
17	22 ^h 4 ^m 38.1 ^s	+ 21° 12' 30.2"	78.8°	-27.0°	10.2	35.9	54.5	71.6
18	22 ^h 5 ^m 10.1 ^s	+ 21° 50' 30.1"	79.4°	-26.6°	10.5	27.8	17.8	53.4
19	22 ^h 51 ^m 18.1 ^s	+ 18° 35' 30.1"	87.1°	-35.8°	39.6	-359.4	-306.6	-316.4
20	23 ^h 3 ^m 14.1 ^s	+ 23° 15' 30.2"	93.0°	-33.2°	10.9	69.5	122.5	170.3
21	23 ^h 36 ^m 10.1 ^s	+ 22° 34' 30.1"	101.0°	-37.1°	3.9	28.7	111.3	61.3

Table 3.2. Observational Characteristics for Group 1 Dwarf Galaxy Candidates

ID number	$T_{B,max}$ K	$N_{HI,peak}$ (10^{19} cm^{-2})	$M_{HI,300kpc}$ ($10^5 M_{\odot}$)	$M_{HI,Dmatch}$ ($10^5 M_{\odot}$)	D_{match} kpc	Selection Characteristic	Apex Plot Location σ
1	3.4	3.5	4.35	6.73	373	N_{HI}	$<+3\sigma$
2	2.4	1.8	2.29	3.77	385	N_{HI}	$<+3\sigma$
3	2.7	1.5	2.19	1.41	241	N_{HI}	$<+3\sigma$
4	1.8	0.7	1.00	0.362	181	T_B	-1 to 0σ
5	1.2	6.0	3.78	8.29	14066	N_{HI}	$<-3\sigma$
6	1.9	1.1	1.35	1.21	285	T_B	$<-3\sigma$
7	2.3	2.5	2.29	11.8	681	N_{HI}	-1 to -3σ
8	1.8	1.6	1.85	3.04	384	N_{HI}	$<-3\sigma$
9	2.6	3.4	4.26	12.9	522	N_{HI}	-3 to -1σ
10	1.6	0.9	1.40	1.05	260	T_B	0 to $+1\sigma$
11	11.4	14.9	17.22	13.0	261	N_{HI}	$>+3\sigma$
12	1.7	2.3	2.94	14.9	676	N_{HI}	$>+3\sigma$
13	1.9	3.2	3.47	31.87	909	N_{HI}	$>+3\sigma$
14	3.6	4.1	4.36	5.38	334	N_{HI}	$>+3\sigma$
15	5.3	4.1	5.02	1.35	156	N_{HI}	$>+3\sigma$
16	1.7	1.8	2.09	6.31	521	N_{HI}	$>+3\sigma$
17	3.8	3.5	4.12	2.75	245	N_{HI}	$>+3\sigma$
18	4.9	4.7	6.07	2.62	197	N_{HI}	$>+3\sigma$
19	1.2	4.2	2.04	607.2	5170	N_{HI}	$>+3\sigma$
20	1.9	1.8	2.07	7.59	574	N_{HI}	$>+3\sigma$
21	3.2	1.1	1.87	0.126	78	T_B	$>+3\sigma$

Table 3.3. Coordinates and Kinematics for Group 2 Galaxy Candidates

ID number	α (J2000)	δ (J2000)	ℓ	b	V_{FWHM} (km s ⁻¹)	V_{lsr} (km s ⁻¹)	V_{gsr} (km s ⁻¹)	V_{lgsr} (km s ⁻¹)
22	0 ^h 14 ^m 45.9 ^s	+ 10° 49′ 30.1″	108.5°	-51.0°	48.0	239.6	398.6	457.8
23	1 ^h 19 ^m 13.9 ^s	+ 11° 7′ 30.1″	133.8°	-51.2°	113.9	617.1	748.2	811.6
24	1 ^h 22 ^m 1.9 ^s	+ 32° 46′ 30.2″	130.3°	-29.7°	3.7	30.9	72.1	44.7
25	2 ^h 58 ^m 57.9 ^s	+ 13° 37′ 30.1″	164.2°	-38.8°	40.2	528.1	594.3	619.5
26	3 ^h 31 ^m 5.9 ^s	+ 21° 51′ 30.2″	165.2°	-27.6°	8.5	60.6	-110.5	-132.2
27	4 ^h 14 ^m 57.9 ^s	+ 33° 18′ 30.2″	164.6°	-12.6°	11.0	461.7	667.3	685.7
28	5 ^h 37 ^m 34.0 ^s	+ 24° 2′ 30.2″	183.2°	-4.1°	15.2	150.1	45.5	16.6
29	5 ^h 45 ^m 46.0 ^s	+ 10° 46′ 30.1″	195.7°	-9.3°	86.9	595.7	427.0	439.4
30	6 ^h 3 ^m 38.0 ^s	+ 30° 53′ 30.2″	180.3°	4.4°	9.4	265.3	337.1	375.3
31	6 ^h 8 ^m 34.0 ^s	+ 9° 29′ 30.1″	199.6°	-5.1°	3.7	586.9	513.9	466.2
32	6 ^h 33 ^m 46.0 ^s	+ 27° 5′ 30.2″	186.7°	8.4°	28.5	102.6	220.8	206.7
33	6 ^h 39 ^m 50.0 ^s	+ 36° 41′ 30.3″	178.4°	13.7°	103.9	423.9	482.5	484.4
34	6 ^h 43 ^m 34.0 ^s	+ 9° 13′ 30.1″	203.8°	2.5°	62.4	318.5	255.3	177.0
35	7 ^h 44 ^m 46.0 ^s	+ 24° 53′ 30.2″	195.4°	22.2°	42.1	73.3	-47.6	-11.9
36	8 ^h 34 ^m 50.0 ^s	+ 31° 39′ 30.2″	191.7°	34.7°	53.6	78.5	88.3	34.8
37	9 ^h 8 ^m 46.0 ^s	+ 15° 26′ 30.1″	213.7°	37.2°	42.0	91.0	109.0	71.8
38	9 ^h 22 ^m 18.0 ^s	+ 26° 45′ 30.2″	200.8°	43.7°	25.2	69.1	17.2	-42.4
39	9 ^h 34 ^m 42.0 ^s	+ 12° 51′ 30.1″	220.1°	42.0°	8.3	212.4	196.4	251.7
40	9 ^h 48 ^m 6.0 ^s	+ 7° 8′ 30.1″	229.0°	42.2°	90.6	519.9	504.7	525.2
41	10 ^h 48 ^m 26.0 ^s	+ 12° 31′ 30.1″	233.7°	57.7°	34.8	446.6	525.9	500.4
42	11 ^h 31 ^m 50.0 ^s	+ 4° 41′ 30.0″	259.2°	60.6°	34.7	68.6	-64.1	-60.7
43	12 ^h 29 ^m 54.0 ^s	+ 7° 58′ 30.1″	287.0°	70.2°	32.7	472.7	375.6	339.9
44	12 ^h 35 ^m 26.0 ^s	+ 14° 30′ 30.1″	285.7°	76.8°	146.4	393.7	399.7	373.8
45	14 ^h 23 ^m 26.0 ^s	+ 4° 33′ 30.0″	351.2°	58.5°	148.5	212.4	267.4	264.4
46	21 ^h 38 ^m 42.1 ^s	+ 36° 29′ 30.3″	85.2°	-11.9°	30.8	27.4	-31.5	-19.4

Table 3.3—Continued

ID number	α (J2000)	δ (J2000)	ℓ	b	V_{FWHM} (km s ⁻¹)	V_{lsr} (km s ⁻¹)	V_{gsr} (km s ⁻¹)	V_{lgsr} (km s ⁻¹)
47	21 ^h 47 ^m 34.1 ^s	+ 20° 16′ 30.1″	74.9°	-25.0°	14.3	61.9	-49.5	-127.7
48	21 ^h 56 ^m 30.1 ^s	+ 16° 16′ 30.1″	73.4°	-29.3°	16.6	70.6	171.9	146.5
49	21 ^h 56 ^m 34.1 ^s	+ 17° 47′ 30.1″	74.6°	-28.2°	8.2	59.8	216.5	289.7
50	22 ^h 7 ^m 6.1 ^s	+ 20° 59′ 30.1″	79.1°	-27.6°	6.9	310.0	403.6	403.5
51	22 ^h 48 ^m 26.1 ^s	+ 20° 33′ 30.1″	87.8°	-33.8°	5.3	199.2	230.6	304.2

Table 3.4. Observational Characteristics for Group 2 Galaxy Candidates

ID number	$T_{B,max}$ K	$N_{HI,peak}$ (10^{19} cm^{-2})	$M_{HI,300kpc}$ ($10^5 M_{\odot}$)	$M_{HI,Dmatch}$ ($10^5 M_{\odot}$)	D_{match} kpc	Selection Characteristic	Apex Plot Location
22	0.7	2.9	2.8	919.2	5480	$V_{lsr} > 150 \text{ km s}^{-1}$	$>+3\sigma$
23	0.5	5.4	3.8	18604.2	20872	$V_{lsr} > 150 \text{ km s}^{-1}$	$>+3\sigma$
24	0.7	0.2	0.4	2.55	247	local V_{lsr} outlier	$>+3\sigma$
25	0.6	2.2	2.3	614.4	4854	$V_{lsr} > 150 \text{ km s}^{-1}$	$>+3\sigma$
26	1.2	0.9	1.0	2.31	450	local V_{lsr} outlier	0 to $+1\sigma$
27	0.7	0.7	0.8	4.44	726	$V_{lsr} > 150 \text{ km s}^{-1}$	$>+3\sigma$
28	0.4	0.6	0.5	19.9	1930	$V_{lsr} > 150 \text{ km s}^{-1}$	+1 to $+3\sigma$
29	0.6	4.5	3.0	3055	9602	$V_{lsr} > 150 \text{ km s}^{-1}$	$>+3\sigma$
30	1.1	0.9	1.4	1.12	271	$V_{lsr} > 150 \text{ km s}^{-1}$	$>+3\sigma$
31	0.8	0.3	0.4	0.237	246	$V_{lsr} > 150 \text{ km s}^{-1}$	$>+3\sigma$
32	0.5	1.4	1.0	474.8	6440	local V_{lsr} outlier	0 to $+1\sigma$
33	1.7	16.2	12.5	1896.2	3693	$V_{lsr} > 150 \text{ km s}^{-1}$	$>+3\sigma$
34	0.4	2.3	1.6	1712.5	9916	$V_{lsr} > 150 \text{ km s}^{-1}$	+1 to $+3\sigma$
35	0.3	1.1	0.8	5851.7	24963	local V_{lsr} outlier	0 to $+1\sigma$
36	0.4	1.7	1.4	2206.9	11938	local V_{lsr} outlier	+1 to $+3\sigma$
37	0.3	1.1	0.8	15713	42569	local V_{lsr} outlier	-1 to 0σ
38	0.3	0.7	0.5	252.6	6477	local V_{lsr} outlier	0 to $+1\sigma$
39	0.3	0.2	0.3	4.50	1255	$V_{lsr} > 150 \text{ km s}^{-1}$	+1 to $+3\sigma$
40	0.4	3.0	2.4	8050	17459	$V_{lsr} > 150 \text{ km s}^{-1}$	$>+3\sigma$
41	0.4	1.1	1.0	276.6	4902	$V_{lsr} > 150 \text{ km s}^{-1}$	$>+3\sigma$
42	0.4	1.2	1.0	978.1	9191	local V_{lsr} outlier	-3 to -1σ
43	0.4	11.2	1.2	256.7	4349	$V_{lsr} > 150 \text{ km s}^{-1}$	+1 to $+3\sigma$
44	0.8	10.1	4.8	46219	29299	$V_{lsr} > 150 \text{ km s}^{-1}$	+1 to $+3\sigma$
45	0.4	5.6	2.3	63918	50000	$V_{lsr} > 150 \text{ km s}^{-1}$	0 to $+1\sigma$
46	1.5	4.2	3.0	280.0	2907	local V_{lsr} outlier	$>+3\sigma$

Table 3.4—Continued

ID number	$T_{B,max}$ K	$N_{HI,peak}$ (10^{19} cm^{-2})	$M_{HI,300kpc}$ ($10^5 M_{\odot}$)	$M_{HI,Dmatch}$ ($10^5 M_{\odot}$)	D_{match} kpc	Selection Characteristic	Apex Plot Location
47	0.8	1.1	1.1	11.1	973	local V_{lsr} outlier	$>+3\sigma$
48	0.4	0.6	0.7	77.7	3224	local V_{lsr} outlier	$>+3\sigma$
49	1.1	0.8	0.9	2.14	469	local V_{lsr} outlier	$>+3\sigma$
50	0.7	0.5	0.4	1.29	541	$V_{lsr} > 150 \text{ km s}^{-1}$	$>+3\sigma$
51	0.6	0.3	0.5	0.332	239	$V_{lsr} > 150 \text{ km s}^{-1}$	$>+3\sigma$

Table 3.5. Range and Mean Values for Candidate Clouds as Compared to Leo T

	Leo T	Grp 1 Mean	Grp1 Range	Grp 2 Mean	Grp 2 Range
V_{lsr} (km s ⁻¹)	35	-11	-359.4:69.5	255	27.4:617
V_{FWHM} (km s ⁻¹)	10	13.8	3.9:56.1	42.5	3.7:148.5
Size (')	5.0	11.6	7.0:24.6	7.2	4.2:21.0
T_{max} (K)	2.7	3.0	1.2:11.4	0.6	0.3:1.7
N_{HI} (10 ¹⁹ cm ⁻²)	13	3.3	0.7:14.9	3.1	0.2:16.2

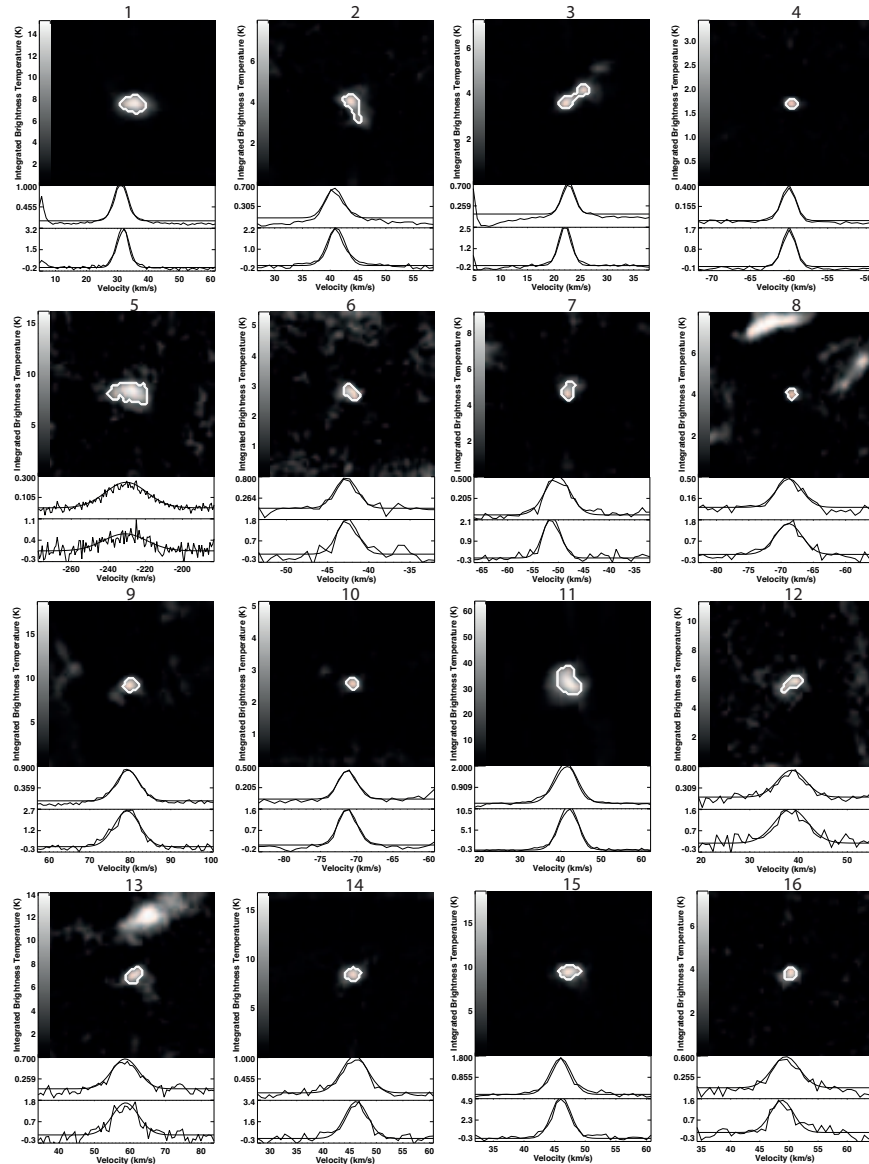


Figure 3.1 Integrated brightness temperature maps for the Group 1 dwarf candidate clouds. Scaling varies between maps. Under the maps are two velocity profiles for each candidate. The top profile is the intensity-weighted spectrum in the region of interest of the cloud, while the bottom profile is the average spectrum across the region of interest. The region of interest is outlined in white on each map, and is determined by the automated region finder used to create the GALFA cloud catalog.

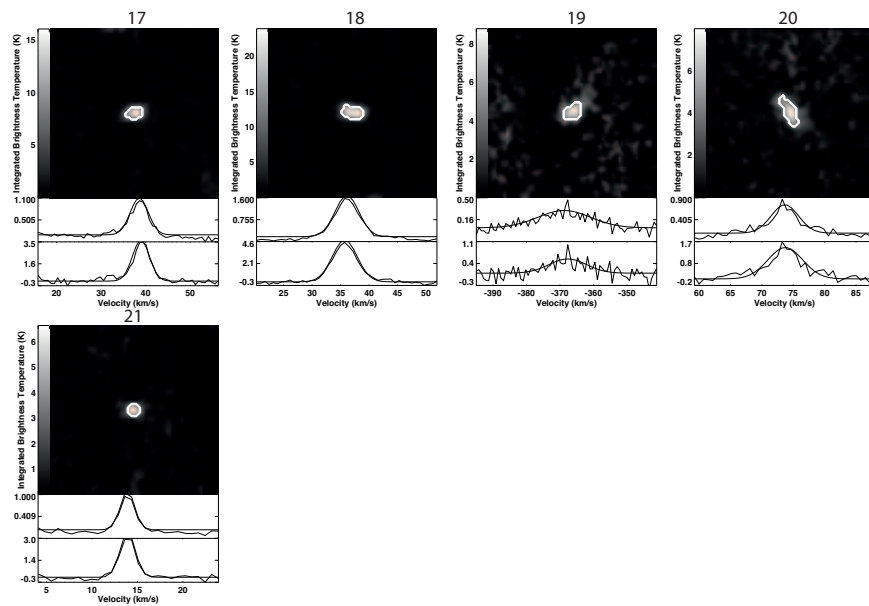


Figure 3.2 Continued: Integrated brightness temperature maps for the Group 1 dwarf candidate clouds. Scaling varies between maps. Under the maps are two velocity profiles for each candidate. The top profile is the intensity-weighted spectrum in the region of interest of the cloud, while the bottom profile is the average spectrum across the region of interest. The region of interest is outlined in white on each map, and is determined by the automated region finder used to create the GALFA cloud catalog.

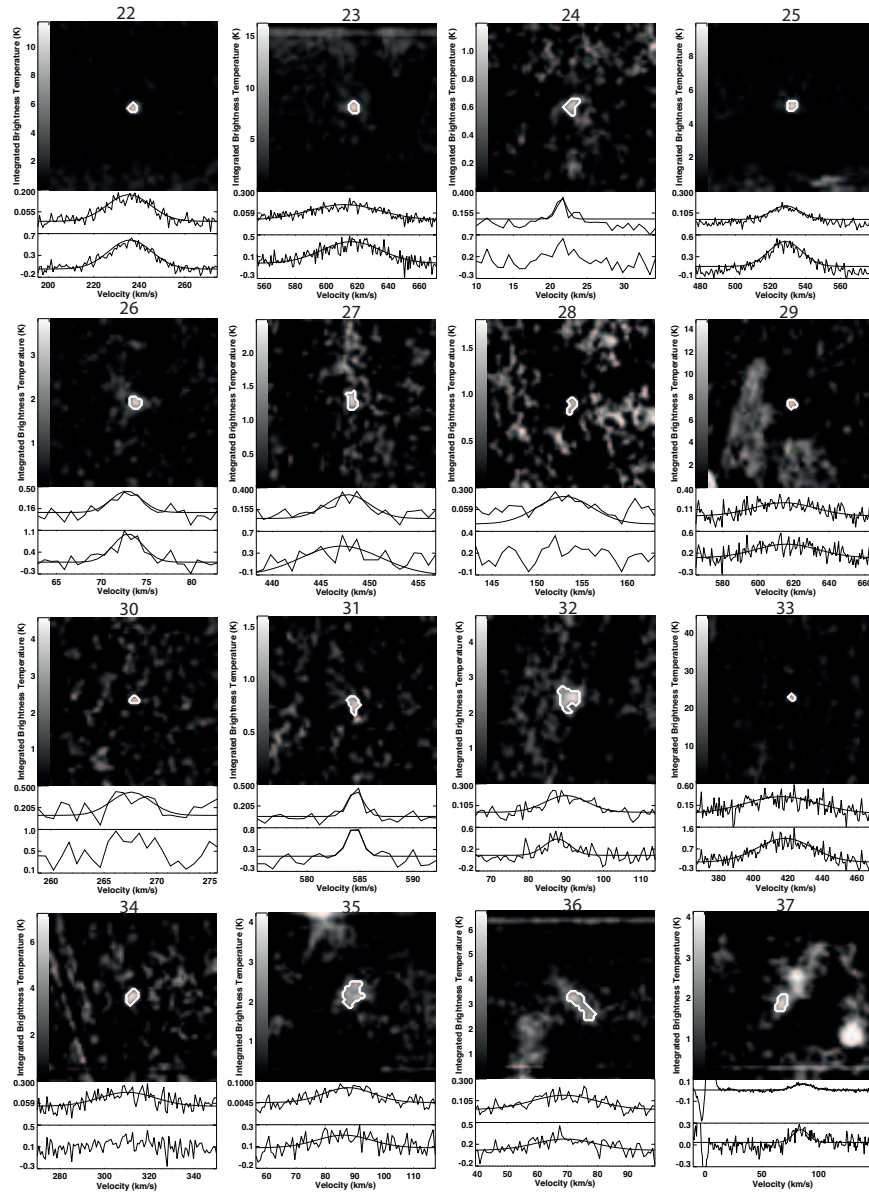


Figure 3.3 Integrated brightness temperature maps for the Group 2 dwarf candidate clouds. Scaling varies between maps. Under the maps are two velocity profiles for each candidate. The top profile is the intensity-weighted spectrum in the region of interest of the cloud, while the bottom profile is the average spectrum across the region of interest. The region of interest is outlined in white on each map, and is determined by the automated region finder used to create the GALFA cloud catalog.

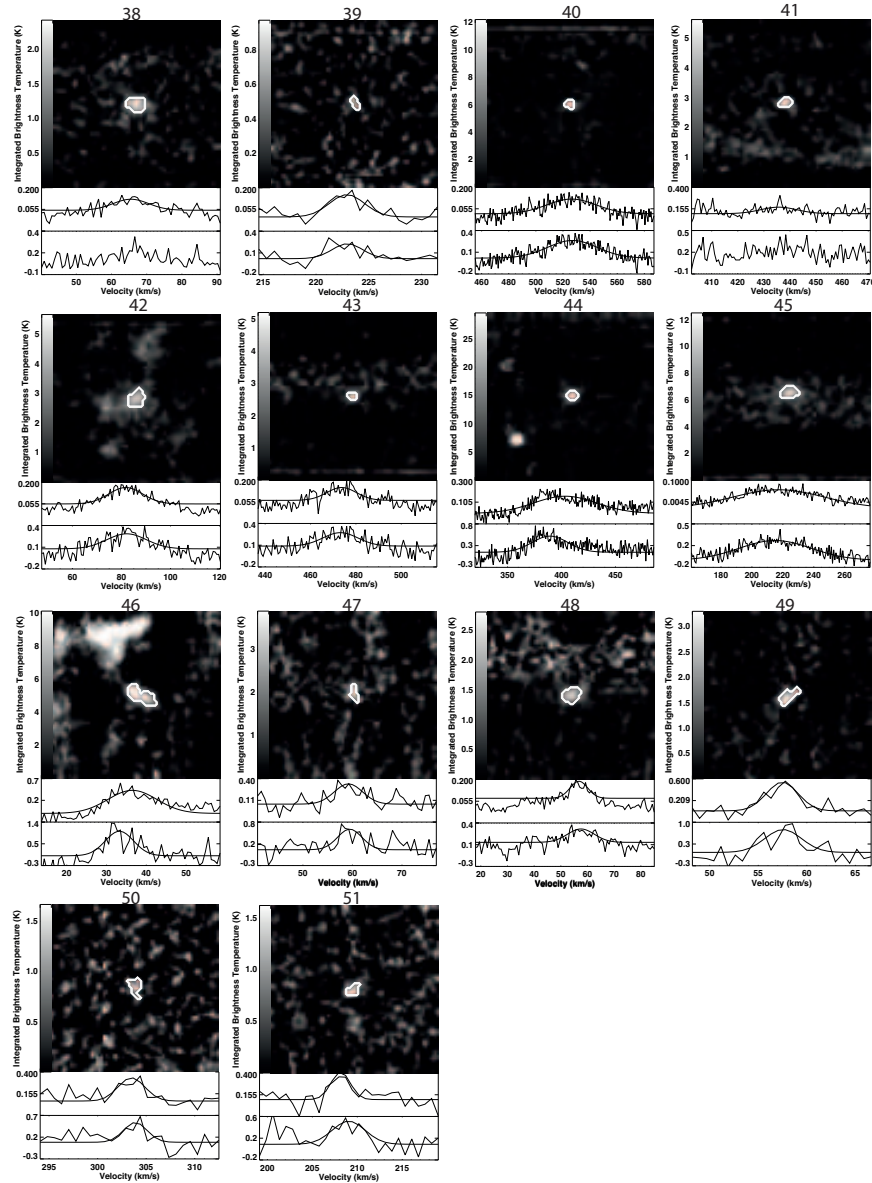


Figure 3.4 Continued: Integrated brightness temperature maps for the Group 2 dwarf candidate clouds. Scaling varies between maps. Under the maps are two velocity profiles for each candidate. The top profile is the intensity-weighted spectrum in the region of interest of the cloud, while the bottom profile is the average spectrum across the region of interest. The region of interest is outlined in white on each map, and is determined by the automated region finder used to create the GALFA cloud catalog.

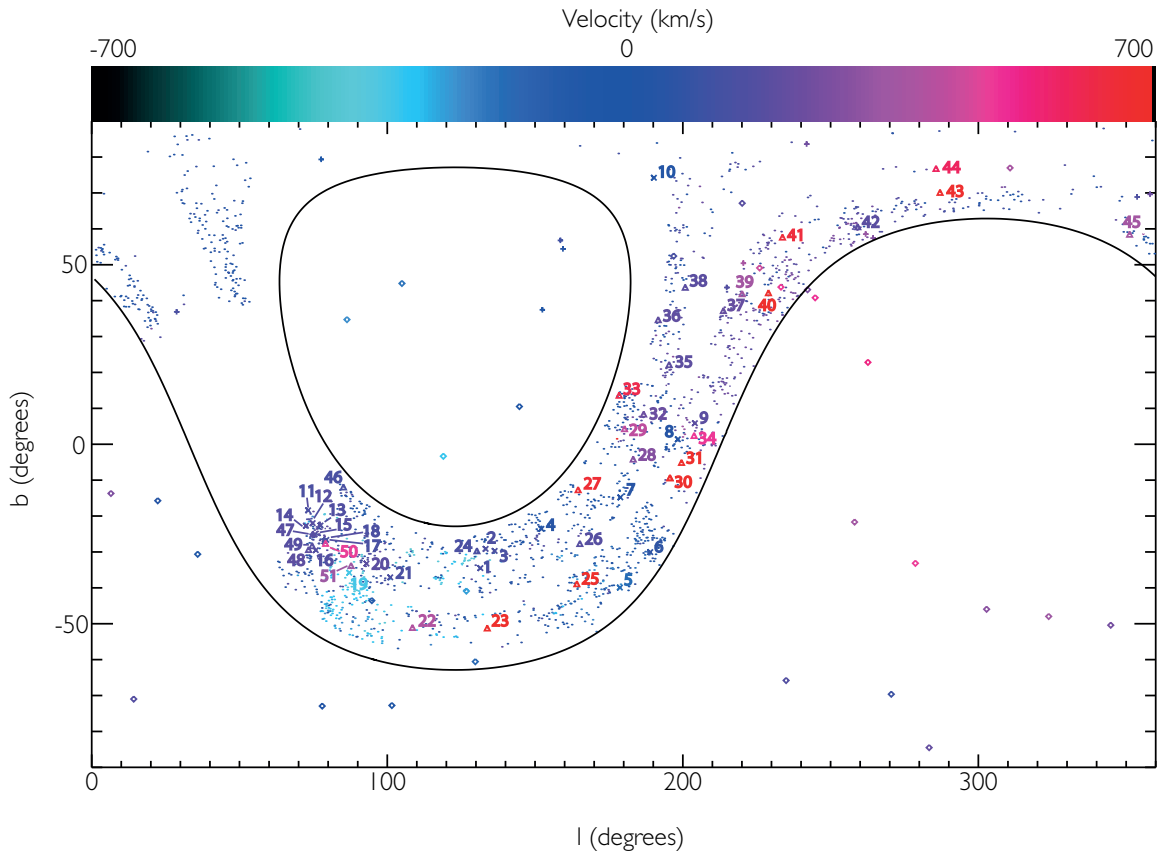


Figure 3.5 The spatial and kinematic distribution of all compact clouds from Saul et al. (2012) (dots), classical Local Group dwarfs (diamonds), ultra-faint Local Group dwarfs (pluses), the Group 1 dwarf candidates (crosses), the Group 2 dwarf candidates (triangles). Galactic coordinates are shown and the LSR velocity. The solid lines show the limits of the Arecibo sky.

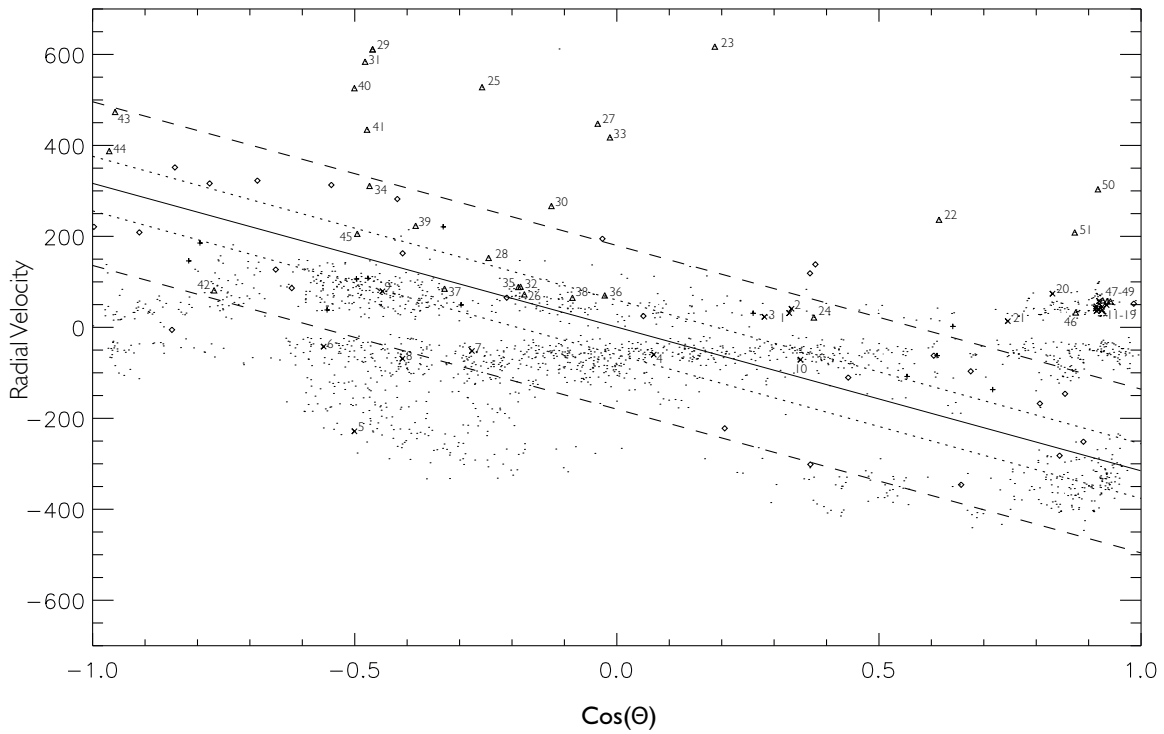


Figure 3.6 V_r versus the angle to the apex of solar motion. Dots represent compact clouds from Saul et. al. (2012), diamonds represent classical Local Group dwarf galaxies, pluses ultra-faint dwarf galaxies, crosses Group 1 candidates, and triangles Group 2 candidates. The solid line is the best fit to known Local Group dwarfs, the dotted lines bound the 1σ variation from that line, and the dot-dashed line the 3σ variation.

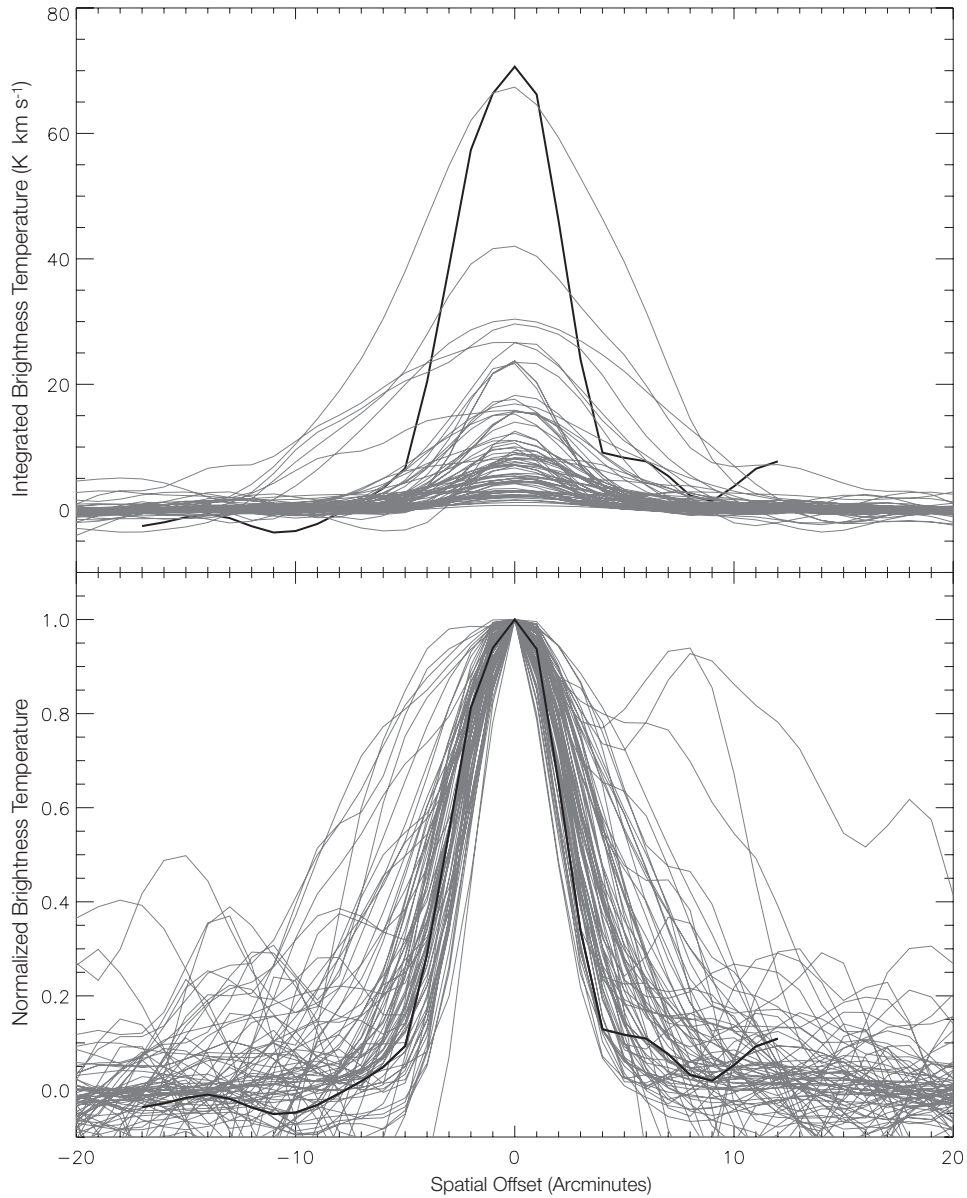


Figure 3.7 Grey lines are the integrated spatial profiles for all candidates, averaged over two perpendicular spatial cuts. The black profile represents the profile of Leo T. The bottom plot has the peak of the candidates scaled to match the peak of Leo T to examine the shape of the profiles in more detail.

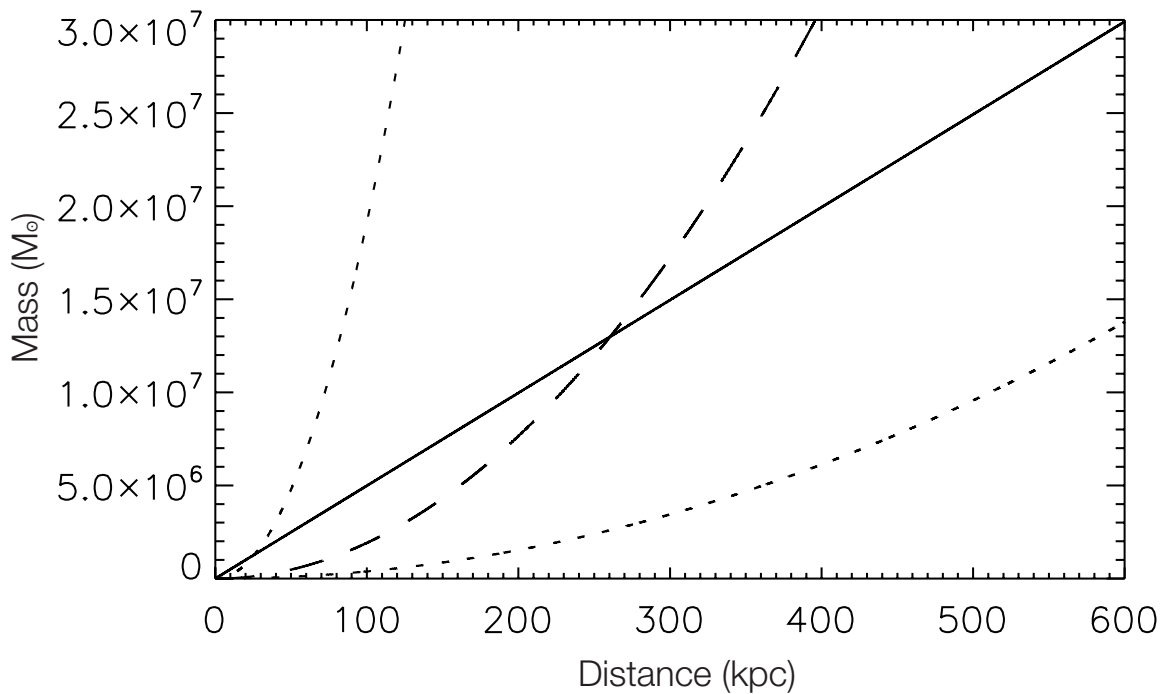


Figure 3.8 Example of the mass estimation method using candidate 11. The solid line is the dynamical mass interior to the HI radius as calculated from the gas dispersion and the dashed line represents the total mass determined from the HI line flux for an assumed 10% HI mass fraction. The dotted line shows masses estimated from the HI line flux assuming a 1% and 50% gas fractions. The intersection of the dashed and solid lines represents the self-consistent match distance and corresponding mass for the fiducial HI fraction of 10%. Uncertainties in the HI gas fractions can lead to large variations in the match distance and mass.

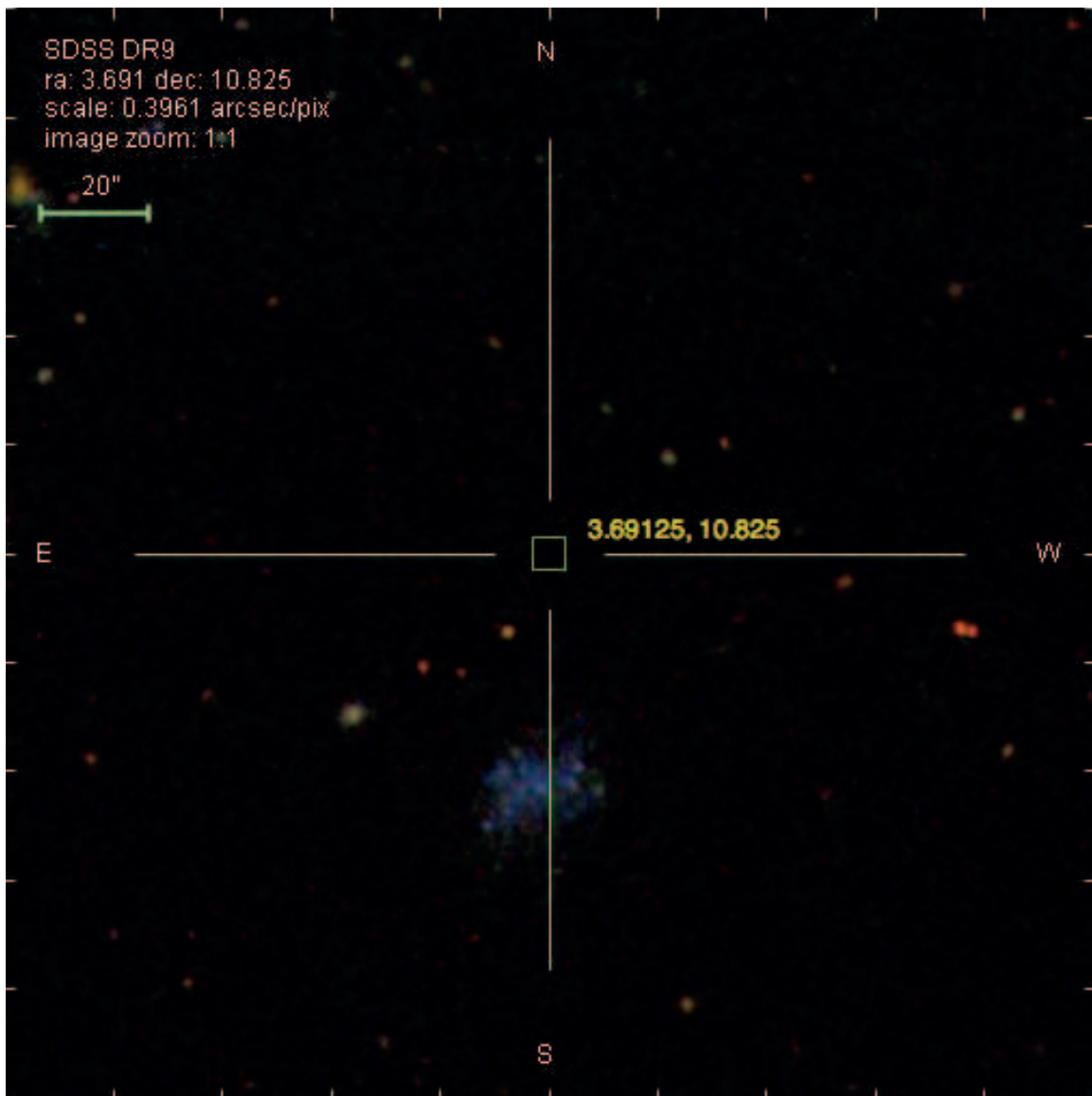


Figure 3.9 SDSS image for the vicinity of candidate 22.

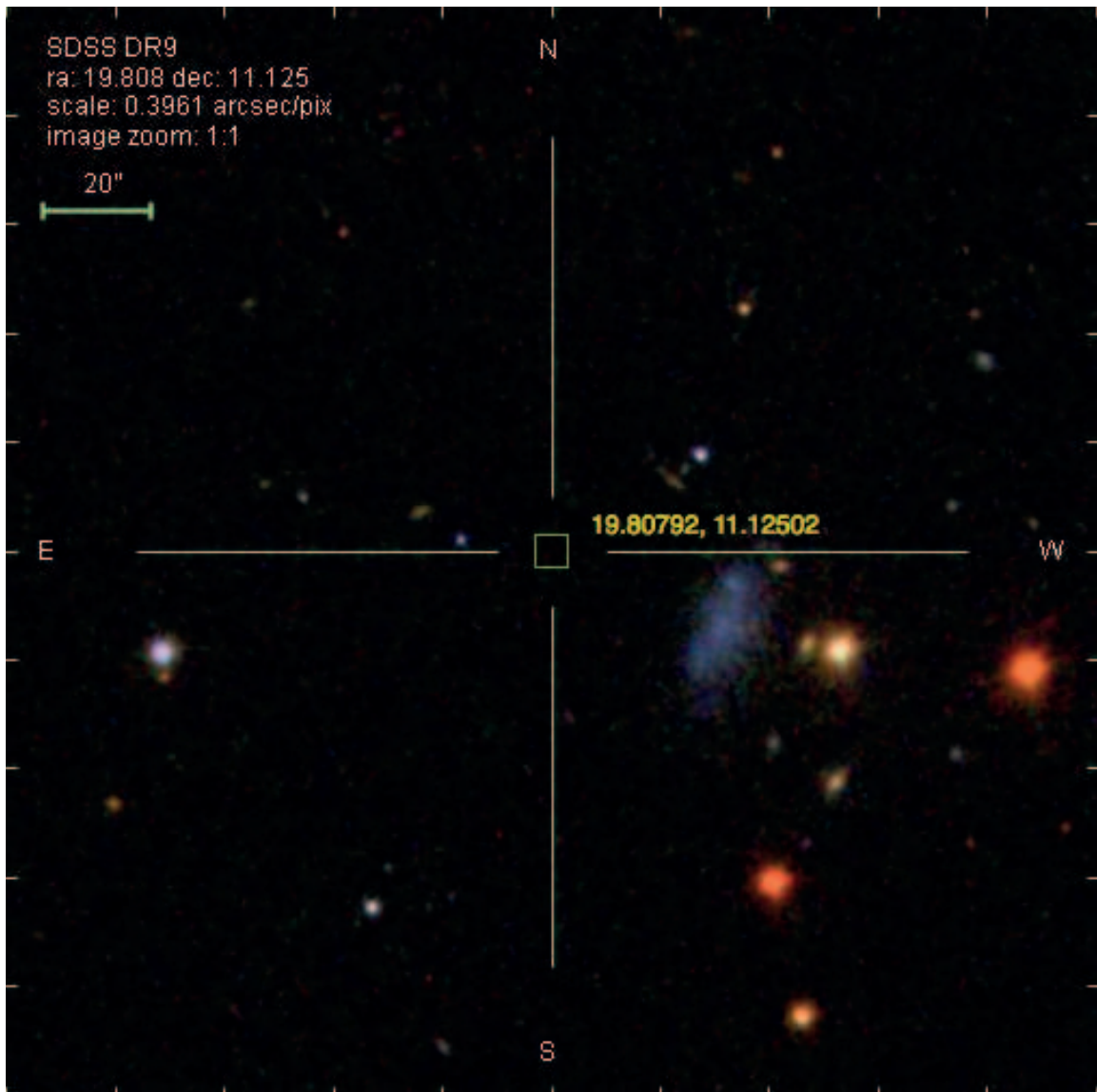


Figure 3.10 SDSS image for the vicinity of candidate 23.

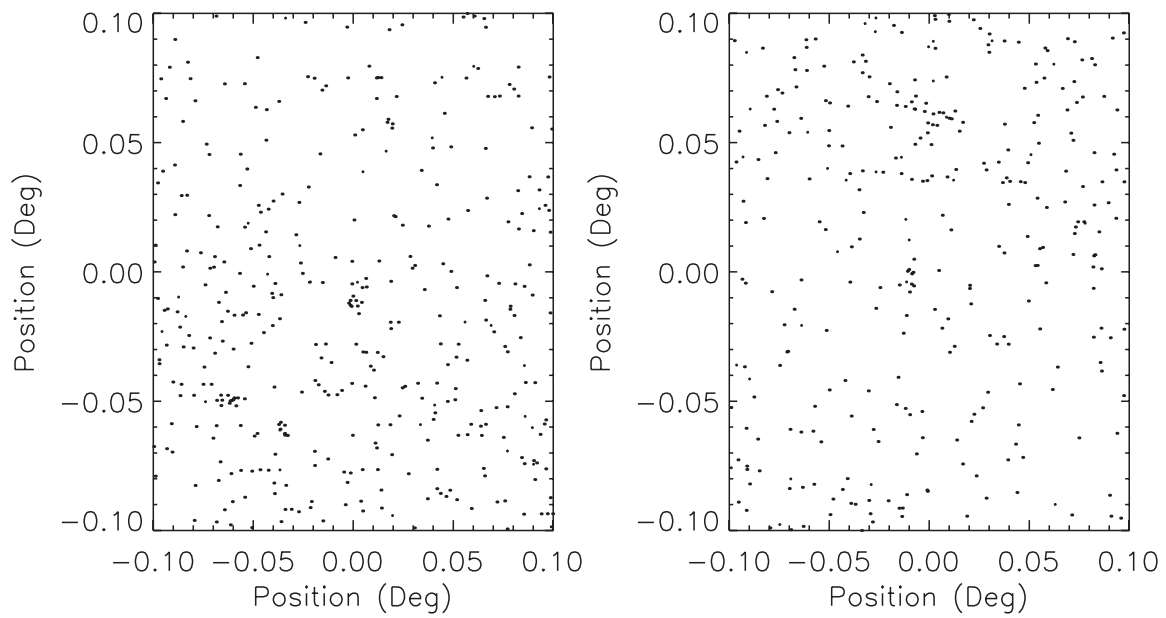


Figure 3.11 SDSS identified stars near the position of candidate 22 (left) and candidate 23 (right).

Chapter 4

Simulations of Mass Loss in Dwarf Satellite Galaxies

4.1 Introduction

The dwarf galaxies of the Local Group are an enigma; dwarf irregular (dIrr) galaxies and dwarf spheroidal galaxies (dSph) share many characteristics, including similar masses, luminosities, and an exponential light distribution, yet differ in their gas content and morphology (Lin & Faber 1983; Kormendy 1985; Grebel et al. 2003). The effect of reionization on the gas of a forming dwarf has been proposed as an origin of dSph galaxies (Dekel & Silk 1986; Gnedin 2000; Bullock et al. 2000; Benson et al. 2002; Somerville 2002; Madau et al. 2008; Bovill & Ricotti 2009; Muñoz et al. 2009). Effects of this process should be observed in the star formation histories of the dwarfs, with stars forming before reionization and little star formation at intermediate redshift. Local group dwarf galaxies do typically have

a dominant, very old (>10 Gyr) population, and many - such as Draco, Ursa Minor, and the majority of the ultra-faint dwarfs - only show a very old population. However, the observed star formation histories of most Local Group dwarfs suggest extended periods of low efficiency star formation, including the ultra-faint dwarfs Leo T and Canis Venatici I (Weisz et al. 2011; Brown et al. 2012).

There have been many suggestions that instead of forming in distinct ways, some dSph form from dIrr galaxies - a reasonable suggestion since we know dSph must have contained gas in order to have formed stars early in their history. Supernova feedback likely affects the gas distributions in dwarf galaxies, although for dwarfs with halo masses as small as $10^8 M_{\odot}$, simulations suggest that star formation alone is not efficient enough to remove most gas (Mori et al. 2002; Mayer & Moore 2004). Other mass loss mechanisms include ram pressure stripping, dynamical stripping, and tides. Mass loss due to these various mechanisms is likely not independent. For example dynamical and ram pressure stripping can induce compression which may trigger star formation, while mass loss can redistribute gas, making it easier to remove via stellar feedback.

A clue to the relationship between dIrr and dSph galaxies are the environments in which they are seen. Due to their faintness, these types of galaxies have primarily been observed in the Local Group. Even among the lowest mass dwarfs, there is an correlation between Galactocentric radius and HI content for Local Group dwarf galaxies, which suggests a distance dependent mechanism is at work (Grebel et al. 2003; Grcevich & Putman 2009). Tidal interactions also likely play a role, but simulations which include the effects of both tides and ram pressure suggest that ram pressure is the dominant mass loss

mechanism for the majority of dwarfs, particularly those at large galactocentric distances (Mayer et al. 2006).

Gas loss due to the interaction between a satellite galaxy's gas and the hot halo medium of the host galaxy occurs via several mechanisms. Ram pressure stripping occurs when the pressure exerted on a satellite's gas exceeds the ability of the dwarf to gravitationally contain its gas (Mori & Burkert 2000; Mayer et al. 2006). Similarly, dynamical stripping occurs from hydrodynamical instabilities at the dwarf/halo interface, and acts over much longer timescales (Nulsen 1982; Murray et al. 1993; Quilis & Moore 2001; Mori & Burkert 2000; Heitsch & Putman 2009).

The magnitude of gas loss depends on the characteristics of the dwarf's gas, the Milky Way's hot halo, and the relative velocity between the two gaseous media. The density and distribution of hot halo gas is not well constrained, and this component of the ISM may harbor a significant fraction of a galaxy's total baryons (the missing baryon problem, see Shull et al. (2011); Fukugita (2004); Fukugita et al. (1998)). For a dwarf with known gas, dark matter, and orbital characteristics, the presence or absence of gas can be used to infer limits on the halo density. Although there is variety in the concentration of hot halo gas around massive galaxies in various theoretical models, many predict a medium present at densities sufficient surrounding massive spiral galaxies to impact the gas within low mass satellite galaxies (Kaufmann et al. 2007, 2008; Sommer-Larsen 2006; Maller & Bullock 2004). The proper motion measurements of satellite galaxy orbits show that several penetrate regions of the hot halo which exceed a density of $5 \times 10^{-5} \text{ cm}^{-3}$. In the case of the Milky Way, which has 27 known satellite galaxies, 17 currently lie within

100 kpc. Indirect constraints such as those provided by the gas content of dwarf galaxies may be able to rule out given halo models.

We present wind tunnel simulations of a low-mass (Leo-T-like) dwarf galaxy undergoing a constant velocity wind. This wind has a density similar to that expected for the Milky Way's hot halo. Many studies have examined the effects of ram-pressure stripping on more massive galaxies in cluster environments, and a few studies have concentrated on dSphs in cluster environments, but only a small number deal with dSph orbiting in a Milky Way-like halo or Local Group medium (Mori & Burkert 2000; Murakami & Babul 1999). While the effects of ram pressure have been studied in simulations which model dwarf galaxies orbiting within a Milky Way like halo, these simulations were run with smoothed particle hydrodynamic (SPH) codes. These codes cannot resolve small scale hydrodynamic instabilities, in contrast to the grid-based simulations presented here (Mayer et al. 2006; Lufkin et al. 2004). The use of a grid-based code combined with the small physical scale of the modeled galaxies should improve results. The set of six two-dimensional simulations presented here are a first step towards accurate ram-pressure and dynamical mass loss rates for low mass Local Group galaxies orbiting within the Milky Way's hot halo.

4.2 Simulation Setup

4.2.1 The Code

Simulations are run with a fixed cartesian grid hydrodynamic solver Proteus (Slyz et al. 2002, Xu 2001, Slyz & Prendergast 1999, Prendergast & Xu 1993). Proteus is based on the Bhatnagar, Gross, and Krook (BGK) scheme, in which the collision term in the Boltzmann equation is approximated by the difference between the initial distribution and the equilibrium distribution, divided by the collision time. Mass, momentum, and total energy are conserved. Heating and cooling is active throughout the simulation, and is calculated with a tabulated cooling function which depends on density and temperature. The equilibrium curve in both the lower and upper temperature regime is adapted from Koyama & Inutsuka and Dalgarno & McCray but modified for lower radiation fields as discussed in Wolfire et. al. 1995. It recreates the warm neutral medium (WNM) and cold neutral medium (CNM). The equilibrium curve in the high temperature regime is constructed to recreate the observed densities and temperatures of the hot ionized medium (HIM) and warm ionized medium (WIM).

4.2.2 Basic Characteristics

The simulations are two dimensional with a resolution of 1024 by 2048 which corresponds to a physical scale of 2.0 kpc \times 4.0 kpc. We simulate a set of dwarf galaxies which is similar to the ultra-faint dwarfs and with HI characteristics modeled after the only ultra-faint dwarf galaxy to have detected HI, Leo T (Ryan-Weber et al. 2008). The characteristics

of each model are summarized in Table 4.1.

The simulations consist of wind tunnel models with a wind which ramps up to a constant velocity of either 200 km s^{-1} or 300 km s^{-1} over a period of 11 Myr. This wind simulates the movement of the dwarf galaxy through the ambient medium, and velocities are chosen which correspond to estimated perigalacticon velocities. For those Milky Way satellite galaxies with orbits constrained via proper motion studies, the range of the estimated perigalacticon velocities are 231 to 443 km s^{-1} (Grcevich & Putman 2009; Piatek et al. 2003, 2005, 2006, 2002; Walker et al. 2008).

4.2.3 Gravitational Potential

Mass to light ($\frac{M}{L_V}$) ratios for several ultra-faint dwarf galaxies have been derived from their stellar velocity dispersions, and range from 138 to an impressive $1722 \frac{M_\odot}{L_\odot}$ (Simon & Geha 2007). This indicates that the gravitational potential is strongly dominated by the dark matter component of these dwarfs, and that ultra-faints are even more strongly dark matter dominated than any other known galaxies. Although there is increasing evidence from simulations that stellar feedback can affect the dark matter distribution in more massive galaxies, leading to a softening of the central dark matter cusp (Governato et al. 2012), it is much less likely that internal baryonic effects could significantly redistribute the dark matter in these extremely dark matter dominated systems, and the gravitational potential of dwarf spheroidal galaxies is well constrained except for at the very center and at large radii (Walker 2012). Ram pressure and dynamical stripping occur only through hydrodynamic interactions and would not affect the dark matter component.

Tidal effects could affect the dark matter distribution, but because the tidal force goes as $\frac{1}{r^3}$ this would not be a significant effect for dwarfs which remain at large Galactocentric distances. Therefore, a static dark matter potential is a fair assumption for the majority of possible orbits.

The gravitational potential used for these simulations is the Navarro, Frenk, & White or NFW potential (Navarro et al. 1995) which has the form:

$$\Phi = -4\pi G\rho_0 a^2 \frac{\ln(1 + \frac{r}{a})}{(\frac{r}{a})} \quad (4.1)$$

Where the two free parameters are the central density (ρ_0) and the scale length (a). Central dark matter densities for the ultra-faints have been estimated to range between 0.8 and 2.09 $M_\odot \text{ pc}^{-3}$ (Simon & Geha 2007). The observed common mass scale for Milky Way satellite galaxies is $10^7 M_\odot$ interior to 300 kpc (Strigari et al. 2008), so the NFW scale length of the models is set at 500 kpc in order to approximately reproduce this result.

4.2.4 Gas Profile

We want to create a stable gas cloud as possible to represent the gas content of our simulated dwarf galaxy. In the adiabatic case, where gas cooling is neglected, one can find a stable gas distribution through hydrostatic equilibrium

$$\frac{\partial P(r)}{\partial r} = -\rho(r) \frac{\partial \Phi(r)}{\partial r} \quad (4.2)$$

for the NFW potential and the adiabatic pressure-temperature relation

$$P^{1-\gamma}T^\gamma = \text{Constant} \quad (4.3)$$

However, if cooling is included, some gas will cool to temperatures between 10^4 and 10^6 K. This is problematic due to the instability of gas at these temperatures, leading to discontinuities in the density and temperature profiles.

A simpler quasi-equilibrium gas distribution can be found by making some reasonable simplifying assumptions which are still consistent with the observed properties of dwarf galaxies. Self-gravity of the gas is negligible because the mass in dark matter to gas mass ratio is so high. Gas within the galaxy has a temperature on the order of 10^4 K and a density greater than 10^{-3} cm^{-3} , while the hot halo medium of the host galaxy has a temperature greater than 10^6 and density less than 10^{-4} cm^{-3} . In both sets of temperature-density regimes, the equation of state can be well approximated by the isothermal case. We use an equilibrium pressure/temperature curve which reproduces the two-phase ISM and is approximately linear in these two regimes.

In these simulations the interior regime includes the area interior to a matching radius, $R_m = 300 \text{ pc}$, chosen to match the HI extent of Leo T (Ryan-Weber et al. 2008). The interior region has a temperature T_1 , on the order of 10^4 , a density profile $\rho_1(r)$, and a sound speed c_{s1} . The external regime primarily represents the hot halo medium of the more massive host galaxy, with a temperature T_2 on the order of 10^6 K, a density profile $\rho_2(r)$, and a sound speed c_{s2} .

In order to construct a stable density profile, we begin with the equilibrium gas profile for an NFW potential in the isothermal case. Considering each regime independently

yields

$$\rho_1(r < R_m) = C_{\rho 1} \exp\left(\frac{C_\Phi}{c_{s1}^2} \ln\left(1 + \frac{r}{b}\right)\right) \quad (4.4)$$

$$\rho_2(r > R_m) = C_{\rho 2} \exp\left(\frac{C_\Phi}{c_{s2}^2} \ln\left(1 + \frac{r}{b}\right)\right) \quad (4.5)$$

The requirement that the pressure needs to be continuous across the density/temperature discontinuity adds an additional constraint:

$$\rho_1(R_m) c_{s1}^2 = \rho_2(R_m) c_{s2}^2 \quad (4.6)$$

In order to determine the constants of integration $C_{\rho 1,2}$, we first need to set values for the density at the interior/exterior region interface. For each equilibrium curve, there is a pressure which corresponds to exactly two temperature/density sets. These are the temperatures (T_1, T_2) and densities (ρ_1, ρ_2) at the matching radius (R_m). The constant of integration $C_{\rho 2}$ can be found by setting $\rho_2(R_m)$ equal to the lower of the two matching densities. Provided the potential is steep enough, the matching radius can be found by numerically solving for the root of the equation

$$\rho_2(R_m) = C_{\rho 2} \exp\left(\frac{C_\Phi}{c_{s2}^2} \ln\left(1 + \frac{R_m}{b}\right)\right) \quad (4.7)$$

The final unknown quantity, $C_{\rho 1}$, can then be found. This method determines a continuous pressure profile and temperature and density profiles which are discontinuous

at the dwarf galaxy/ambient medium interface. The temperature and density profiles are convolved with a hyperbolic tangent function which smoothes them just enough to avoid numerical issues. The resulting gas profile is in near equilibrium with the background potential, but not in perfect equilibrium due to two factors: the equation of state not being perfectly isothermal and the smoothing of the temperature and density profiles.

Modifying the effective ion fraction modifies the equilibrium pressure vs. temperature curves. They still give realistic temperatures and densities for different phases of the ISM, but the slight differences in the temperature and density pairs which result in equal pressure at the dwarf galaxy/ambient halo medium interface lead to different equilibrium gas density profiles. Several equilibrium curves are chosen to cover a range of realistic densities for the ambient halo medium. However, changing the equilibrium curve affects both the density of the halo medium and the density profile of the dwarf galaxy. For this reason each model represents a different set of initial conditions - dwarf galaxies with different characteristics - and one should focus on the ram pressure force and fractional gas mass loss when comparing them. The relevant densities, temperatures, and characteristic scales for this set of six 2D models is given in Table 4.1.

4.3 Results

4.3.1 Stripping Timescales

The fraction of mass remaining in the original 300 pc extent of the dwarfs as a function of time is plotted in Figure 4.1. Sets of models are labeled A to C in order of increasing

background halo density and dwarf mass, while models labeled 1 have a 200 km s^{-1} wind and those labeled 2 have a 300 km s^{-1} wind. In both models A2 and B2, there is rapid mass loss which lasts approximately 440 Myr for model B2 and 470 Myr for model A2. By 600 Myr, both models A2 and B2 have no cold gas within the dark matter potential well, and the simulated dwarf galaxies are stripped of all material. They show what might be linear mass loss for periods of 350 and 450 Myr for A2 and B2 respectively, and then diverge to extremely rapid mass loss events in which the remainder of the gas in these dwarfs are stripped. As seen in Figures 4.2 and 4.3 (bottom panels), these models both are significantly disrupted by 500 Myr, and by 600 Myr there is no sign of gas in the underlying dark matter halo. In contrast, models A1, B1, and C2 show linear mass loss over the vast majority of their simulated lifetimes, with only model A1 diverging from the linear trend when only 20% of the initial gas mass remains (See Figure 4.2, Figure 4.3, and Figure 4.4). B1 and C2 still have 38% and 65% of their initial gas mass remaining at the end of the simulated time period of 1.2 Gyrs. Extrapolating this linear mass loss in models A1, B1, and C2, suggests stripping times of 1.3, 2.2, and 3.25 Gyrs respectively.

4.3.2 Gas Loss Trends

Models B1 and C1 show linear gas loss over time until the end of the simulated time period, 1.2 Gyr, while model C2 shows linear mass loss until the end of its simulated time period at 600 Myr. Model A2 and B2 appear not to show linear mass loss, with a steeper curve in the fractional mass remaining over time, which is particularly sharp after 350 Myr or 40% gas mass remaining for model A2 and 450 years or 40% gas mass remaining

for model B2. The difference in character between the stripping modes seen is likely due to the dominance of either ram pressure stripping vs dynamical stripping in particular models, and is discussed later in detail.

4.3.3 Resolution Study

Klein et al. (1994) quote a required resolution of 100 cells over the cloud to resolve dynamical instabilities. Our initial resolution is 600 cells across the dwarf's gas diameter, and although the effective radius of the cloud decreases from the initial radius due wind effects, it does not fall below 100 cells until the very end stages of disruption.

To investigate the effects of resolution on the results, a pair of models matching the initial conditions of models B1 and B2 was run at 2048×4096 versus the original resolution of 1024×2048 in order to check the possible effects of resolution on mass loss trends. Figure 4.5 shows the fractional mass loss over time for the original B1 and B2 runs and their high resolution versions. The higher resolution models show a larger degree of oscillation in the mass. While this oscillation is seen in the lower resolution models, in those the mass oscillations are limited to 10% or less the total mass of the dwarf, where in the high resolution versions, it varies up to 50%. The oscillation is due to the fact that the region defined as the original dwarf boundary is very close to the The dwarfs modeled at higher resolution gain mass during the initial 100 Myr as compared to the lower resolution models. The overall behavior from this point is qualitatively very similar. B1 and its high resolution counterpart show either linear mass loss, or oscillations which average to a similar mass loss rate over time. The B2 model and its high resolution

counterpart diverge slightly at initial times, but then the high resolution model seems to track the qualitative behavior of the original B2 model. Importantly, it seems that the timescale for total stripping, the change in fractional mass over time, or the presence of a rapid stripping event does not depend on resolution, although further resolution studies should be done to confirm this result.

4.3.4 Discussion

4.3.5 Ram Pressure Stripping

As first stated in Gunn & Gott 1972 , in order for instantaneous ram pressure stripping to occur, the ram pressure from the ambient medium must exceed the gravitational restoring force per unit area; in pressure supported systems the gravitational restoring force is comparable to the thermal pressure. In the case of a dSph galaxy (Grebel et al. 2003; Blitz & Robishaw 2000), if ρ_{halo} is the mass density of a homogenous hot halo, v_{sat} the relative velocity of the satellite dwarf galaxy, M_0 the core mass of the dwarf galaxy, and $\rho_{sat,0}$ the central mass density of the satellite dwarf galaxy, then instantaneous ram pressure stripping occurs when

$$\rho_{halo} v_{sat}^2 > \frac{GM_0 \rho_{sat,0}}{3r_0} \quad (4.8)$$

It may seem counterintuitive that those models which have a less dense wind (representing a less dense static halo through which a dwarf is moving) are stripped in the 300 km s⁻¹ wind models (A2 and B2) while a model with a denser halo, which also experiences

a 300 km s^{-1} wind, does not undergo a rapid stripping event by 600 Myr. However, the central density varies greatly between these two models, and so this result is consistent with predictions from the ram pressure analysis.

The magnitude of ram pressure exerted on the gas in a dwarf can be approximated by ρv^2 where ρ is the halo density and v is the relative velocity of the dwarf with respect to the hot halo gas. In Figure 4.6, the ram pressure criterion for instantaneous stripping is shown by the solid line. In the simplest model of ram pressure stripping, satellites which lie above this line are expected to be entirely stripped of their gas on relatively rapid timescales, whereas those that lie below the line are expected to retain their gas. Of the simulated dwarf galaxies, two (A2 and B2) meet the criteria for ram pressure stripping, while four of the models (A1, B1, C1, and C2) do not.

Figure 4.1 shows the fraction of the initial gas mass remaining as a function of time. For those simulated dwarfs meeting the ram pressure criteria, both show a rapid, nearly instantaneous stripping event which occurs soon after they begin to experience the wind. The period of very rapid mass loss leading to complete destruction seen in models A2 and B2 at 440 Myr and 470 Myr respectively indicates these dwarfs undergo ram pressure stripping. Remaining models show a period of linear mass loss. This behavior is likely due to characteristic instabilities, primarily the Kelvin-Helmholtz instability on the dwarf/hot halo interface, and which can be clearly seen in Figure 4.2, Figure 4.3, and Figure 4.4.

4.3.6 Kelvin-Helmholtz Instability

Instantaneous ram pressure stripping is not the only means by which an orbiting satellite galaxy may lose gas. The Kelvin-Helmholtz (KH) instability occurs at the interface between two fluids experiencing shear motion. As a satellite dwarf galaxy orbits a more massive host, a KH instability can develop between the hot ambient ISM of the host galaxies and the gas within the dwarf galaxy. This can lead to gas loss in addition to ram-pressure stripping. While ram pressure stripping is taken to be an instantaneous or nearly instantaneous process, dynamical stripping due to the KH instability occurs over a non-negligible period of time.

Following Nulsen (1982) mass loss rate of a galaxy due to the KH instability can be estimated by taking the cross section of the dwarf times the momentum imparted by the ambient medium,

$$\dot{M}_{KH} = \pi r_0^2 \rho_{halo} v_{sat} \quad (4.9)$$

where r_0 is the radius of the dwarf as it experiences the effective wind, ρ_{halo} is the ambient hot halo density, and v_{sat} is the relative velocity between the satellite and halo medium. In our models, the radius r_0 can be determined from the simulations by direct measurement after the wind has been applied and the dwarf has stabilized in size. As measured from the gas profiles of the models over time, r_0 remains fairly constant over the length of our simulations. ρ_{halo} and v_{sat} are constant within each model, and can be found in Table 4.1.

Consistent with the analytic mass loss equation, the mass loss rate due to KH insta-

bilities does not vary over time. For the vast majority of the lifetime of the dwarf, the mass loss rate is independent of the remaining HI mass of the satellite. The mass loss rate for run A1 shows this in Figure 4.1, where the mass loss shows a fixed rate from the time when 90% of the dwarf's gas mass remains to when only 20% of the initial gas mass remains. Only in the very late stages of stripping, when less than 20% of the original mass of the dwarf remains, there is a short divergence from the linear trend.

However, these simulations do not agree with the dependencies of the analytic description. In the case of identical dwarf galaxies being stripped by the same halo medium and having varying orbital speeds, one would expect the mass loss to scale linearly with velocity. This is the case of models C1 and C2, which are below the ram pressure criterion, have identical initial conditions, and vary only in the wind velocity. This makes them a very clean test of the dependency of mass loss on the wind velocity. In C2, the wind velocity is 1.5 times the wind velocity of C1. Both C1 and C2 show linear mass loss over their simulated lifetimes. However, the extrapolated survival time for C1 is 3250 years, while that of C2 is 1300. Thus the lifetimes differ by a factor of 2.5 times. This is due to one of two scenarios. It is either possible that the result that the swept-up mass as described by Nulsen does not accurately describe the mass loss due to the relevant instabilities. The second is that this reflects a limitation of the models presented here due to complex interactions with the dwarf which are not well modeled by the wind tunnel with constant wind or due to the two dimensionality of the simulations.

4.3.7 Models as Compared to Observations

The initial conditions of the models compare well to the expected characteristics of Local Group dwarfs and their environment. The true halo density at a given distance is not well constrained because the hot halo is difficult to detect directly, but according to models the values are typical of galactocentric distances less than 200 kpc (Kaufmann et al. 2007, 2008; Sommer-Larsen 2006). In order to include some models which were expected to be dominated by ram-pressure stripping as well some expected to be dominated by dynamical stripping, the chosen velocities are a bit higher than the average expected orbital velocities for dwarf galaxies. They are still well within the range of observed optical velocities of dwarf galaxies. Observationally, four Local Group dwarfs have measured proper motions, and their expected perigalacticon velocities agree with the values of 200 km s^{-1} and 300 km s^{-1} adopted for the models.

As discussed in Chapter 1, all known ultra-faint dwarfs in the Local Group except for Leo T lack detectable HI gas. All known ultra-faint satellites of the Milky Way except Leo T also have galactocentric distances within 250 kpc, and classical dwarfs with gas tend to lie within 270 kpc (see Chapter 1). The lack of gas for low mass dwarfs at low galactocentric radii is in agreement with these models. As long as these dwarfs have been orbiting within or near their current Galactocentric radius for at least several Gyr, their gas should be removed through interactions with the halo medium as seen in the models presented here. For dwarfs which are not on a first passage, this is a reasonable assumption since dwarfs are expected to be preferentially observed near apogalacticon rather than perigalacticon due to timing arguments. The halo medium at distances of Leo

T (420 kpc) are expected to fall below the minimum halo densities tested here, and so the presence of HI in Leo T or dwarfs on the outskirts of the Local Group does not conflict with these models, although further simulations of lower density halo media are needed to see if dwarfs at these distances would be predicted to retain gas.

Some classical Local Group dwarf galaxies frequently show gas clouds in the vicinity but offset from the optical center of the dwarf, as in the case of Sculptor and Fornax. It is possible that these clouds represent gas which was stripped from these galaxies, although proving this association would be difficult in practice. However, we also do not see gas being stripped in a coherent, high column clouds in these models.

4.3.8 Implications for Dwarf Galaxy Evolution

Gas loss due to ram pressure and dynamical stripping has the potential to significantly impact the evolution of low-mass dwarf galaxies. If the lowest mass dwarfs are susceptible to complete stripping on timescales of a few Gyr at velocities and densities typical of what they would experience in the course of their orbits, this could quench star formation and fundamentally alter the nature of the dwarfs. Compression is seen on the leading edge of the dwarf, which could trigger star formation. Alternately, disruption, redistribution, or loss of the dwarf's gas may reduce the efficiency of star formation. The loss of significant quantities of gas obviously reduces the total available star formation fuel for the dwarf. Confirmation of these results with an evolving wind is necessary, but it is likely that ram pressure and dynamical stripping can remove a significant fraction of gas mass in Local Group dwarfs with typical characteristics of ultra-faint dwarfs, and likely have

contributed to the removal of gas in these dwarfs if the gas has not been already removed by other mechanisms. This mechanism is most likely to be at work for dwarf galaxies which have intermediate age stellar populations, as this indicates they retained sufficient gas to form stars over a non-negligible fraction of their lifespan. Examples of dwarfs are the classical dSph population, as well as Leo T and Canis Venatici I.

4.4 Summary

The results of these simulations support the hypothesis that rapid gas loss occurs when the ram pressure stripping criterion is met, and that complete stripping of the dwarf galaxy occurs with a timescale of about half a Gyr for the dwarf galaxies simulated here. This stripping would occur in less than an orbital period as these dwarfs have typical orbital periods on the order of a few Gyrs.

In the cases where the ram pressure criterion is not met, there is still a significant level of gas loss experienced by the dwarfs. This gas loss appears to occur at a linear rate which is mainly independent of the remaining dwarf gas mass. For the 2D models presented here, the dependencies of the mass loss rate on velocity do not agree with the predictions of simple analytical models of gas loss due to the Kelvin-Helmholtz instability. This likely indicates that either the models are inaccurate or that our models are limited due to being two-dimensional.

Extrapolating the stripping timescales for those dwarf models which do not meet the ram pressure stripping criterion, we expect the survival timescales of these dwarfs to be between 1.1 and 3.3 Gyr, depending on the specific original characteristics of the

dwarf and halo medium. This suggests that dSph dwarfs may have been significantly affected by their interaction with the medium of their host galaxy on timescales which are comparable to the orbital timescales of the dwarf galaxies, even if they do not meet the ram pressure criterion. These models suggest that the observed lack of gas in classical dSph within 250 kpc can be explained through ram-pressure and dynamical mass loss occurring due to interactions between the satellite galaxy and hot halo gas.

Table 4.1. Parameters for Models

Model Name	Halo Gas Gas Density ρ_2 (cm^{-3})	Halo Gas Temperature T_2 (K)	Central Dwarf Density ρ_0 (cm^{-3})	Dwarf Gas Temperature T_1 (K)	$M_{gas,sat}$ $r < 300\text{pc}$ (M_\odot)	Matching Radius R_m (pc)	M_{DM} $r < 300\text{pc}$ (M_\odot)	v_{wind} (km s^{-1})
A1	4.6×10^{-5}	7.4×10^5	0.05	9.2×10^3	1.4×10^4	300	1×10^7	200
A2	4.6×10^{-5}	7.4×10^5	0.05	9.2×10^3	1.4×10^4	300	1×10^7	300
B1	1.5×10^{-4}	7.5×10^5	0.35	8.1×10^3	5.6×10^4	300	1×10^7	200
B2	1.5×10^{-4}	7.5×10^5	0.35	8.1×10^3	5.6×10^4	300	1×10^7	300
C1	4.5×10^{-4}	8.1×10^5	1.7	7.2×10^3	2.3×10^5	300	1×10^7	200
C2	4.5×10^{-4}	8.1×10^5	1.7	7.2×10^3	2.3×10^5	300	1×10^7	300

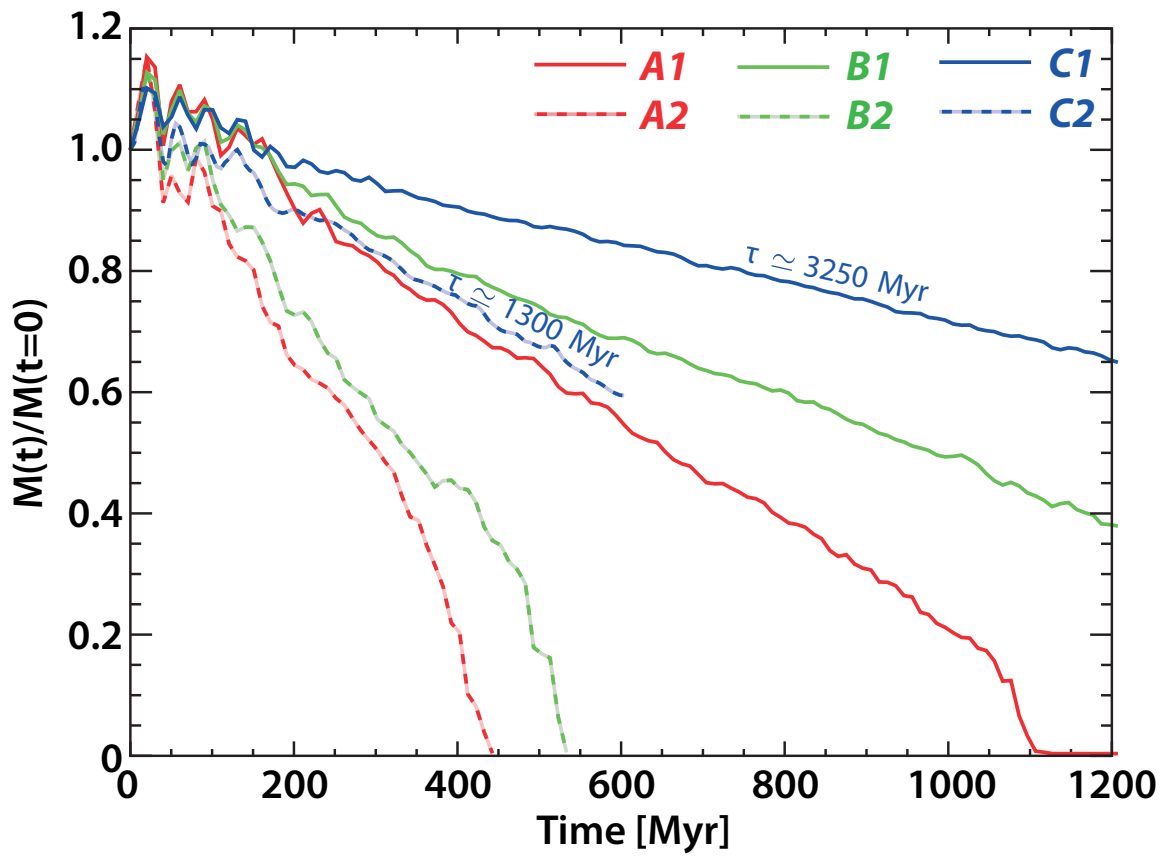


Figure 4.1 Fractional gas mass in the dwarf's original extent ($r = 300$ pc) over time.

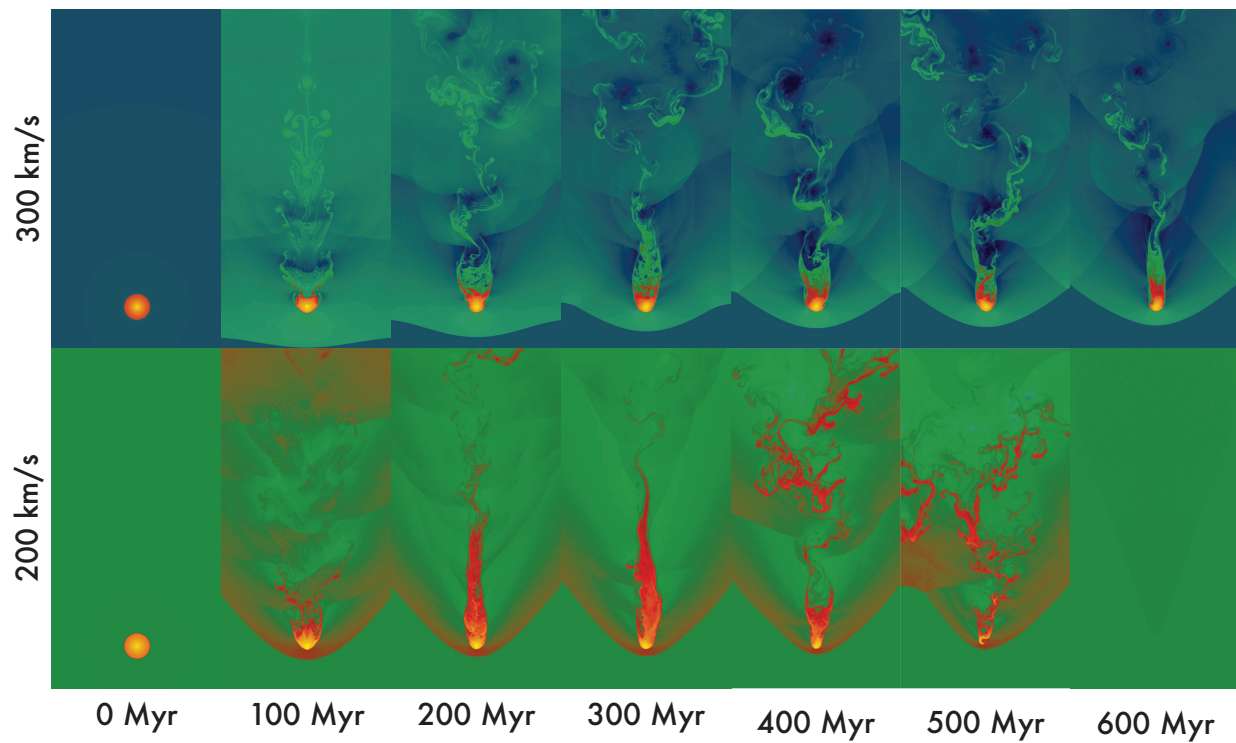


Figure 4.2 Model A1 (Top) and A2 (Bottom). Simulations are shown at 7 intermediate timesteps each. Scaling is consistent between time periods but varies between models to show detail. Density is on a log scale ranging from 0.05 to $4.6 \times 10^{-5} \text{ cm}^{-3}$.

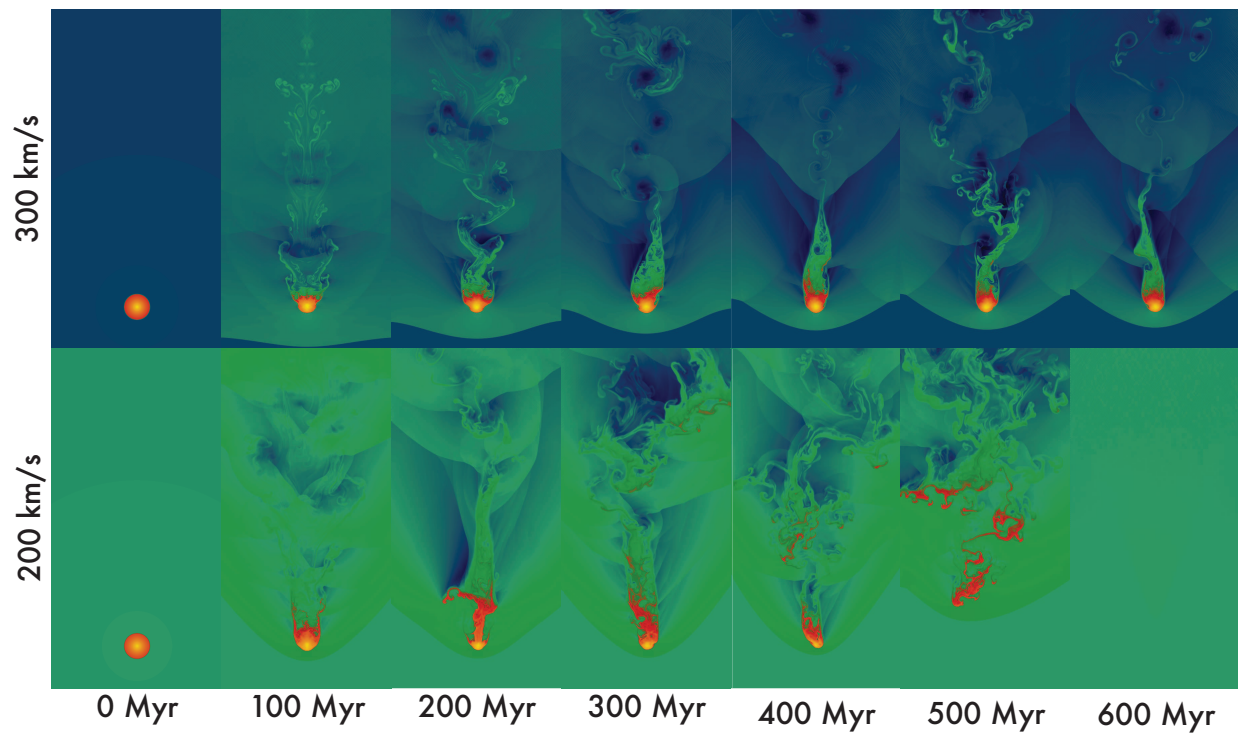


Figure 4.3 Models B1 (Top) and B2 (Bottom). Simulations are shown at 7 intermediate timesteps each. Scaling is consistent between time periods but varies between models to show detail. Density is on a log scale ranging from 0.35 to $1.5 \times 10^{-4} \text{ cm}^{-3}$.

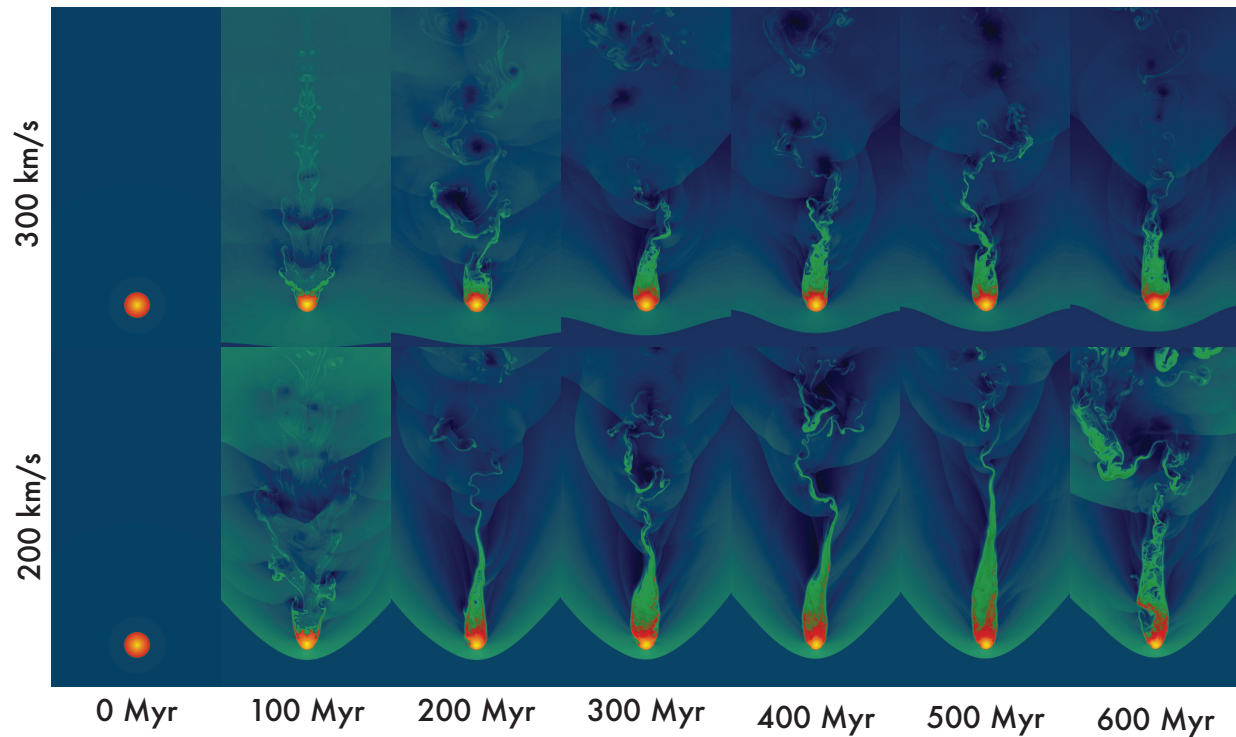


Figure 4.4 Models C1 (Top) and C2 (Bottom). Simulations are shown at 7 intermediate timesteps each. Scaling is consistent between time periods but varies between models to show detail. Density is on a log scale ranging from 1.7 to $4.5 \times 10^{-4} \text{ cm}^{-3}$.

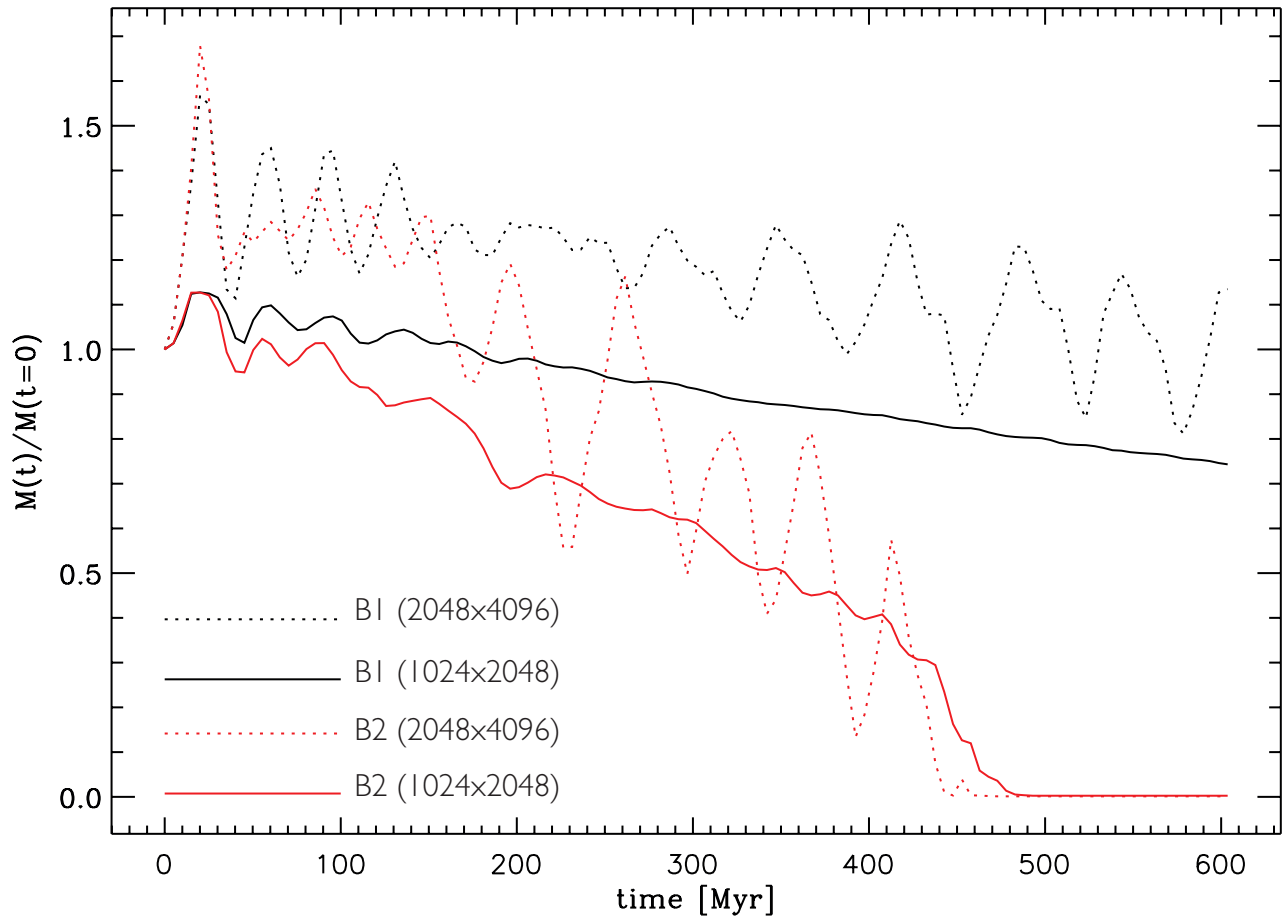


Figure 4.5 Fractional mass loss for the B1 and B2 models, which have resolutions of 1024 x 2048, along with models having identical initial conditions and wind characteristic, but twice the resolution (2048 x 4096)

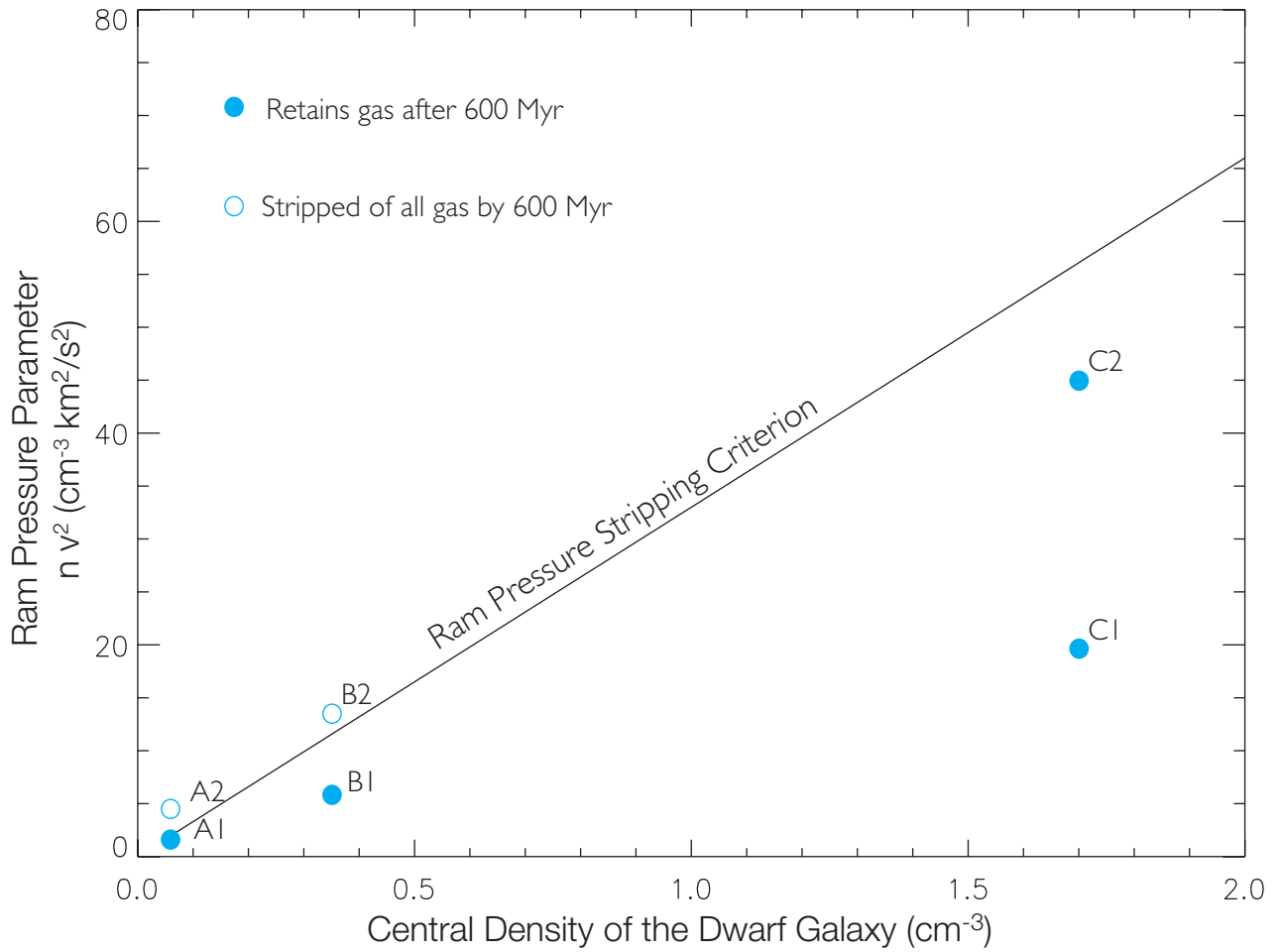


Figure 4.6 Ram pressure strength vs. the initial central density of the dwarf for the six models. Red dots have a 300 km/s wind, blue a 200 km/s wind.

Chapter 5

Conclusion

5.1 Future Work

5.1.1 Searching for Unknown Local Group Dwarf Galaxies

The identification of the 51 candidate clouds presented in Chapter 3 is promising for the prospects of HI-motivated dwarf galaxy searches. Deep optical observations of a small subset ($n = 10$) of the dwarf galaxies candidates has been undertaken at the 2.4m Hiltner telescope at MDM observatory, and additional observations are scheduled at the 3.5m WIYN telescope using the One Degree Imager (ODI). No obvious presence of galaxies at the position of the candidates was seen in the calibrated images from completed observations, but none would be expected. Once photometry is complete, deeper CMDs for these galaxies can be constructed which may reveal stellar populations. In addition, the GALFA-HI survey is ongoing, and processing the data from additional regions of sky

through the cataloging algorithm may reveal additional candidates.

5.1.2 Dwarf Galaxy Simulations

The natural next step is to extend the simulations presented in Chapter 4 to simulations including an evolving velocity and density wind which would more accurately model a low-mass dwarf galaxy's orbit. In addition, extending the simulations to three dimensions may increase their accuracy. The framework for both these extensions of the models already exist. The eventual goal is an analytic description of the dependency of the mass loss rates on the satellite's gas characteristics, dark matter halo properties, background density, and hot halo characteristics.

As the proper motions of stars within Local Group dwarf galaxies is measured more accurately, better constrained orbital histories of the dwarfs will become available. Combining the orbital histories with analytical models of stripping would help to tease out the relative impact of processes such as stellar feedback, ionizing radiation, and dynamical/ram pressure stripping in individual dwarfs. It may also be fruitful to combine analytical models of mass loss rates derived from high resolution ram-pressure stripping simulations with lower resolution cosmological simulations. This "meet in the middle" approach to physical processes which are unresolved in simulations shows promise to improve over either strategy in isolation. For example, Starckenburg et al. 2012 have combined the Aquarius dark matter simulations with semi-analytic models of galaxy formation, and well reproduce the luminosity function, luminosity-metallicity relation, and radial distribution of Milky Way satellites. They note that there is an environmentally

dependent effect on the satellite's gas due to ram-pressure stripping, but their simulated satellite galaxies have too much cold gas as compared to observations. The authors note that this discrepancy might be solved by including more accurate ram pressure stripping (Starkenburger et al. 2012), but as seen in the models of Chapter 4, low level dynamical stripping of cold gas over long timescales might help to ameliorate this discrepancy.

Combining accurate mass loss rates, dark matter only cosmological simulations, and a suite of hot halo models could yield an expected distribution of gas-rich and gas-poor dwarfs on the smallest mass scales. Another approach is to improve the gas loss approximations used in semi-analytic cosmological simulations including gas, which are far from resolving these small scale effects. In either case, once one has a predicted distribution of gas-containing satellites, a comparison to the observed distribution of such dwarfs could be conducted. While other mass loss factors are likely at play, these generally work to increase the gas loss rates, and so the presence of too many gas-rich dwarfs at a given galactocentric radius may rule out certain halo densities at that distance.

5.2 Conclusion

Our picture of Local Group dwarf galaxies has changed dramatically over the past decade. Not only have half the current members of the Local Group been discovered in that time, but our understanding of their nature has vastly improved. For example, studies of the resolved stellar populations of the lowest mass dwarf galaxies allow insight into their evolution through their distribution, metallicity, and ages. While these advances on the stellar front are exciting, stars are not the only means by which to study low mass dwarfs.

Neutral hydrogen in dwarf galaxies, and particularly faint, low mass dwarfs, can provide evidence for environmental gas loss mechanisms, measure the hot halo gas of the Milky Way, and reveal the presence of hidden ultra-faint dwarfs.

Bibliography

Abazajian, K. N., Adelman-McCarthy, J. K., Agüeros, M. A., Allam, S. S., Allende Prieto, C., An, D., Anderson, K. S. J., Anderson, S. F., Annis, J., Bahcall, N. A., & et al. 2009, *ApJS*, 182, 543

Armandroff, T. E., Davies, J. E., & Jacoby, G. H. 1998, *AJ*, 116, 2287

Armandroff, T. E., Jacoby, G. H., & Davies, J. E. 1999, *AJ*, 118, 1220

Arnal, E. M., Bajaja, E., Larrarte, J. J., Morras, R., & Pöppel, W. G. L. 2000, *A&AS*, 142, 35

Bailin, J., & Ford, A. 2007, *MNRAS*, 375, L41

Bajaja, E., Arnal, E. M., Larrarte, J. J., Morras, R., Pöppel, W. G. L., & Kalberla, P. M. W. 2005, *A&A*, 440, 767

Barnes, D. G., Staveley-Smith, L., de Blok, W. J. G., Oosterloo, T., Stewart, I. M., Wright, A. E., Banks, G. D., Bhathal, R., Boyce, P. J., Calabretta, M. R., Disney, M. J., Drinkwater, M. J., Ekers, R. D., Freeman, K. C., Gibson, B. K., Green, A. J., Haynes, R. F., te Lintel Hekkert, P., Henning, P. A., Jerjen, H., Juraszek, S., Kesteven, M. J., Kilborn, V. A., Knezek, P. M., Koribalski, B., Kraan-Korteweg, R. C., Malin, D. F., Marquarding, M.,

- Minchin, R. F., Mould, J. R., Price, R. M., x, M. E., Ryder, S. D., Sadler, E. M., Schröder, A., Stootman, F., Webster, R. L., Wilson, W. E., & Ye, T. 2001, *MNRAS*, 322, 486
- Battaner, E., & Florido, E. 2000, *Fundamentals of Cosmic Physics*, 21, 1
- Belokurov, V., Evans, N. W., Irwin, M. J., Lynden-Bell, D., Yanny, B., Vidrih, S., Gilmore, G., Seabroke, G., Zucker, D. B., Wilkinson, M. I., Hewett, P. C., Bramich, D. M., Fellhauer, M., Newberg, H. J., Wyse, R. F. G., Beers, T. C., Bell, E. F., Barentine, J. C., Brinkmann, J., Cole, N., Pan, K., & York, D. G. 2007a, *ApJ*, 658, 337
- . 2007b, *ApJ*, 658, 337
- Belokurov, V., Walker, M. G., Evans, N. W., Faria, D. C., Gilmore, G., Irwin, M. J., Koposov, S., Mateo, M., Olszewski, E., & Zucker, D. 2008, *ArXiv e-prints*, 807
- Belokurov, V., Zucker, D. B., Evans, N. W., Gilmore, G., Vidrih, S., Bramich, D. M., Newberg, H. J., Wyse, R. F. G., Irwin, M. J., Fellhauer, M., Hewett, P. C., Walton, N. A., Wilkinson, M. I., Cole, N., Yanny, B., Rockosi, C. M., Beers, T. C., Bell, E. F., Brinkmann, J., Ivezić, Ž., & Lupton, R. 2006a, *ApJ*, 642, L137
- Belokurov, V., Zucker, D. B., Evans, N. W., Kleyana, J. T., Koposov, S., Hodgkin, S. T., Irwin, M. J., Gilmore, G., Wilkinson, M. I., Fellhauer, M., Bramich, D. M., Hewett, P. C., Vidrih, S., De Jong, J. T. A., Smith, J. A., Rix, H.-W., Bell, E. F., Wyse, R. F. G., Newberg, H. J., Mayeur, P. A., Yanny, B., Rockosi, C. M., Gnedin, O. Y., Schneider, D. P., Beers, T. C., Barentine, J. C., Brewington, H., Brinkmann, J., Harvanek, M., Kleinman, S. J., Krzesinski, J., Long, D., Nitta, A., & Snedden, S. A. 2007c, *ApJ*, 654, 897

- Belokurov, V., Zucker, D. B., Evans, N. W., Wilkinson, M. I., Irwin, M. J., Hodgkin, S., Bramich, D. M., Irwin, J. M., Gilmore, G., Willman, B., Vidrih, S., Newberg, H. J., Wyse, R. F. G., Fellhauer, M., Hewett, P. C., Cole, N., Bell, E. F., Beers, T. C., Rockosi, C. M., Yanny, B., Grebel, E. K., Schneider, D. P., Lupton, R., Barentine, J. C., Brewington, H., Brinkmann, J., Harvanek, M., Kleinman, S. J., Krzesinski, J., Long, D., Nitta, A., Smith, J. A., & Snedden, S. A. 2006b, *ApJ*, 647, L111
- Benson, A. J., Frenk, C. S., Lacey, C. G., Baugh, C. M., & Cole, S. 2002, *MNRAS*, 333, 177
- Bhatnagar, P. L., Gross, E. P., & Krook, M. 1954, *Physical Review*, 94, 511
- Binggeli, B. 1994, in *Panchromatic View of Galaxies. Their Evolutionary Puzzle*, ed. G. Hensler, C. Theis, & J. S. Gallagher, 173
- Bland-Hawthorn, J., Veilleux, S., Cecil, G. N., Putman, M. E., Gibson, B. K., & Maloney, P. R. 1998, *MNRAS*, 299, 611
- Blitz, L., & Robishaw, T. 2000, *ApJ*, 541, 675
- Bouchard, A., Carignan, C., & Staveley-Smith, L. 2006, *AJ*, 131, 2913
- Bouchard, A., Jerjen, H., Da Costa, G. S., & Ott, J. 2005, *AJ*, 130, 2058
- Bovill, M. S., & Ricotti, M. 2009, *ApJ*, 693, 1859
- Brown, T. M., Tumlinson, J., Geha, M., Kirby, E. N., Vandenberg, D. A., Muñoz, R. R., Kalirai, J. S., Simon, J. D., Avila, R. J., Guhathakurta, P., Renzini, A., & Ferguson, H. C. 2012, *ApJ*, 753, L21

Brown, W. R., Geller, M. J., Kenyon, S. J., & Kurtz, M. J. 2007, *ApJ*, 666, 231

Brüns, C., Kerp, J., Staveley-Smith, L., Mebold, U., Putman, M. E., Haynes, R. F., Kalberla, P. M. W., Muller, E., & Filipovic, M. D. 2005, *A&A*, 432, 45

Bullock, J. S., Kravtsov, A. V., & Weinberg, D. H. 2000, *ApJ*, 539, 517

—. 2001, *ApJ*, 548, 33

Burles, S., Nollett, K. M., & Turner, M. S. 2001, *ApJ*, 552, L1

Cannon, J. M., Giovanelli, R., Haynes, M. P., Janowiecki, S., Parker, A., Salzer, J. J., Adams, E. A. K., Engstrom, E., Huang, S., McQuinn, K. B. W., Ott, J., Saintonge, A., Skillman, E. D., Allan, J., Erny, G., Fliss, P., & Smith, A. 2011, *ApJ*, 739, L22

Carignan, C., Beaulieu, S., Côté, S., Demers, S., & Mateo, M. 1998, *AJ*, 116, 1690

Carignan, C., Beaulieu, S., & Freeman, K. C. 1990, *AJ*, 99, 178

Chiappini, C., Matteucci, F., & Romano, D. 2001, *ApJ*, 554, 1044

Clementini, G., Cignoni, M., Contreras Ramos, R., Federici, L., Ripepi, V., Marconi, M., Tosi, M., & Musella, I. 2012, *ApJ*, 756, 108

Dalgarno, A., & McCray, R. A. 1972, *ARA&A*, 10, 375

Dekel, A., & Silk, J. 1986, *ApJ*, 303, 39

Diemand, J., Kuhlen, M., & Madau, P. 2007, *ApJ*, 667, 859

Dijkstra, M., Haiman, Z., Rees, M. J., & Weinberg, D. H. 2004, *ApJ*, 601, 666

Efstathiou, G. 1992, MNRAS, 256, 43P

Einasto, J., Saar, E., Kaasik, A., & Chernin, A. D. 1974, Nature, 252, 111

Fenner, Y., & Gibson, B. K. 2003, Publications of the Astronomical Society of Australia, 20, 189

Ferguson, A. M. N., Gallagher, J. S., & Wyse, R. F. G. 2000, AJ, 120, 821

Fukugita, M. 2004, in IAU Symposium, Vol. 220, Dark Matter in Galaxies, ed. S. Ryder, D. Pisano, M. Walker, & K. Freeman, 227

Fukugita, M., Hogan, C. J., & Peebles, P. J. E. 1998, ApJ, 503, 518

Gaensler, B. M., Madsen, G. J., Chatterjee, S., & Mao, S. A. 2008, ArXiv e-prints

Giovanelli, R., Haynes, M. P., Kent, B. R., & Adams, E. A. K. 2010, ApJ, 708, L22

Gnedin, N. Y. 2000, ApJ, 542, 535

Gnedin, N. Y., & Kravtsov, A. V. 2006, ApJ, 645, 1054

Governato, F., Zolotov, A., Pontzen, A., Christensen, C., Oh, S. H., Brooks, A. M., Quinn, T., Shen, S., & Wadsley, J. 2012, MNRAS, 422, 1231

Grcevich, J., & Putman, M. E. 2009, ApJ, 696, 385

Grebel, E. K., & Gallagher, III, J. S. 2004, ApJ, 610, L89

Grebel, E. K., Gallagher, III, J. S., & Harbeck, D. 2003, Astronomische Nachrichten Supplement, 324, 90

Gunn, J. E., & Gott, J. R. I. 1972, *ApJ*, 176, 1

Harbeck, D., Grebel, E. K., Holtzman, J., Guhathakurta, P., Brandner, W., Geisler, D., Sarajedini, A., Dolphin, A., Hurley-Keller, D., & Mateo, M. 2001, *AJ*, 122, 3092

Hartmann, D., & Burton, W. B. 1997, *Atlas of Galactic Neutral Hydrogen* (*Atlas of Galactic Neutral Hydrogen*, by Dap Hartmann and W. Butler Burton, pp. 243. ISBN 0521471117. Cambridge, UK: Cambridge University Press, February 1997.)

Heitsch, F., & Putman, M. E. 2009, *ApJ*, 698, 1485

Hoffman, G. L., Salpeter, E. E., Farhat, B., Roos, T., Williams, H., & Helou, G. 1996, *ApJS*, 105, 269

Huchra, J. P., Vogeley, M. S., & Geller, M. J. 1999, *ApJS*, 121, 287

Huchtmeier, W. K., & Richter, O. G. 1986, *A&AS*, 63, 323

Huchtmeier, W. K., & Richter, O.-G. 1988, *A&A*, 203, 237

Hulsbosch, A. N. M., & Wakker, B. P. 1988, *A&AS*, 75, 191

Humason, M. L., Mayall, N. U., & Sandage, A. R. 1956, *AJ*, 61, 97

Ibata, R., Martin, N. F., Irwin, M., Chapman, S., Ferguson, A. M. N., Lewis, G. F., & McConnachie, A. W. 2007, *ApJ*, 671, 1591

Irwin, J. A., Hoffman, G. L., Spekkens, K., Haynes, M. P., Giovanelli, R., Linder, S. M., Catinella, B., Momjian, E., Koribalski, B. S., Davies, J., Brinks, E., de Blok, W. J. G., Putman, M. E., & van Driel, W. 2009, *ApJ*, 692, 1447

Irwin, M., & Tolstoy, E. 2002, *MNRAS*, 336, 643

Irwin, M. J., Belokurov, V., Evans, N. W., Ryan-Weber, E. V., de Jong, J. T. A., Koposov, S., Zucker, D. B., Hodgkin, S. T., Gilmore, G., Prema, P., Hebb, L., Begum, A., Fellhauer, M., Hewett, P. C., Kennicutt, Jr., R. C., Wilkinson, M. I., Bramich, D. M., Vidrih, S., Rix, H.-W., Beers, T. C., Barentine, J. C., Brewington, H., Harvanek, M., Krzesinski, J., Long, D., Nitta, A., & Snedden, S. A. 2007, *ApJ*, 656, L13

Irwin, M. J., Ferguson, A. M. N., Huxor, A. P., Tanvir, N. R., Ibata, R. A., & Lewis, G. F. 2008, *ApJ*, 676, L17

Jarosik, N., Bennett, C. L., Dunkley, J., Gold, B., Greason, M. R., Halpern, M., Hill, R. S., Hinshaw, G., Kogut, A., Komatsu, E., Larson, D., Limon, M., Meyer, S. S., Nolta, M. R., Odegard, N., Page, L., Smith, K. M., Spergel, D. N., Tucker, G. S., Weiland, J. L., Wollack, E., & Wright, E. L. 2011, *ApJS*, 192, 14

Kalberla, P. M. W., Burton, W. B., Hartmann, D., Arnal, E. M., Bajaja, E., Morras, R., & Pöppel, W. G. L. 2005, *A&A*, 440, 775

Karachentsev, I. D., & Karachentseva, V. E. 1999, *A&A*, 341, 355

Kaufmann, T., Bullock, J. S., Maller, A., & Fang, T. 2008, *ArXiv e-prints*, 801

Kaufmann, T., Mayer, L., Wadsley, J., Stadel, J., & Moore, B. 2007, *MNRAS*, 375, 53

Klypin, A., Kravtsov, A. V., Valenzuela, O., & Prada, F. 1999, *ApJ*, 522, 82

Knapp, G. R., Kerr, F. J., & Bowers, P. F. 1978, *AJ*, 83, 360

Komatsu, E., Smith, K. M., Dunkley, J., Bennett, C. L., Gold, B., Hinshaw, G., Jarosik, N., Larson, D., Nolta, M. R., Page, L., Spergel, D. N., Halpern, M., Hill, R. S., Kogut, A., Limon, M., Meyer, S. S., Odegard, N., Tucker, G. S., Weiland, J. L., Wollack, E., & Wright, E. L. 2011, *ApJS*, 192, 18

Koposov, S., Belokurov, V., Evans, N. W., Hewett, P. C., Irwin, M. J., Gilmore, G., Zucker, D. B., Rix, H. ., Fellhauer, M., Bell, E. F., & Glushkova, E. V. 2007a, *ArXiv e-prints*, 706

Koposov, S., de Jong, J. T. A., Belokurov, V., Rix, H.-W., Zucker, D. B., Evans, N. W., Gilmore, G., Irwin, M. J., & Bell, E. F. 2007b, *ApJ*, 669, 337

—. 2007c, *ApJ*, 669, 337

Koribalski, B., Johnston, S., & Otrupcek, R. 1994, *MNRAS*, 270, L43+

Kormendy, J. 1985, *ApJ*, 295, 73

Koyama, H., & Inutsuka, S.-I. 2000, *ApJ*, 532, 980

Kuhlen, M. 2010, *Advances in Astronomy*, 2010

Lake, G., & Skillman, E. D. 1989, *AJ*, 98, 1274

Lewis, G. F., Ibata, R. A., Chapman, S. C., McConnachie, A., Irwin, M. J., Tolstoy, E., & Tanvir, N. R. 2007, *MNRAS*, 375, 1364

Li, Z., Wang, Q. D., & Hameed, S. 2007, *MNRAS*, 376, 960

Lin, D. N. C., & Faber, S. M. 1983, *ApJ*, 266, L21

Lo, K. Y., Sargent, W. L. W., & Young, K. 1993, *AJ*, 106, 507

Longmore, A. J., Hawarden, T. G., Goss, W. M., Mebold, U., & Webster, B. L. 1982, *MNRAS*, 200, 325

Lufkin, G., Quinn, T., Wadsley, J., Stadel, J., & Governato, F. 2004, *MNRAS*, 347, 421

Madau, P., Kuhlen, M., Diemand, J., Moore, B., Zemp, M., Potter, D., & Stadel, J. 2008, ArXiv e-prints

Majewski, S. R., Beaton, R. L., Patterson, R. J., Kalirai, J. S., Geha, M. C., Muñoz, R. R., Seigar, M. S., Guhathakurta, P., Gilbert, K. M., Rich, R. M., Bullock, J. S., & Reitzel, D. B. 2007, *ApJ*, 670, L9

Maller, A. H., & Bullock, J. S. 2004, *MNRAS*, 355, 694

Martin, N. F., Ibata, R. A., Chapman, S. C., Irwin, M., & Lewis, G. F. 2007, *MNRAS*, 380, 281

Martin, N. F., Ibata, R. A., Irwin, M. J., Chapman, S., Lewis, G. F., Ferguson, A. M. N., Tanvir, N., & McConnachie, A. W. 2006, *MNRAS*, 371, 1983

Martin, N. F., McConnachie, A. W., Irwin, M., Widrow, L. M., Ferguson, A. M. N., Ibata, R. A., Dubinski, J., Babul, A., Chapman, S., Fardal, M., Lewis, G. F., Navarro, J., & Rich, R. M. 2009, *ApJ*, 705, 758

Mateo, M. L. 1998, *ARA&A*, 36, 435

Mayer, L., Mastropietro, C., Wadsley, J., Stadel, J., & Moore, B. 2006, *MNRAS*, 369, 1021

Mayer, L., & Moore, B. 2004, MNRAS, 354, 477

McConnachie, A. W. 2012, AJ, 144, 4

McKernan, B., Yaqoob, T., & Reynolds, C. S. 2004, ApJ, 617, 232

Merrett, H. R., Merrifield, M. R., Douglas, N. G., Kuijken, K., Romanowsky, A. J., Napolitano, N. R., Arnaboldi, M., Capaccioli, M., Freeman, K. C., Gerhard, O., Coccato, L., Carter, D., Evans, N. W., Wilkinson, M. I., Halliday, C., & Bridges, T. J. 2006, MNRAS, 369, 120

Moore, B., Diemand, J., Madau, P., Zemp, M., & Stadel, J. 2006, MNRAS, 368, 563

Moore, B., Ghigna, S., Governato, F., Lake, G., Quinn, T., Stadel, J., & Tozzi, P. 1999, ApJ, 524, L19

Mori, M., & Burkert, A. 2000, ApJ, 538, 559

Mori, M., Ferrara, A., & Madau, P. 2002, ApJ, 571, 40

Morrison, H. L., Harding, P., Hurley-Keller, D., & Jacoby, G. 2003, ApJ, 596, L183

Muñoz, J. A., Madau, P., Loeb, A., & Diemand, J. 2009, MNRAS, 400, 1593

Murakami, I., & Babul, A. 1999, MNRAS, 309, 161

Murray, S. D., White, S. D. M., Blondin, J. M., & Lin, D. N. C. 1993, ApJ, 407, 588

Navarro, J. F., Frenk, C. S., & White, S. D. M. 1995, MNRAS, 275, 56

- Newberg, H. J., Yanny, B., Cole, N., Beers, T. C., Re Fiorentin, P., Schneider, D. P., & Wilhelm, R. 2007, *ApJ*, 668, 221
- Newberg, H. J., Yanny, B., Rockosi, C., Grebel, E. K., Rix, H.-W., Brinkmann, J., Csabai, I., Hennessy, G., Hindsley, R. B., Ibata, R., Ivezić, Z., Lamb, D., Nash, E. T., Odenkirchen, M., Rave, H. A., Schneider, D. P., Smith, J. A., Stolte, A., & York, D. G. 2002, *ApJ*, 569, 245
- Nulsen, P. E. J. 1982, *MNRAS*, 198, 1007
- O'Meara, J. M., Burles, S., Prochaska, J. X., Prochter, G. E., Bernstein, R. A., & Burgess, K. M. 2006, *ApJ*, 649, L61
- Oosterloo, T., Da Costa, G. S., & Staveley-Smith, L. 1996, *AJ*, 112, 1969
- Peek, J. E. G., Heiles, C., Douglas, K. A., Lee, M.-Y., Grcevich, J., Stanimirović, S., Putman, M. E., Korpela, E. J., Gibson, S. J., Begum, A., Saul, D., Robishaw, T., & Krčo, M. 2011, *ApJS*, 194, 20
- Peek, J. E. G., Putman, M. E., McKee, C. F., Heiles, C., & Stanimirović, S. 2007, *ApJ*, 656, 907
- Peek, J. E. G., Putman, M. E., & Sommer-Larsen, J. 2008, *ApJ*, 674, 227
- Pettini, M., Zych, B. J., Murphy, M. T., Lewis, A., & Steidel, C. C. 2008, *MNRAS*, 391, 1499
- Piatek, S., Pryor, C., Bristow, P., Olszewski, E. W., Harris, H. C., Mateo, M., Minniti, D., & Tinney, C. G. 2005, *AJ*, 130, 95

—. 2006, *AJ*, 131, 1445

Piatek, S., Pryor, C., Olszewski, E. W., Harris, H. C., Mateo, M., Minniti, D., Monet, D. G., Morrison, H., & Tinney, C. G. 2002, *AJ*, 124, 3198

Piatek, S., Pryor, C., Olszewski, E. W., Harris, H. C., Mateo, M., Minniti, D., & Tinney, C. G. 2003, *AJ*, 126, 2346

Prendergast, K. H., & Xu, K. 1993, *Journal of Computational Physics*, 109, 53

Putman, M. E., de Heij, V., Staveley-Smith, L., Braun, R., Freeman, K. C., Gibson, B. K., Burton, W. B., Barnes, D. G., Banks, G. D., Bhathal, R., de Blok, W. J. G., Boyce, P. J., Disney, M. J., Drinkwater, M. J., Ekers, R. D., Henning, P. A., Jerjen, H., Kilborn, V. A., Knezek, P. M., Koribalski, B., Malin, D. F., Marquarding, M., Minchin, R. F., Mould, J. R., Oosterloo, T., Price, R. M., Ryder, S. D., Sadler, E. M., Stewart, I., Stootman, F., Webster, R. L., & Wright, A. E. 2002, *AJ*, 123, 873

Putman, M. E., Staveley-Smith, L., Freeman, K. C., Gibson, B. K., & Barnes, D. G. 2003, *ApJ*, 586, 170

Putman, M. E., Thom, C., Gibson, B. K., & Staveley-Smith, L. 2004, *ApJ*, 603, L77

Quilis, V., & Moore, B. 2001, *ApJ*, 555, L95

Rasmussen, J., Ponman, T. J., Mulchaey, J. S., Miles, T. A., & Raychaudhury, S. 2006, *MNRAS*, 373, 653

Ricotti, M., & Gnedin, N. Y. 2005, *ApJ*, 629, 259

Rubin, V. C., & Ford, Jr., W. K. 1970, *ApJ*, 159, 379

Ryan-Weber, E. V., Begum, A., Oosterloo, T., Pal, S., Irwin, M. J., Belokurov, V., Evans, N. W., & Zucker, D. B. 2008, *MNRAS*, 384, 535

Santiago-Figueroa, N., Putman, M. E., Werk, J., Meurer, G. R., & Ryan-Weber, E. 2011, *PASA*, 28, 271

Saul, D., Peek, J. E. G., Grcevich, J. M., & Putman, M. 2011, *ApJ*, submitted

Seigar, M. S., Barth, A. J., & Bullock, J. S. 2007, in *IAU Symposium, Vol. 235, IAU Symposium*, ed. F. Combes & J. Palous, 135–135

Sembach, K. R., Wakker, B. P., Savage, B. D., Richter, P., Meade, M., Shull, J. M., Jenkins, E. B., Sonneborn, G., & Moos, H. W. 2003, *ApJS*, 146, 165

Shull, J. M., Smith, B. D., & Danforth, C. W. 2011, *ArXiv e-prints*

Simon, J. D., & Geha, M. 2007, *ApJ*, 670, 313

Skillman, E. D., Terlevich, R., Teuben, P. J., & van Woerden, H. 1988, *A&A*, 198, 33

Slyz, A., & Prendergast, K. H. 1999, *A&AS*, 139, 199

Slyz, A. D., Devriendt, J. E. G., Silk, J., & Burkert, A. 2002, *MNRAS*, 333, 894

Somerville, R. S. 2002, *ApJ*, 572, L23

Sommer-Larsen, J. 2006, *ApJ*, 644, L1

Stanek, K. Z., & Garnavich, P. M. 1998, *ApJ*, 503, L131+

Stanimirović, S., Putman, M., Heiles, C., Peek, J. E. G., Goldsmith, P. F., Koo, B.-C., Krčo, M., Lee, J.-J., Mock, J., Muller, E., Pandian, J. D., Parsons, A., Tang, Y., & Werthimer, D. 2006, *ApJ*, 653, 1210

Starkenburg, E., Helmi, A., De Lucia, G., Li, Y.-S., Navarro, J. F., Font, A. S., Frenk, C. S., Springel, V., Vera-Ciro, C. A., & White, S. D. M. 2012, *ArXiv e-prints*

Strigari, L. E., Bullock, J. S., Kaplinghat, M., Diemand, J., Kuhlen, M., & Madau, P. 2007, *ApJ*, 669, 676

Strigari, L. E., Bullock, J. S., Kaplinghat, M., Simon, J. D., Geha, M., Willman, B., & Walker, M. G. 2008, *Nature*, 454, 1096

Thuan, T. X., & Martin, G. E. 1979, *ApJ*, 232, L11

Tollerud, E. J., Bullock, J. S., Strigari, L. E., & Willman, B. 2008, *ApJ*, 688, 277

Tolstoy, E., Hill, V., & Tosi, M. 2009, *ARA&A*, 47, 371

Tolstoy, E., & Irwin, M. 2000, *MNRAS*, 318, 1241

Tolstoy, E., Irwin, M., Cole, A., Fraternali, F., Szeifert, T., & Marconi, G. 2004, *The Messenger (ESO)*, 115, 32

van den Bergh, S. 1972, *ApJ*, 171, L31+

van den Bergh, S. 1999, in *IAU Symposium, Vol. 192, The Stellar Content of Local Group Galaxies*, ed. P. Whitelock & R. Cannon, 3–+

—. 2006, *AJ*, 132, 1571

van Loon, J. T., Stanimirović, S., Evans, A., & Muller, E. 2006, *MNRAS*, 365, 1277

Wakker, B., York, D. G., Wilhelm, R., Barentine, J. C., Richter, P., Beers, T. C., Ivezić, Ž., & Howk, J. C. 2008, *ApJ*, 672, 298

Wakker, B. P., Savage, B. D., Fox, A. J., Benjamin, R. A., & Shapiro, P. R. 2012, *ApJ*, 749, 157

Wakker, B. P., & van Woerden, H. 1997, *ARA&A*, 35, 217

Walker, M. G. 2012, ArXiv e-prints

Walker, M. G., Mateo, M., & Olszewski, E. W. 2008, *ApJ*, 688, L75

Walsh, S. M., Jerjen, H., & Willman, B. 2007, *ApJ*, 662, L83

Walsh, S. M., Willman, B., & Jerjen, H. 2009, *AJ*, 137, 450

Wang, Q. D., Yao, Y., Tripp, T. M., Fang, T.-T., Cui, W., Nicastro, F., Mathur, S., Williams, R. J., Song, L., & Croft, R. 2005, *ApJ*, 635, 386

Weisz, D. R., Dalcanton, J. J., Williams, B. F., Gilbert, K. M., Skillman, E. D., Seth, A. C., Dolphin, A. E., McQuinn, K. B. W., Gogarten, S. M., Holtzman, J., Rosema, K., Cole, A., Karachentsev, I. D., & Zaritsky, D. 2011, *ApJ*, 739, 5

White, S. D. M., & Frenk, C. S. 1991, *ApJ*, 379, 52

Whiting, A. B., Hau, G. K. T., & Irwin, M. 1999, *AJ*, 118, 2767

Willman, B., Blanton, M. R., West, A. A., Dalcanton, J. J., Hogg, D. W., Schneider, D. P., Wherry, N., Yanny, B., & Brinkmann, J. 2005a, *AJ*, 129, 2692

Willman, B., Dalcanton, J. J., Martinez-Delgado, D., West, A. A., Blanton, M. R., Hogg, D. W., Barentine, J. C., Brewington, H. J., Harvanek, M., Kleinman, S. J., Krzesinski, J., Long, D., Neilsen, Jr., E. H., Nitta, A., & Snedden, S. A. 2005b, *ApJ*, 626, L85

Wilman, R. J., Edge, A. C., Johnstone, R. M., Fabian, A. C., Allen, S. W., & Crawford, C. S. 2002, *MNRAS*, 337, 63

Wolfire, M. G., McKee, C. F., Hollenbach, D., & Tielens, A. G. G. M. 1995, *ApJ*, 453, 673

York, D. G., Adelman, J., Anderson, Jr., J. E., Anderson, S. F., Annis, J., Bahcall, N. A., Bakken, J. A., Barkhouser, R., Bastian, S., Berman, E., Boroski, W. N., Bracker, S., Briegel, C., Briggs, J. W., Brinkmann, J., Brunner, R., Burles, S., Carey, L., Carr, M. A., Castander, F. J., Chen, B., Colestock, P. L., Connolly, A. J., Crocker, J. H., Csabai, I., Czarapata, P. C., Davis, J. E., Doi, M., Dombeck, T., Eisenstein, D., Ellman, N., Elms, B. R., Evans, M. L., Fan, X., Federwitz, G. R., Fiscelli, L., Friedman, S., Frieman, J. A., Fukugita, M., Gillespie, B., Gunn, J. E., Gurbani, V. K., de Haas, E., Haldeman, M., Harris, F. H., Hayes, J., Heckman, T. M., Hennessy, G. S., Hindsley, R. B., Holm, S., Holmgren, D. J., Huang, C.-h., Hull, C., Husby, D., Ichikawa, S.-I., Ichikawa, T., Ivezić, Ž., Kent, S., Kim, R. S. J., Kinney, E., Klaene, M., Kleinman, A. N., Kleinman, S., Knapp, G. R., Korienek, J., Kron, R. G., Kunszt, P. Z., Lamb, D. Q., Lee, B., Leger, R. F., Limmongkol, S., Lindenmeyer, C., Long, D. C., Loomis, C., Loveday, J., Lucinio, R., Lupton, R. H., MacKinnon, B., Mannery, E. J., Mantsch, P. M., Margon, B., McGehee, P., McKay, T. A., Meiksin, A., Merelli, A., Monet, D. G., Munn, J. A., Narayanan, V. K., Nash, T., Neilsen, E., Neswold, R., Newberg, H. J., Nichol, R. C., Nicinski, T., Nonino, M., Okada, N., Okamura, S.,

Ostriker, J. P., Owen, R., Pauls, A. G., Peoples, J., Peterson, R. L., Petravick, D., Pier, J. R., Pope, A., Pordes, R., Prosapio, A., Rechenmacher, R., Quinn, T. R., Richards, G. T., Richmond, M. W., Rivetta, C. H., Rockosi, C. M., Ruthmansdorfer, K., Sandford, D., Schlegel, D. J., Schneider, D. P., Sekiguchi, M., Sergey, G., Shimasaku, K., Siegmund, W. A., Smee, S., Smith, J. A., Snedden, S., Stone, R., Stoughton, C., Strauss, M. A., Stubbs, C., SubbaRao, M., Szalay, A. S., Szapudi, I., Szokoly, G. P., Thakar, A. R., Tremonti, C., Tucker, D. L., Uomoto, A., Vanden Berk, D., Vogeley, M. S., Waddell, P., Wang, S.-i., Watanabe, M., Weinberg, D. H., Yanny, B., & Yasuda, N. 2000, *AJ*, 120, 1579

Young, L. M., & Lo, K. Y. 1997, *ApJ*, 476, 127

Zucker, D. B., Belokurov, V., Evans, N. W., Gilmore, G., & Wilkinson, M. I. 2006a, in *Bulletin of the American Astronomical Society*, Vol. 38, American Astronomical Society Meeting Abstracts, 178.05

Zucker, D. B., Belokurov, V., Evans, N. W., Kleyna, J. T., Irwin, M. J., Wilkinson, M. I., Fellhauer, M., Bramich, D. M., Gilmore, G., Newberg, H. J., Yanny, B., Smith, J. A., Hewett, P. C., Bell, E. F., Rix, H.-W., Gnedin, O. Y., Vidrih, S., Wyse, R. F. G., Willman, B., Grebel, E. K., Schneider, D. P., Beers, T. C., Kniazev, A. Y., Barentine, J. C., Brewington, H., Brinkmann, J., Harvanek, M., Kleinman, S. J., Krzesinski, J., Long, D., Nitta, A., & Snedden, S. A. 2006b, *ApJ*, 650, L41

Zucker, D. B., Belokurov, V., Evans, N. W., Wilkinson, M. I., Irwin, M. J., Sivarani, T., Hodgkin, S., Bramich, D. M., Irwin, J. M., Gilmore, G., Willman, B., Vidrih, S., Fellhauer, M., Hewett, P. C., Beers, T. C., Bell, E. F., Grebel, E. K., Schneider, D. P., Newberg,

H. J., Wyse, R. F. G., Rockosi, C. M., Yanny, B., Lupton, R., Smith, J. A., Barentine, J. C., Brewington, H., Brinkmann, J., Harvanek, M., Kleinman, S. J., Krzesinski, J., Long, D., Nitta, A., & Snedden, S. A. 2006c, *ApJ*, 643, L103

Zucker, D. B., Kniazev, A. Y., Bell, E. F., Martínez-Delgado, D., Grebel, E. K., Rix, H.-W., Rockosi, C. M., Holtzman, J. A., Walterbos, R. A. M., Annis, J., York, D. G., Ivezić, Ž., Brinkmann, J., Brewington, H., Harvanek, M., Hennessy, G., Kleinman, S. J., Krzesinski, J., Long, D., Newman, P. R., Nitta, A., & Snedden, S. A. 2004a, *ApJ*, 612, L121

Zucker, D. B., Kniazev, A. Y., Bell, E. F., Martínez-Delgado, D., Grebel, E. K., Rix, H.-W., Rockosi, C. M., Holtzman, J. A., Walterbos, R. A. M., Ivezić, Ž., Brinkmann, J., Brewington, H., Harvanek, M., Kleinman, S. J., Krzesinski, J., Lamb, D. Q., Long, D., Newman, P. R., Nitta, A., & Snedden, S. A. 2004b, *ApJ*, 612, L117

Zucker, D. B., Kniazev, A. Y., Martínez-Delgado, D., Bell, E. F., Rix, H.-W., Grebel, E. K., Holtzman, J. A., Walterbos, R. A. M., Rockosi, C. M., York, D. G., Barentine, J. C., Brewington, H., Brinkmann, J., Harvanek, M., Kleinman, S. J., Krzesinski, J., Long, D., Neilsen, Jr., E. H., Nitta, A., & Snedden, S. A. 2007, *ApJ*, 659, L21

Zwicky, F. 1933, *Helvetica Physica Acta*, 6, 110